Estimating Leaf Area Index from Airborne Laser Scanning in *Pinus radiata* Forests

---

A thesis submitted in partial fulfilment of the requirements for the Degree of Doctor of Philosophy in Forestry by Grant Dennis Pearse

---

School of Forestry

University of Canterbury

2017

for Simon

Contents

List of Figures

List of Tables

Abstract

Leaf area index (LAI) quantifies the amount of leaf surface area per unit ground area. LAI in forest ecosystems regulates the upper limit of possible light interception, atmospheric gas exchange, and primary production. These properties make LAI one of the most important ecophysiological variables with a wide range of potential applications. In the context of forests managed for production, knowledge of LAI offers the potential to align management activities with fundamental biophysical properties. For example, LAI offers the potential to precisely target and monitor management activities such as fertiliser application or disease control. Despite the potential benefits knowledge of LAI offers, usage is seldom seen outside of research applications. A key reason for this is the difficulty in obtaining LAI measurements over large areas, with field based optical methods largely constrained to use under uniform, diffuse sky conditions. Remote sensing of LAI offers one potential solution to obtain large-scale estimates of LAI. However, promising spectral-based approaches have been shown to have limited usefulness for forests with high LAI such as intensively managed coniferous plantations. Airborne laser scanning (ALS) data (lidar) offers enhanced ability to estimate LAI in a range of forest types with a high degree of accuracy, but the optimum methods for estimating LAI from lidar are not well established.

This thesis aims to develop and demonstrate a method for estimating LAI from lidar in New Zealand's intensively managed *Pinus radiata* D. Don forests. To accomplish this, two distinct areas of research are addressed. First, this thesis addresses the need for acquiring a large number of LAI field measurements covering a range of stand conditions in order to calibrate ALS-LAI models. This was accomplished by validating the use of the newly developed LAI-2200C (LI-COR Biosciences Inc., Lincoln, NE, USA). This instrument allows measurement of LAI under clear sky conditions through the application of a model to correct for the impact of scattered light on gap fraction estimates. This thesis presents the first *in situ* comparison of LAI measurements acquired under diffuse and clear sky conditions in a coniferous forest. These results were obtained by repeatedly measuring LAI in plots of pure *P. radiata* in New Zealand. In addition, the thesis presents the first assessment of the importance of acquiring accurate needle spectra to parameterise the scattering correction model. These values were acquired using newly developed methods that allow accurate spectra to be acquired from needle-leaved species via spectroradiometer. The thesis also addresses the stability of needle optical properties with respect to position in the canopy, abaxial and adaxial measurements, and variability between individual trees.

The second part of this thesis used a large number of LAI measurements made possible by the new instrumentation to address key questions on the topic of estimating LAI from lidar.

To date, most ALS-LAI research has been divided between establishing empirical or physical links between lidar metrics and LAI. This has resulted in a proliferation of proposed methods and lidar metrics for estimating LAI, and few studies have compared these approaches. In addition, factors known to impact ALS-LAI estimation such as the choice of plot parameters have gone relatively unexplored, as has the use of new statistical learning approaches. This thesis attempts to offer the first simultaneous assessment of the optimum combination of lidar metrics, plot parameters, and modelling approaches for estimating LAI from ALS lidar data in *P. radiata* forests.

Results from the instrument validation suggest that the scattering correction model performs well in coniferous forests. Overall, clear sky LAI measurements were higher on average than diffuse sky measurements. However, there was evidence that this difference resulted from a reduction in erroneous readings obtained from the largest outer sensor ring under diffuse sky conditions. Traditionally, data from this part of the instrument have been error-prone and there was some evidence that clear sky LAI measurements offer increased accuracy by reducing scattering induced error across the range of zenith angles observed by the instrument. The method used to obtain spectroradiometer measurements from needle-leaved specimens was well suited to collecting accurate needle reflectance and transmittance for use in the scattering correction model. Use of these values improved agreement between clear and diffuse sky LAI measurements and reduced the magnitude of the largest differences at the extremes of the range. The results demonstrated that *P. radiata* spectra did not differ significantly with canopy position and were reasonably stable between trees. Measured *P. radiata* needle spectra are presented as part of this thesis and values are suggested for future users of the LAI-2200C scattering correction model in this forest type. Overall, use of measured spectra in combination with masking of outer ring data allowed LAI to be measured under both clear and diffuse sky conditions; however, clear sky conditions offered considerable reductions in the maximum potential measurement error resulting from changes in sky condition over time and between sensor locations.

Results presented in the second part of this thesis demonstrate that LAI can be accurately estimated from lidar data in *P. radiata* forests. A key finding from this work was that use of standard approaches developed for use in other forest types produced some of the worst models of all those trialled, indicating that successful ALS-LAI estimation in *P. radiata*

depends on careful selection of lidar metrics, plot parameters, and modelling approach. Specifically, results showed that (1) metrics that form a proxy for gap fraction by computing the ratio of returns above and below a chosen height threshold (ratio metrics) were key predictors of LAI; (2) choice of height threshold for ratio metrics strongly impacted model performance and *P. radiata* appeared to require higher thresholds than other forest types; (3) the concept of a variable height threshold was beneficial in accommodating differences in tree height across plots and led to improved estimates of LAI; (4) a larger fixed plot radius generally improved model performance; (5) use of a variable plot radius linked to instrument view distance was better than any fixed radius trialled; (6) metrics linking lidar penetration to the Beer-Lambert law were only marginally less accurate than empirical models and showed strong predictive ability. This approach may offer a means of estimating LAI without calibration by inverting the Poisson model using gap fraction from lidar and an empirical projection coefficient. Finally, the research found a high level of correlation present between lidar metrics, strongly emphasising the need for modelling approaches robust to these effects. Regularised regression via the elastic net was found to be a useful method for providing both variable and model selection in high-dimensional space while accounting for the presence of high correlation between metrics. Results from models produced by the random forests algorithm were similar to results from elastic net but provided some useful insights into variable importance.

Acknowledgements

The author would like to thank my two thesis supervisors Drs. Michael Watt and Justin Morgenroth, as well as several anonymous reviewers and Mr Jonathan Dash for providing helpful written feedback on the thesis and published works. I would also like to thank Timberlands Ltd. for providing access to forest plots and associated data, as well as providing valuable staff time to assist with the preparations for data collection.

I would like to acknowledge the financial support received from the University of Canterbury in the form of a scholarship (UC Canterbury Scholarship 2013-2016) and generous support from the Growing Confidence in Forestry's Future (GCFF) research program administered by Scion New Zealand and the Ministry of Business, Innovation and Employment (contract number: CO4X1306).

Chapter 1 - Background and Introduction

1.1 Applications and measurement of leaf area index

Leaf area index (LAI) quantifies the amount of leaf surface area per unit ground area. In forest ecosystems, the unit-less quantity LAI provides a measure of the leaf tissue available for photosynthesis. As such, LAI is a fundamental determinant of a range of ecosystem processes including gas and energy exchange, water and nutrient cycling, canopy health and primary production (Bréda, 2008). LAI is also closely linked to site fertility, with poor fertility being strongly associated with lower values of LAI (Raison & Myers, 1992). Despite the fundamental importance of LAI to forest managers and scientists, usage has been limited by the difficulty of obtaining accurate and cost-effective LAI measurements (Jonckheere et al., 2004). This difficulty is primarily the result of the following factors:

- LAI varies greatly across forest ecosystems, at both local and global scales (Bréda, 2008).
- Intra and inter-seasonal variation can be large and species dependent (Bréda, 2008; Raison & Myers, 1992).
- Environmental factors such as climate and site fertility can have large impacts on LAI (Raison & Myers, 1992).
- Management activities such as fertilisation and thinning can impact LAI for several years (Peduzzi, Wynne, Fox, Nelson, & Thomas, 2012; Raison & Myers, 1992).
- Interactions between the above factors are common, further complicating assessment.

Therefore, the use of LAI in forest science and forest management necessitates methods for LAI assessment that are (1) suitable for fine-scale surveys, (2) suitable for use across a range of locations, and (3) can be used repeatedly to assess change. At present, managers and

researchers interested in LAI have several options to acquire *in situ* LAI measurements, although all have significant limitations:

- Direct assessment through leaf litter traps or destructive sampling is accurate and well tested, but this method is costly, laborious, and limited to suitable (deciduous) forest types (Jonckheere et al., 2004).
- Allometric models relating sapwood to LAI are accurate but highly stand specific (Bréda, 2008).
- Optical methods using cameras or specialised light sensors can produce accurate measurements of LAI by inversion of the Beer-Lambert law. However, these methods include non-photosynthetic light blocking elements and can be used only under diffuse sky conditions to collect LAI measurements from small areas (J. M. Chen et al., 2006; J. M. Chen, Rich, Gower, Norman, & Plummer, 1997; Zhang, Chen, & Miller, 2005).

In practice, optical LAI methods are usually selected for LAI measurement. A considerable body of work has developed demonstrating variable relationships between LAI and effective LAI (including light-blocking, non-photosynthetic canopy elements) (J. M. Chen et al., 1997; Fassnacht, Gower, Norman, & McMurtric, 1994; Gower, Kucharik, & Norman, 1999; Mason, Diepstraten, Pinjuv, & Lasserre, 2012). Despite observed discrepancies between directly measured LAI and effective LAI (hereafter LAI), optical methods remain the *de facto* standard for measurement of LAI, and measurements retrieved using these methods retain strong links to ecophysiological variables of interest such as (1) monitoring of insect driven defoliation events (Solberg, Næsset, Hanssen, & Christiansen, 2006); (2) fertiliser mediated increases in foliar biomass, nutrition, and retention (Amponsah, Comeau, Brockley, & Lieffers, 2005); and (3) relating fertiliser application to changes in LAI and light interception (Balster & Marshall, 2000). In practice, optical measurements of LAI are strongly impacted by sky conditions and measurement must usually be conducted under uniform, diffuse sky conditions (Kobayashi, Ryu, Baldocchi, Welles, & Norman, 2013; Zhang et al., 2005). Suitable conditions can be rare and can greatly reduce the number of LAI measurements obtainable during a given time frame or season (Solberg et al., 2009).

1.2 Remote sensing for leaf area index

The development of remote sensing technologies has produced the first readily available LAI assessment tools for large areas. The spectral properties of vegetation have been used to produce a wide variety of LAI products, including a global LAI map as part of NASA's MODIS satellite product suite (Knyazikhin, Martonchik, Diner, et al., 1998; Knyazikhin, Martonchik, Myneni, Diner, & Running, 1998). These resources have been useful to the scientific community interested in large scale issues with the MODIS LAI product finding uses in a wide variety of ecological studies (Yang et al., 2006). Forest managers and researchers interested in smaller scale applications have found these tools less useful. With a resolution of 1 km, the MODIS product is not well suited to fine-scale assessment of LAI, and comparative studies using newer techniques have found algorithm-dependent variations in the accuracy of MODIS LAI products (Jensen, Humes, Hudak, Vierling, & Delmelle, 2011). The resolution of forest LAI mapping may be improved through the use of newer high-resolution sensors combined with the inclusion of textural metrics alongside spectral metrics (Pu & Cheng, 2015). However, passive optical methods remain of limited use for forest-LAI estimation due to high data costs and the need for complicated image processing techniques (Fang & Liang, 2008). One of the most significant limitations of existing spectral techniques is the inability to derive estimates of LAI above certain thresholds. Saturation of spectral bands occurs in areas with high LAI values such as tropical forests - and importantly - conifer plantations (Bréda, 2008; Peduzzi et al., 2012). Development of spectral indices intended to address sensor saturation such as the enhanced vegetation index (EVI), or those addressing the effect of background pixels such as the soil-adjusted vegetation index (SAVI), have not reliably shown improvement in forest LAI estimation (Kamal, Phinn, & Johansen, 2016). Retrieval of LAI in coniferous forests has been attempted through the use of spectral-based methods in conjunction with sophisticated radiative transfer models similar to those developed for MODIS but with newer, finer resolution earth observation data; however, the high levels of LAI and unique canopies of coniferous species have confounded reliable estimation of LAI from these approaches (Kuusk, Lang, Kodar, & Sims, 2015).

1.3 Lidar and LAI

The advent of relatively inexpensive methods and instruments for acquiring light detection and ranging (lidar) data from airborne laser scanning (ALS) campaigns has had a profound impact on remote sensing of forested areas. This technology has emerged as a useful, and often superior, tool for a range of forestry applications including estimation of forest biomass, standing volume, stand height, log grade product mix, canopy structure, tree crown diameter, and species classification (Dash, Marshall, & Rawley, 2015; Leeuwen & Nieuwenhuis, 2010; Peduzzi et al., 2012). In the context of LAI, an emerging body of research has shown that ALS-based estimation of LAI can accurately predict LAI in a range of forest types, including planted coniferous forests (Peduzzi et al., 2012; Riaño, Valladares, Condés, & Chuvieco, 2004). Furthermore, ALS-based estimates of LAI have been shown to be less sensitive to saturation at high LAI levels, and more accurate than other assessment methods (Lefsky et al., 1999; Zheng & Moskal, 2009). As such, ALS-based estimation of LAI offers the first practical method for achieving large-scale, accurate assessment of LAI over large areas of plantation forest. However, previous work has demonstrated that the techniques to achieve accurate ALS-LAI estimates are forest and site specific, with limited transferability, even from similar forest types (Sumnall et al., 2016). Indeed, the majority of research estimating LAI from lidar data relies on the development of models using *in situ* measurements of LAI, usually acquired from optical methods (Jensen, Humes, Vierling, & Hudak, 2008; Morsdorf, Kötz, Meier, Itten, & Allgöwer, 2006; Peduzzi et al., 2012; Solberg et al., 2006). For reasons described in Section 1.1, the acquisition of field measurements can be challenging and can limit the availability of field measurements (Solberg et al., 2009), and introduce uncertainty associated with optical measurement of LAI (K. Zhao & Popescu, 2009). In addition, the methods for describing lidar in order to derive LAI covariates for inclusion in ALS-LAI models range from largely empirical (Jensen et al., 2011, 2008) approaches to those directly connecting the properties of lidar to the Beer-Lambert law underpinning optical methods of LAI measurement (Morsdorf et al., 2006; Solberg et al., 2009). Several aspects of the development of ALS-LAI models have been identified as important factors in determining the strength of ALS-LAI relationships, including: (1) the optimum type and combination of lidar metrics for use in model development, (2) choice of plot radius used to extract lidar data, (3) the height threshold used in ratio-based metrics, and (4) choice of an appropriate modelling approach (K. Zhao & Popescu, 2009).

1.4 Thesis context

At present, very limited research on ALS-LAI estimation has been conducted in New Zealand's managed forests of *Pinus radiata* D. Don. These forests are commercially important and provide a wide range of commercial and social goods. Intensive management practices such as fertiliser application, disease control, and site preparation are often employed in these forests. Assessment of LAI is appealing to managers of these forests as a tool for targeting and monitoring the aforementioned interventions and for monitoring forest growth and health. To the best of our knowledge, only a single study by Beets et al. (2011) has examined the potential to estimate LAI from lidar in this forest type. Results from this study demonstrated that simple lidar metrics could provide accurate estimates of LAI (R^2=0.8) for stands of *P. radiata*. While these results appear promising, this research relied on destructive measurement of LAI for model development, and hence was limited to a small area comprising a single age class with limited variations in stand conditions. The work of Beets et al. (2011) focused on validation of national carbon accounting models and their work did not address the optimal methods required to achieve reliable ALS-LAI estimates across varied stand conditions.

In conclusion, the potential to develop ALS-based methods for estimating LAI in forests of planted *P. radiata* remains largely unexplored. In addition, new methods for acquiring *in situ* measurements of LAI for the calibration of ALS-LAI models have recently been proposed (Kobayashi et al., 2013). These methods have not yet been validated in coniferous forest types. However, if validated they offer the potential to greatly enhance the practicality and scope for acquiring a large number of LAI samples in order to better train and validate ALS-LAI models.

1.5 Thesis objectives and layout

The primary objective of this thesis is to develop and assess models predicting LAI from lidar data acquired over planted forests of *P. radiata*. In order to achieve this, the thesis addressed two distinct problems. Firstly, an instrument validation was conducted on the LAI-2200C (LI-COR Biosciences Inc., Lincoln, NE, USA). This instrument represents the latest iteration of the well tested LAI-2000 and LAI-2200 that have been widely used to acquire field measurements of LAI for use in ALS-LAI studies (e.g. Peduzzi et al., 2012; Solberg et al., 2009). However, the newer version has been developed to allow for measurement of LAI

in the presence of direct sunlight i.e. under clear sky conditions as well as diffuse sky conditions. This is accomplished by attempting to remove the impact of scattered light, which would usually cause severe underestimation of LAI, by implementing a scattering correction model during post-processing of the measurements. The scattering correction model is strongly dependent on the properties of the forest canopy and on the accurate characterisation of sky condition at the time of measurement. Importantly, the model has not been directly tested using *in situ* measurements from coniferous forests and relies to an unknown extent on the availability of measured needle spectral properties to compensate for scattered light from canopy elements. The first part of this thesis presents a comparison of diffuse and clear sky LAI measurements obtained using the LAI-2200C in forest plots of pure *P. radiata*. The study also acquired measured needle spectra from a large sample of *P. radiata* foliage. Measurements were acquired using a newly developed method allowing accurate spectroradiometer measurements to be acquired from needle leafed foliage. The results are presented in the form of a published journal article incorporated in this manuscript as Chapter 3.

The second part of this thesis utilises a large number of LAI measurements afforded by the new instrumentation to develop ALS-LAI models for *P. radiata* forests. In doing so, the study addresses several important research questions that have emerged in the field of lidar estimation of LAI including (1) Performing a comparison of the large number of metrics proposed or used for ALS-LAI studies; (2) assessing the impact of a range of fixed plot radii and variable plot radii based on the height of trees within the plot; (3) evaluating the optimal choice and importance of a height threshold for metrics computed by dividing points according to the chosen height threshold; (4) trialling the use of modern statistical learning approaches to account for the high dimensionality and inter-correlation encountered in the study. The results are presented in the form of a manuscript under review, incorporated here as Chapter 4. The remaining sections provide additional information, discussions and conclusions not included in the works submitted for publication.

Chapter 2 - Literature Review

2.1 Introduction

Leaf area index (LAI) was initially defined as the one-sided area of photosynthetic tissue per unit ground area. However, this definition was not well suited to species with multiple sided leaf structures such as cylindrical or hemi-cylindrical needles (Jonckheere et al., 2004). To overcome this, a definition based on the projected leaf was proposed whereby LAI is taken to be the area enclosed by the largest projected outline of the leaf (Smith, 1991). However, Chen & Black (1992) demonstrated that this approach was also unsuitable for use on species with multiple sided or folded leaf structures. When averaged across all radiation incidence angles these leaf structures absorb considerably more light than a flat leaf with a similar maximum projected area. Using numerical simulation Chen & Black (1992) demonstrated that a projection coefficient of 0.5 should be applied to the total needle area per unit ground area of these species. While a variety of definitions continue to be used in the literature, one-half the total leaf area per unit ground surface is now generally accepted as the standard means of defining LAI in conifer forests (Jonckheere et al., 2004).

The link to surface area available for energy transformation and gas exchange makes LAI a fundamental determinant of primary productivity in the terrestrial biosphere (Bréda, 2008; Jonckheere et al., 2004). As such, LAI is also the primary determinant of water interception and use, energy and nutrient flux, and a key driver of many ecosystem processes (Bréda, 2008). Knowledge of LAI is therefore of great interest to researchers seeking to characterise and study these ecosystems and processes (Fang & Liang, 2008). In the context of forestry, LAI relates to a range of canopy properties such as canopy structure, canopy microclimate, rainfall interception, below canopy conditions and the ability of the canopy to support other species (Bréda, 2008). For managers of forest ecosystems LAI also provides an important link to the growth and productivity of forests, being both an important input into emerging ecophysiological models to predict future growth (Mason et al., 2012), as well as an important tool for assessing forest health in response to insect or pathogen attack (Solberg et al., 2006).

To utilise the information available from LAI it is necessary to understand the complex interaction between climate, site, and tree species traits which influence forest LAI both spatially and temporally. The primary factors known to impact LAI are outlined in the following section.

2.2 LAI and site quality

Site quality assessment in forestry is focused on matching species to appropriate sites and quantifying the productivity of a given region for the selected species. In the New Zealand context, several indices have been developed for the major commercial species *Pinus radiata*. Site Index (SI) and the 300 Index have emerged as the most important of these. Both are empirically derived by assessing stands according to a set of criteria at reference ages and silvicultural treatments. The index value for a site reflects the complex interaction between site, climate, and soil factors that determine tree growth (Kimberley, West, Dean, & Knowles, 2005). M. S. Watt et al. (2010) used regression analysis to evaluate the relative importance of environmental factors to both 300 Index and SI. The findings revealed that SI depended strongly on mean annual temperature and fraction of mean annual available root zone water storage. For 300 Index, seasonal ground frost and root zone water were the two most important factors. These findings highlight the requirement for knowledge of a range of environmental variables when attempting to determine productivity for a given site. Historic climate data is available at a reasonable resolution for much of New Zealand (Leathwick, Wilson, & Stephens, 2002). Data on soil properties is less accurate, with coverage for much of the country suffering from a range of issues including inaccuracy, poor or outdated methodology, low sampling intensity and missing values (Pearse, Moltchanova, & Bloomberg, 2015). New approaches aimed at developing improved soil maps may offer incremental improvements (Lilburne, Hewitt, & Webb, 2012) but these new data sources have yet to be validated. This limitation is particularly relevant given the importance of soil properties in determining available root zone water – a key variable for determining both 300 Index and SI. In addition to water storage, soil characteristics are a key determinant of nutrient availability within an ecosystem (McLaren & Cameron, 1996, p. 178). The reliance on indices provides a means of bypassing the complexity of site and environmental interactions by directly observing their impacts (Kimberley et al., 2005). To this end, LAI may offer a direct and fine-grained substitute for these indices, as it is also the product of complex environmental variables such as soil nutrient and water availability.

2.2.1 Nutrient status and LAI

Although LAI is the product of many variables, climate, and edaphic conditions explain much of the global variability in LAI (Bréda, 2008). Fertility, as measured by the availability of nitrogen, phosphorus, and potassium, is strongly linked to LAI and fertilisation with these nutrients can induce a positive response in LAI in several plant species (Bréda, 2008). The response of LAI to increased nutrient availability is more complex in forest ecosystems. For coniferous species, LAI response to fertiliser addition, especially nitrogen, is the product of increased needle count per fascicle, needle volume, needle length and increased fascicle count per tree (Fife & Nambiar, 1997; Rubilar et al., 2013a; Vose et al., 1994). Additional nitrogen is also associated with increased production of chlorophyll, as reflected by increased foliar N concentration. This is associated with an increase in needle efficiency and these impacts are reflected in increased ratios of net primary productivity (NPP) to needle mass (Beets & Whitehead, 1996; Carlyle, 1998; Fife & Nambiar, 1997).

However, in forest ecosystems, the LAI response to nutrient inputs is strongly impacted by other factors such as water availability, mean temperature, and light availability. Thus, additional nutrient inputs may fail to induce a large increase in LAI in the presence of restricted water supply or heavy shading. Added to this are the effects of canopy dynamics on resource availability. Research on the interaction of these factors on LAI for *P. radiata* forests shows several broad trends worth noting.

2.2.1.1 Combined impact of environmental factors on LAI

Soil nutrition, specifically nitrogen and phosphorous availability, is strongly and positively associated with foliar biomass, needle length, needle mass, foliage density, and LAI for a broad range of pine species. However, extensive research has shown mixed foliar response to fertiliser application alone. Large responses in LAI have been observed but the magnitude of the response has been found to be strongly dependent on other potentially limiting environmental or edaphic factors (Neilsen, Pataczek, Lynch, & Pyrke, 1992; Raison & Myers, 1992; Vose et al., 1994). Of these factors, soil water availability is frequently the most important moderator of LAI response to changes in nutrient availability. Raison & Myers (1992) conducted a detailed examination of the influence of water and nutrition on LAI in stands of *P. radiata*. Their findings indicated that available water in the year of needle formation was the most important factor influencing changes to LAI, needle extension, and foliar mass in the following year. Added nitrogen had some impact on LAI but was far more effective when combined with irrigation. The findings indicate that in this setting, annual

variation in LAI was largely determined by water stress. However, in the absence of water stresses the study showed that soil N content was strongly and positively correlated with LAI and NPP. Vose et al. (1994) reviewed a range of studies examining the factors influencing LAI of several pine species. The results consistently demonstrate a positive impact (+14% on average) on LAI from fertilisation in *P. radiata*, with irrigation resulting in additive effects on LAI (+54%). These results are supported by additional findings from a study of *P. radiata* in Chile. In this study, Rubilar et al. (2013b) trialled a number of silvicultural interventions including weed control and fertilisation. The results demonstrated that weed control produced a marked increase in LAI of up to 15% due to reduced water stress. Weed control also increased soil nutrient availability, limiting the impact of the added fertiliser in plots with both treatments. This study also provided some insight into the value of LAI as a measure of productivity. Detailed measurements of stem volume increment allowed the authors to construct a model of LAI and volume increment. The model demonstrated a strong positive relationship between LAI and volume, with changes in LAI able to explain 80-97% of the observed variation in stem volume increment. The authors note that their results are similar to those observed elsewhere for both *P. radiata* and loblolly pine (*Pinus taeda* L.).

2.2.2 Impact of canopy conditions and development on LAI

LAI response to fertility is also strongly influenced by canopy structure and light conditions. As the forest canopy matures and closes, light conditions may become limiting. At the point of canopy closure, the rate of LAI increase shows a marked decline and stabilises at a maximum value soon after this point (Vose et al., 1994). Once canopy closure is obtained, changes in LAI are largely restricted to shifts in the vertical profile, with stable LAI usually reflecting a normal distribution along the vertical axis. In *P. radiata* this shift to a normal distribution has been observed around age 13, but the timing is strongly related to factors influencing canopy closure, such as stand density and growth rate (Vose et al., 1994). In these conditions, additional fertilisation may induce a skew in foliar distribution as LAI increases in the upper canopy where light conditions are most favourable. In contrast to this, thinning and pruning may induce skewing in the opposite direction, shifting LAI towards the lower canopy in response to the altered light environment (Vose et al., 1994). At the stand level, thinning has a dramatic impact on LAI, with reductions of up to 50% being recorded. The post-thinning response in the remaining trees may be somewhat delayed as trees initially respond through increased productivity from existing needles, aided by re-allocation of

resources. In the absence of limiting factors, LAI will usually show a rapid increase towards pre-thinning levels in the years following stand thinning (Carlyle, 1998).

2.2.3 Summary of factors affecting LAI

In summary, LAI values may be influenced by many edaphic, climatic, and silvicultural factors, but there is a strong and well-established link between LAI and nutrient and water availability in particular. LAI, in turn, is strongly associated with tree growth. Many authors have noted this association, and it has been suggested that LAI may be an excellent proxy for determining site quality owing to the close link to both nutrient and water availability observed across many species (Carlyle, 1998; Vose et al., 1994). The strong link between LAI and volume increment found by Rubilar et al. (2013b) demonstrates that LAI may also be effective for identifying sites where interventions such as weed control, irrigation, and fertilisation may have beneficial impacts on timber production. Furthermore, the relationship between LAI and volume increment would allow forest managers to monitor LAI response and evaluate the benefits of interventions in terms of timber production and hence forest value. Measuring LAI also offers a practical means of overcoming the inherent difficulty in assessing soil fertility and water availability across a spatially heterogeneous landscape. Moreover, using LAI as a proxy for soil fertility and water status provides a direct assessment of plant useable resources, as opposed to soil testing and other techniques which may not reflect the ability of a species to access resources as presented in the environment. Finally, measurement of LAI also offers an opportunity to detect and monitor the impacts of biotic agents. For example, Swiss needle cast has been observed to greatly reduce LAI in stands of Douglas fir (*Pseudotsuga menziesii* var. *menziesii* [Mirb] Franco) (Weiskittel & Maguire, 2007). While in forests dominated by Scots pine (*Pinus silvestris* L.), measurement of LAI by optical means clearly reflected the progress of a severe insect attack causing widespread defoliation (Solberg et al., 2006).

It is clear that LAI values are the product of a complex set of interactions that may be difficult or impossible to model without extensive data for a range of factors. This suggests that measurements of LAI would be of particular interest in commercial forestry where site productivity and silvicultural management are key concerns. Despite these applications, LAI is seldom used in this setting, and this can be partially attributed to the difficulty of obtaining LAI measurements in commercial forests. In these settings, many approaches for measuring LAI are poorly suited to acquiring accurate, repeatable, and cost-effective measurements of

LAI across larger areas. These techniques and the challenges they face, as well as promising new approaches, are outlined in the following sections.

2.3 Measurement of LAI

Several factors make measurement of LAI in forest ecosystems particularly challenging:

- The canopy architecture is complex and varies greatly between forest types (J. M. Chen et al., 1997; Welles & Cohen, 1996).
- The forest canopy includes a large fraction of non-photosynthetic elements that extinguish light but do not contribute to primary productivity (J. M. Chen et al., 1997).
- LAI varies widely on a global scale with values ranging from 0.4–20 LAI (Bréda, 2008; Jonckheere et al., 2004). Climate, edaphic, and temporal factors can also drive large variations on smaller scales (Bréda, 2008).

To address these challenges, a variety of methods for assessing LAI have been developed. None of these methods is without drawbacks and measurement accuracy is often traded for practicality. A summary of the most common methods encountered in the literature is presented below to provide background for the chosen methodology and instrument validation presented in Chapter 3 and used to collect the data for the study presented in Chapter 4.

2.3.1 Non-destructive direct measurement

A common and accurate method in deciduous forests is the use of litter traps. The total surface area of the collected leaves may be assessed and divided by the area of the traps to derive an accurate assessment of LAI (J. M. Chen et al., 1997). This method can provide LAI estimates with up to 95% accuracy in some deciduous forests (Jonckheere et al., 2004). The setting and measuring of litter traps also takes considerable time and effort, and measurements can be confounded in species with fast leaf replacement times (Jonckheere et al., 2004). The use of litter traps is necessarily limited to deciduous species and is not suitable for use with evergreen coniferous species such as *P. radiata*.

2.3.2 Destructive model tree method

In this approach, a number of representative trees are sampled destructively and LAI may be determined by measurement of all leaves from the sample trees or by selective sub-

sampling (Jonckheere et al., 2004). For flat-leaf species, planimetric assessment can be performed using either manual methods or specialist equipment such as the LI-COR LI-3000 electronic leaf area scanner (Liang & Li, 2012, p. 348) For conifer species needle area is often measured by volume displacement methods (Johnson, 1984). It is not practical to use this method on all needles even from a single tree as each specimen must be soaked in detergent to avoid trapped air, and even the weight and meniscus induced by the pin holding fascicles must be accounted for (Beets, 1977; J. M. Chen et al., 1997). Therefore, samples of foliage (or other tree components) are used to derive volume to dry weight ratios, which are in turn used to estimate total values from the dry mass of un-sampled components. Using samples taken from juvenile *P. radiata* trees, Beets (1977) showed that a model-based approach using fascicle weight, density, and length of fascicles may also be used to accurately predict fascicle surface area, somewhat reducing the labour required to obtain these measurements. Model tree data and sub-sampling results can then be used to scale up estimates of LAI and area of woody components to the level of the stand (J. M. Chen et al., 1997; Mason et al., 2012). Where allometric models are to be derived for more general applications, the need for larger samples is required in order to ensure representativeness. Larger studies of this type are very labour intensive tasks and, importantly, require the destruction of all sampled trees (Beets et al., 2011; Perry, Fraser, Thomson, & Norman, 1988).

In summary, direct LAI measurement by means of foliage sampling is resource and labour intensive and impractical for large-scale, routine assessments of the type desired by forest managers and many researchers. However, it is the only source of primary LAI data and retains significant value as a means of calibrating and validating all other methods for indirectly measuring LAI (Jonckheere et al., 2004).

2.3.3 Allometric techniques

As the primary location for energy, water, and gas exchange LAI is closely related to tree growth. The diameter at breast height (DBH) of tree species has been shown to have a strong positive relationship with LAI, with the agreement as high as R^2=0.94 in one study (Le Dantec, Dufrêne, & Saugier, 2000). This relationship is driven by the close association between the area of water conducting sapwood and the leaf surface area – the site of all gas and water exchange. As such, more detailed measurements observing only sapwood area have also shown very strong correlations with needle area (R^2=0.93) (Bartelink, 1996). This would suggest that allometric methods may be used to predict LAI from DBH or sapwood

area measurements. However, Bartelink (1996) found large stand-dependent differences between sapwood and needle area. Similarly, the relationships observed by Le Dantec et al. (2000) were also found to be stand-dependent. The dependency of these relationships is due to physiological differences between species, which alters the sapwood to leaf area relationship. Further differences in the relationship arise from the complex interaction of climate and site on individual tree stands (Bartelink, 1996). In addition to stand-dependent limitations, Zheng & Moskal (2009) note that allometric models also fail to reflect changes in LAI arising from seasonal impacts, forest health conditions, and local climate conditions. The implication is that an allometric relationship may produce LAI estimates of uncertain accuracy when applied outside of the stands or season used to derive these relationships.

In general, it is acknowledged that allometric models tend to overestimate LAI and are limited by their stand-specificity to sites where LAI exceeds 5. In these conditions, alternative methods such as the remote sensing-based LAI measurement techniques discussed in Section 2.4 begin to suffer from sensor saturation (Bréda, 2008; Jonckheere et al., 2004) and allometric models may offer improved estimates where large-scale assessment is required. The limitations of allometric methods are unsurprising given that the range of factors known to impact LAI includes both environmental influences (Raison & Myers, 1992) and management practices (Carlyle, 1998) (see also Section 2.2). Furthermore, allometric models must be derived and validated using destructive sampling for the combinations of site and species for which LAI is to be estimated. A practical alternative to methods involving destructive sampling lies in the use of optical instrumentation to indirectly measure LAI *in situ* and without the need for destructive sampling.

2.3.4 Canopy light interaction

Optical methods for estimating canopy LAI are practical and widely used alternatives to direct measurement (Jonckheere et al., 2004). These methods rely on the interaction between incoming solar radiation and canopy elements. Complex and varied canopy architecture together with variations in incoming solar radiation make the actual canopy light environment difficult to characterise. Various simplifications have been proposed to model LAI and other canopy properties using the observed radiation regime. A common and widely used approach assumes that plant canopies conform to the requirements of an attenuating medium such that the Beer-Lambert law may be applied. The Beer-Lambert law describes an exponential extinction function that can be used to describe the attenuation of light as it passes through a medium according to:

$$I = I_o e^{-kl} \quad 2.1$$

Where *Io* is the light flux observed at the top of the medium, *l* is the length travelled through the medium and *k* gives the extinction coefficient that describes the absorptivity of the medium (assumed to be constant), with the negative sign denoting attenuation. Monsi & Saeki (1953, 2005) presented both theoretical arguments and experimental data demonstrating that, under certain assumptions, the attenuation of light through a plant canopy can indeed be approximated by the Beer-Lambert law. In this approach, a simplified model of the plant canopy with horizontal leaves, perpendicular to incoming solar rays, is assumed to be statistically uniform in terms of the distribution of leaves across the layers. Dividing the canopy into layers containing *s* fraction of the total leaf area spread out over a larger area *S*, the probability of a beam passing through *n* layers is then:

$$P = \left(1 - \frac{s}{S}\right)^n \quad 2.2$$

And total LAI $= sn/S$. As *n* approaches infinity, the probability of a light beam making no contacts through the layers of a canopy with a given LAI is described according to a Poisson distribution (Jonckheere et al., 2004):

$$P_0 = e^{LAI} \quad 2.3$$

P_0 describes the gap fraction – the integrated frequency of all gaps - and represents the fraction of total incoming radiation not absorbed or blocked by the canopy (Weiss, Baret, Smith, Jonckheere, & Coppin, 2004). The contact frequency is the opposite of the gap frequency and represents the probability of a certain number of contacts with light blocking elements as a probe or beam of light passes through the canopy (Wilson, 1959). This is a fundamental concept underpinning many methods of indirectly estimating LAI. This relationship implies that measures of gap fraction are highly nonlinearly related to LAI, and that knowledge of the gap fraction (transmittance) can be used to obtain estimates of LAI by inverting the Poisson model.

Through integration it can also be shown that under the assumption of the canopy as a random, turbid medium with a small probability of foliage overlapping within layers, the attenuation of light passing through the layers of a canopy with LAI = *L* is described by (Monsi & Saeki, 1953, 2005):

$$I_b = I_a e^{-KL} \quad 2.4$$

Where I_a is the irradiance before entering the canopy and $I_b$is the irradiance below the canopy. This is like the Beer-Lambert law, with the ratio of irradiance (I_b/I_a) described as an

exponential function of LAI and an 'extinction coefficient' (*K*) that describes the absorptivity of the medium – in this simple model it is assumed to be complete i.e. *K* = -1.

The assumptions and simplifications underpinning the Poisson model are frequently not met in plant canopies. For example, the random dispersal of foliage within the canopy, with clumping evident in many plant species. Alternative models such as the Markov or Binomial models have been proposed as alternatives that can be adapted to alter the frequency of subsequent contacts with leaves given an initial contact in order to account for clumped foliage. However, the Poisson model remains popular for many applications and can provide reasonable descriptions of canopy light interactions for a range of canopy types (Nilson, 1971, 1999).

The Poisson gap probability model as described in Eq. 2.4 applies only to direct beam radiation entering a canopy from above and intercepted by leaves arranged horizontally. For use in plant canopies, Eq. 2.4 is modified to account for different zenith angles and leaf orientations:

$$P(\theta) = e^{\left[-G(\theta)\times\frac{L}{\cos(\theta)}\right]} \quad 2.5$$

Where *P* is the gap fraction at zenith angle θ, G defines the projection coefficient of foliage area on a plane normal to the solar zenith angle θ and *L* is the leaf area index (Pisek, Ryu, & Alikas, 2011; Stenberg, 2006; Zheng & Moskal, 2009). The need for this modification arises from the fact that leaf orientation within the canopy impacts the probability of light penetrating through the canopy at a given angle of observation. For example, in a canopy with vertically orientated leaves the fraction of direct solar radiation blocked by foliage when the sun is overhead will be much lower (high solar zenith angle leads to *K* approaching 0) than when the sun is close to the horizon (low solar zenith angle leads to *K* approaching infinity). This means that the extinction coefficient varies both with solar angle and the distribution of leaf angles within the plant canopy. In the simple case of fixed leaf angle, the ratio of the projected surface area of the leaf on a horizontal plane to the leaf hemi-surface area (projection coefficient or shadow area) defines *K*. For actual canopies, *K* is related to solar zenith angle and the projection coefficient *G* by (Weiss et al., 2004; Zheng & Moskal, 2009):

$$K = \frac{G\theta}{cos\theta} \quad 2.6$$

In real canopies, the angle of leaves within the canopy is not fixed and instead leaf angles are best described by a probability density function, often called a leaf angle distribution

(LAD). In this instance, *G* is defined as the average projection of leaf area onto a plane perpendicular to the incoming solar rays and *G* is, therefore, a function of both the distribution of leaf angles within the canopy as well as the zenith angle. It follows that the extinction coefficient *K* also varies with both the distribution of leaf angles in the canopy and the solar zenith angle (Stenberg, 2006; W.-M. Wang, Li, & Su, 2007). To invert the Poisson model and estimate LAI from observations of gap fraction at some solar zenith angle, it is necessary to model the leaf angle distribution (LAD) within the canopy to compute the mean projection of foliage and then the extinction coefficient of the canopy for a given zenith angle. Directly measuring leaf angles in a plant canopy is laborious and impractical and it is more common to approximate the LAD within the canopy by a statistical distribution reflecting the dominant leaf angle patterns and to calculate the projection coefficient by relating the mean projected area of the leaves on a plane to leaf surface area (Pisek et al., 2011; W.-M. Wang et al., 2007). It is important to note that LADs often relate only to the inclination angle of leaves from the zenith to the leaf normal, and often do not describe the azimuthal inclination angles. Although some species do show clear patterns of leaf azimuthal angle preference, the distribution of leaf angles is often treated as random to simplifying the calculation of *G* (W.-M. Wang et al., 2007). The spherical model is widely used to approximate the distribution of leaf angles in a plant canopy (Pisek et al., 2011). The spherical distribution is named for the fact that the probability of observed leaf angles is assumed to match the distribution of angles found if foliage were arranged on the surface of a sphere (i.e. randomly distributed). Use of shape-based models, such as the spherical distribution, to represent LADs is useful because it allows the projection coefficient to be calculated as the ratio of the surface area of a geometric shape to the projection of the shape on a horizontal plane. However, it has been observed that the simple spherical distribution is inflexible and does not represent LADs well for all canopy types (Pisek et al., 2011; W.-M. Wang et al., 2007; Weiss et al., 2004). Modification of the spherical distribution to use an ellipsoidal shape model allows representation of LADs that can accommodate canopy types ranging from those with predominantly erectophile leaves to those with predominantly planophile leaves using a single parameter (*X*) describing the ratio of the horizontal and vertical axes of the ellipse (with the spherical distribution being $X = 1$) (Jonckheere et al., 2004; W.-M. Wang et al., 2007; Weiss et al., 2004). Fig. 2.1 shows the density of leaf angles for several alternative representations of LAD for different canopy archetypes alongside the ellipsoidal distribution with 3 different values of *X* (W.-M. Wang et al., 2007). The leaf angle

is measured from the leaf surface normal to the zenith direction; therefore, canopies with erectophile foliage have many fewer leaves with high angles (θ) between leaf and zenith, whereas most leaves in planophile canopies have higher angles between the leaf normal and the zenith.

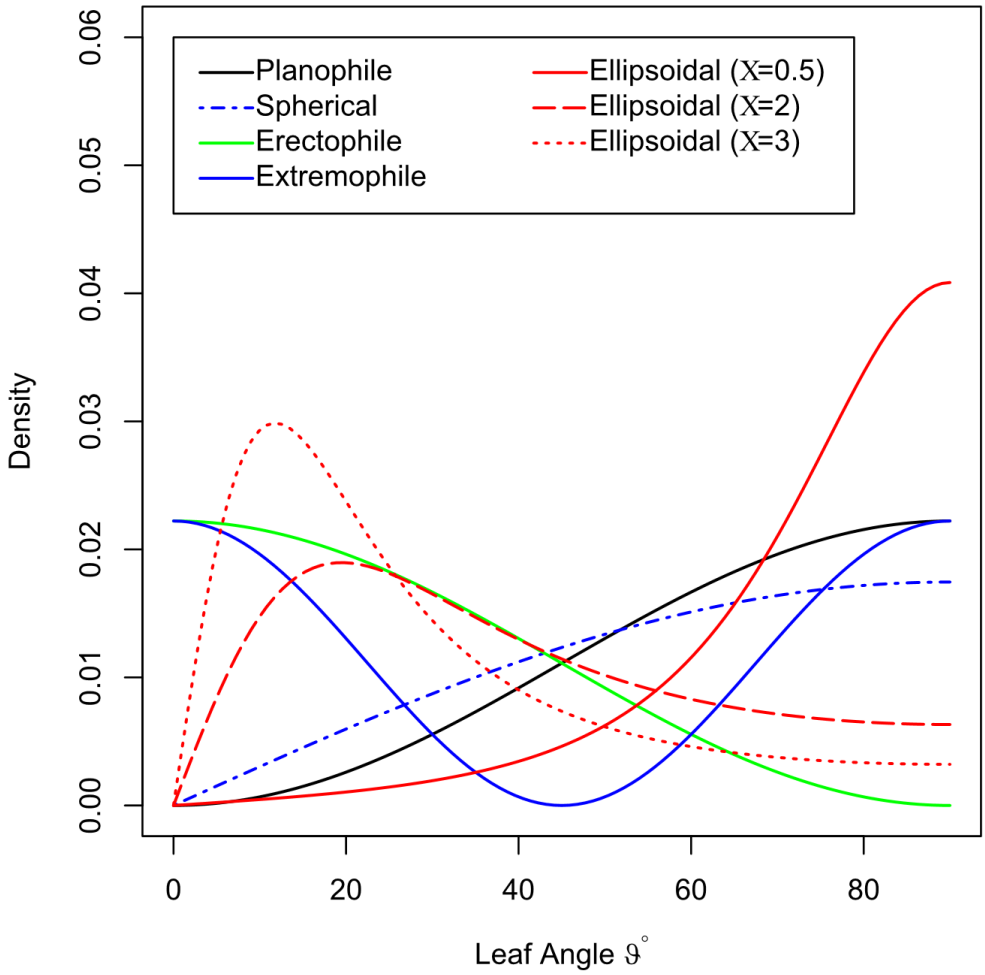

Fig. 2.1. Plot of probability density functions against leaf angle for several common leaf angle distributions used to model forest canopies. The spherical (random) distribution is equivalent to an ellipsoidal distribution with X=1.

As with the spherical approach, the ellipsoidal approach allows G to be computed using the projection of the ellipsoid's shape onto a horizontal plane at different solar zenith angles. The behaviour of G for different LADs at different solar zenith angles is shown graphically in

Fig. 2.2. The value of *K* at any zenith angle is related to the value of *G* for the same zenith angle through Eq. 2.6.

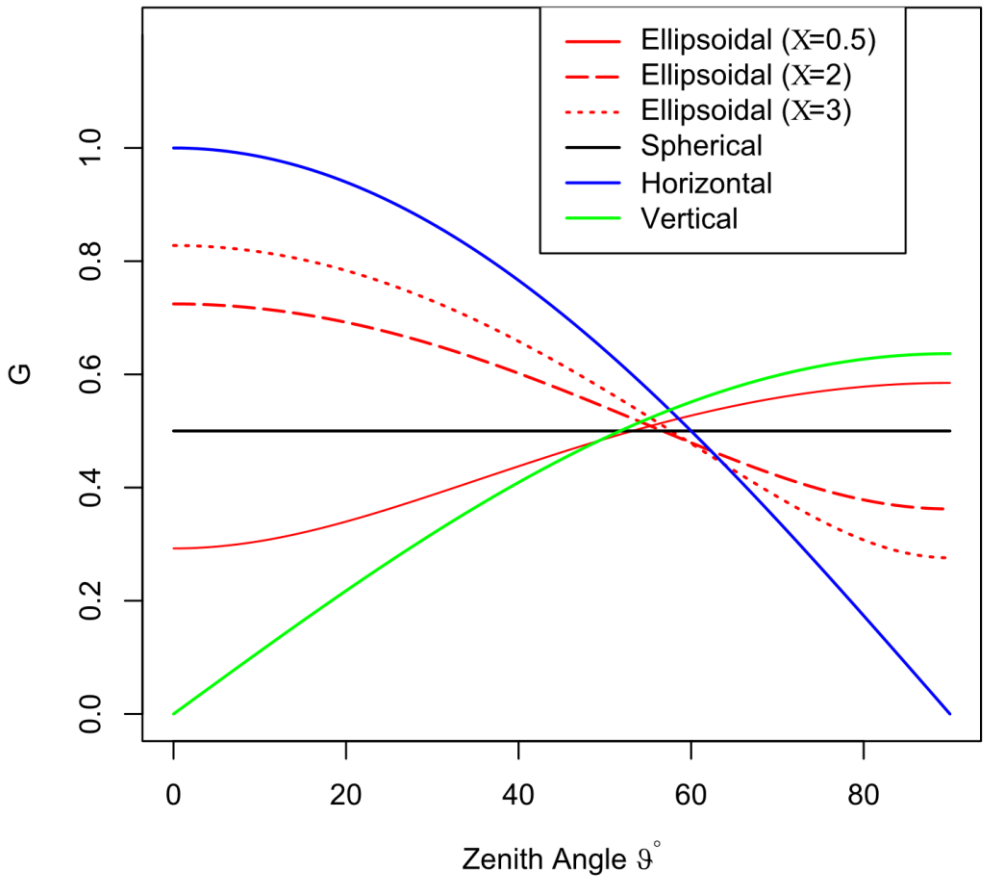

Fig. 2.2. Projection function (*G*) for common leaf angle distributions across the range of zenith angles. Projection coefficients for use in the Poisson model of LAI converge to approximately 0.5 at 1 radian (θ = 57.5°) for all LADs.

It is noteworthy that projection coefficients for all LADs converge to approximately 0.5 when the zenith angle is equal to 1 radian (θ = 57.5°). This is an important property that allows LAI to be estimated using Eq. 2.5 without knowledge of the LAD by observing canopy gap fraction within a narrow band centred on this region, where *G* is independent of the canopy LAD and approximately equal to 0.5, and the extinction coefficient *K* is close to 0.9 for most LADs (Wilson, 1960). The convergence of *G* at this zenith range is also useful for estimation of LAI using alternative methods for inverting the Poisson model (Eq. 2.5) to

estimate LAI from observed gap fraction, such as the solution proposed by Miller (1967) that underpins the LAI-2000 instrument (Section 2.3.6). In this approach, an initial estimate of LAI is computed using measurements of canopy transmissivity at zenith angle 57.5°, where *G* can be assumed to be 0.5, and then an iterative process is used to refine estimates of LAI. Having an initial estimate of LAI from this zenith range allows the form of the relationship between zenith angle and foliage inclination angle to be estimated empirically using regression, and extrapolated to other zenith angles outside of this range (Lang, 1986; Weiss et al., 2004; Welles & Norman, 1991). Ellipsoidal and other geometrically based distributions do not always accurately represent LADs observed in real plant canopies and many other models have been proposed as improvements, with a two-parameter beta distribution suggested as a superior alternative for representing many observed plant canopy LADs (W.-M. Wang et al., 2007).

In summary, application of the Beer-Lambert law to plant canopies provides a means to estimate LAI by measuring observed gap fraction or transmittance and inverting the Poisson model of light extinction through the canopy. Observations of gap fraction across the hemisphere can also be used to estimate the projection function and hence LAD for the canopy. For these methods, the gap fraction (*P*) must be computed across a range of zenith (θ) and azimuthal ($\propto$) angles using the simplified equation:

$$P(\theta, \propto) = \frac{Ps}{Ps + Pns} \qquad 2.7$$

Where *Ps* represents sky fraction (gaps) and *Pns* the non-sky fraction (canopy elements) within a given region (Jonckheere et al., 2004). Using this general approach, it is possible to obtain estimates of LAI using any method that allows *P* to be reliably estimated. For example, Eq. 2.7 may be applied to images taken from hemispherical cameras (Section 2.3.5) where $P(\theta, \propto)$ is the fraction of sky pixels in the specified direction, or the gap fraction may be obtained from measures of light intensity above and below the canopy as in the LAI-2000 (Section 2.3.6). Similarly, active sensors such as terrestrial or airborne laser scanners (Section 2.5) may also be used to obtain estimates of $P(\theta, \propto)$. As such, gap fraction-based approaches allow rapid and automatic calculation of LAI from easily obtainable data.

Despite these advantages, gap fraction techniques do have several limitations. Importantly, most methods of estimating gap fraction are unable to discern light extinction caused by the presence of photosynthetic leaf tissue from that caused by non-photosynthetic elements such as stems and branches (Jonckheere et al., 2004). The term effective LAI (often represented by LAIe) is generally used in scientific literature to distinguish these estimates

from true LAI (often represented by LAIt) incorporating only photosynthetic elements (Zheng & Moskal, 2009). Unless otherwise specified, the term LAI will refer to effective LAI (LAIe) throughout this text. The goal of much of the theory described in Chapter 2 is to produce estimates of LAI that are as close as possible to true LAI, and references to improvement in LAI estimates in this chapter refer to a closer agreement between these two values.

As noted earlier, the Poisson model (Eq. 2.5) assumes randomly distributed foliage and does not account for the clumping and overlapping of foliage elements at multiple scales evident in most plant canopies. This is particularly true of coniferous species that often have strongly clumped foliage and canopies which are non-random and strongly influenced by branch and shoot structures (J. M. Chen et al., 1997).

The violation of these assumptions can cause significant underestimation of LAI in coniferous forests. J. M. Chen et al. (1997) demonstrated that clumping at different scales can result in underestimation of LAI by up to 30% in boreal conifer forests. To obtain reliable estimates of LAI for conifer species the Poisson model (Eq. 2.5) is altered to include a term to account for clumping of canopy elements. This value is referred to as the clumping index (Ω) (Zheng & Moskal, 2009). The modified expression including the correction for clumping is given by:

$$P\,(\theta) = e^{\left[-\,G\,(\theta)\times\,\Omega\,\times\frac{L}{cos(\theta)}\right]} \qquad 2.8$$

J. M. Chen et al. (1997) demonstrated that clumping occurs at both the level of the shoot and at scales greater than the shoot. Both can impact estimates of LAI and so for coniferous forests, Ω must be decomposed into two parts as:

$$\Omega\ = \frac{\Omega e}{Ye} \qquad 2.9$$

Where Ω*e* represents the clumping factor at scales greater than the shoot, and *Ye* represents clumping at the level of the shoot (J. M. Chen et al., 1997). Specialised instruments such as the TRAC device, described in J. M. Chen & Cihlar (1995), have been developed to assess canopy clumping by measuring the size and distribution of canopy gaps, and, in one study, use of the TRAC device improved LAI estimates by up to 30% (J. M. Chen, 1996). Further development of methods which allow clumping to be estimated using only data collected for gap fraction analysis (as described in 2.3.5) have largely negated the need for dedicated instruments, and methods to account for clumping are available for several common instruments for measuring LAI (Chianucci & Cutini, 2012; Ryu et al., 2010).

However, these techniques largely deal with clumping of canopy elements, while neglecting clumping at the scale of the shoot (*Ye*), which can be a significant cause of LAIe underestimation - especially for coniferous species (J. M. Chen & Cihlar, 1995; J. M. Chen et al., 1997). J. M. Chen et al. (1997) demonstrated a method to assess *Ye* for coniferous forests by collecting intact samples and using a video camera and volume displacement to measure shoot projected area and needle surface area. The value for *Ye* then becomes:

$$Ye = \frac{An}{As} \qquad 2.10$$

Where *An* is half the shoot all-sided needle area and *As* is the total shoot intercepting area (also called 'imaginary' area) (J. M. Chen et al., 1997; Zheng & Moskal, 2009). Published values of *Ye* obtained in this way are available for some coniferous species but these have been observed to vary with growth conditions (J. M. Chen et al., 2006), raising questions about the usefulness of these as reference values to correct LAI in similar forests. Information on *Ye* for *P. radiata* in New Zealand could not be found, and work done by Mason et al. (2012) on the same species suggested a single within-shoot correction factor may not be appropriate in some situations.

Despite the complexity of LAI optical LAI measurement, it remains the most practical and widely used method for researchers and commercial users to obtain estimates of this important biophysical measure. Moreover, in practice, the effective LAI values are sufficiently correlated with true LAI that they retain usefulness for a range of applications (Mason et al., 2012; Solberg et al., 2006; Stenberg, Linder, Smolander, & Flower-Ellis, 1994). This has spurred the development of several specialised optical instruments for measuring LAI, most of which utilise gap fraction analysis. Of the available instruments, the LI-COR LAI-2000 plant canopy analyser and hemispherical canopy photography are widely used to estimate LAI in forest canopies.

2.3.5 Gap fraction by hemispherical photography

Gap fraction can be determined from images acquired using hemispherical canopy photography (HCP). These images are acquired using an upward facing camera, often fitted to a self-levelling tripod mount. Images are usually aligned or marked to a reference direction such as magnetic north (Leblanc, 2004; Rich, 1990). Using a fish-eye lens the view angle for each image covers close to 90 degrees in zenith and 360 degrees in azimuth, capturing a view of the canopy in all directions. Once the gap fraction has been calculated (detailed below), effective LAI can be determined by inverting the Poisson model (Eq. 2.5). Early work on

obtaining LAI from HCP relied on the cumbersome digitisation of greyscale photographs followed by classification of sky and canopy pixels. This process was overshadowed by the advent of dedicated instruments (see Section 2.3.6) that offered a simplified means of estimating LAI. However, the recent availability of powerful and cheap digital cameras with very high resolutions, as well as refinement of the processing techniques has seen HCP again become a popular technique for measuring LAI (Chianucci & Cutini, 2012).

2.3.5.1 Advantages of HCP

LAI from HCP images is obtained by classifying images, usually using only the blue band from RGB imagery, into sky and canopy pixels. The classified image is then divided into concentric rings covering defined ranges of zenith angles. These rings are processed individually to obtain a measure of gap fraction (the proportion of visible sky) within each ring (Leblanc, 2004). While similar to related instruments such as the LAI-2000 that automate this process (see Section 2.3.6), HCP has the advantage of allowing images to be segmented using custom zenith and azimuth angle intervals. In this way, HCP allows simultaneous measurement of gap fraction, leaf angle distribution, and canopy architecture across the entire scene, or any chosen area of interest (Zhang et al., 2005). This flexibility avoids some of the difficulties encountered when the physically defined zenith angles of LAI-2000 rings are excluded from analysis. This is frequently required to avoid clearings or obstacles, minimise interference, or reduce scattered light (J. M. Chen et al., 1997; Solberg et al., 2009). Compared with direct assessment, HCP methods have been observed to underestimate LAIt by up to 50% and improved segmentation of the images in this way can reduce, but not eliminate, this tendency (Zhang et al., 2005). Modern cameras can capture HCP images at very high resolutions, greatly improving the ability to identify small canopy gaps, which further improves the accuracy of LAI. However, the optical characteristics of fish-eye lenses do offset some of the improvements in camera resolution (Macfarlane, Grigg, & Evangelista, 2007; Zhang et al., 2005).

Advances in image processing techniques have also contributed to more accurate estimates of LAI from HCP. Efforts such as those by Leblanc et al. (2005) have focused on utilising computer-based processing to analyse gap distribution within HCP images to estimate clumping correction factors (Ωe from Eq. 2.9) to better estimate LAI. Building on this work J. M. Chen et al. (2006) revisited HCP as a substitute for the TRAC device. By using a simulated transect of readings extracted from high-resolution HCP images they could create a string of readings suitable for processing by the TRAC processing software.

Comparison with TRAC values indicated that HCP clumping index was generally within 4% of the TRAC value. This approach allows both effective LAI and the foliage element clumping index to be derived using only images acquired from HCP. Needle to shoot ratio (*Ye* from Eq. 2.9) must still be calculated from somewhat laborious destructive sampling. Another commonly used method for computing the clumping index is based on logarithmic gap averaging, whereby the HCP image is divided into small segments and the natural log of the gap fraction per region is taken to diminish the impact of large, non-random gaps between crowns or canopy elements (Lang & Yueqin, 1986; van Gardingen, Jackson, Hernandez-Daumas, Russell, & Sharp, 1999).

Most software packages for processing HCP images now include several different methods for calculating effective LAI, clumping index, and many other canopy parameters (Chianucci & Cutini, 2012). A further advantage of HCP imagery is that archived imagery may be reprocessed to take advantage of new methods as they emerge. Despite the advances in HCP hardware and software, the technique still suffers from several limitations which must be addressed carefully if accurate estimates of LAI are to be obtained from HCP.

2.3.5.2 Limitations of HCP

Successful estimation of LAI from HCP relies on accurate classification of canopy and sky elements within an image. This is accomplished using automatic or operator-based selection of a digital number (DN) threshold to perform a simple binary classification (Leblanc, Chen, Fernandes, Deering, & Conley, 2005; Mason et al., 2012). Gap fraction estimates, and hence LAI, are highly sensitive to this process, and errors arising from misclassification have been a persistent problem with HCP methods (Jonckheere et al., 2004; Rich, 1990). For manual classification, this issue is further compounded by the subjectivity of operator classification. For example, Seidel et al. (2012) found only 75% correlation in the selection of DN thresholds between two experienced operators. Use of histogram based methods can assist in identifying the optimal DN threshold; however, these methods often produce ‘mixed’ pixels with DNs that could be considered either sky or canopy (Macfarlane, Ryu, Ogden, & Sonnentag, 2014). Mixed pixels are common in small gaps within the canopy, around the edges of canopy elements, and where leaves are located in brightly illuminated regions (Macfarlane et al., 2014). Gamma correction and the use of a dual threshold technique to deal with mixed pixels has been shown to improve image classification (Macfarlane, Grigg, et al., 2007).

Minimising thresholding errors and obtaining good LAI estimates from HCP depends strongly on obtaining images with maximum contrast between canopy and sky elements, and very little over or under-exposure within the scene (J. M. Chen et al., 2006; Macfarlane et al., 2014). A key requirement for obtaining images with these characteristics is to acquire HCP images only under uniformly diffuse sky conditions, with camera exposure set to make sky pixels appear white, and foliage black. Over-exposed images with brighter light levels cause the camera sensor to saturate at a given exposure and these regions bleed into neighbouring, darker canopy elements. This effect is termed blooming, and results in an overestimation of gap fraction, and hence underestimation of LAI (Leblanc et al., 2005; Macfarlane et al., 2014). Conversely, under-exposed images fail to capture small gaps within the canopy, leading to overestimation of LAI, as well as difficulty in assessing canopy clumping index (Zhang et al., 2005).

A considerable amount of research has been conducted to determine the optimal camera and exposure settings for acquiring HCP images, and many of the proposed methods require consideration to be given to some or all of the following: canopy type, gap fraction, gap size and distribution, sky luminance, and camera setup (Beckschäfer, Seidel, Kleinn, & Xu, 2013). These requirements are at least in part due to the fact that camera hardware utilised for HCP is optimised for acquiring aesthetically pleasing images by automatically altering image exposure, grey level, and gamma settings to compensate for changing light conditions. When used under a dense canopy the camera will compensate by increasing exposure. Conversely, a sparse canopy will cause the camera to underexpose the canopy scene. The resulting images acquired using automatic camera settings can have very large errors – up to 900% overestimation of gap fraction in one study (Beckschäfer et al., 2013). In another assessment, Zhang et al. (2005) found that relying on automatic exposure resulted in LAI underestimation of 16-71% for medium and dense canopy and LAI overestimation of 11-29% in sparse canopies. Based on these findings the study authors proposed a method for determining the optimal exposure settings for HCP. In this method, the camera's automatic exposure is recorded while pointed toward open sky and then below canopy images are acquired with the camera set two exposure levels (f-stops) more than the external reference value. This protocol has been demonstrated to work well under a variety of canopy types and has been incorporated into several studies using HCP to measure LAI (J. M. Chen et al., 2006; Macfarlane, Hoffman, et al., 2007).

Despite widespread recognition of the importance of image exposure for obtaining accurate LAI estimates from HCP, and the availability of methods to determine optimal exposure, many researchers still attempt HCP while using automatic exposure settings. In a review of 61 studies using HCP, Beckschäfer et al. (2013) found that auto-exposure remained the most frequent method of determining the exposure of HCP images. In the same review, the authors noted that when exposure was recognised as an issue there was no consensus on how to determine the correct value, and over 10 different methods were observed in the reviewed studies.

In response to this, new techniques have been proposed to simplify exposure selection without reference to light levels outside the canopy. Beckschäfer et al. (2013) proposed the use of image histograms or saturation warnings, available on most modern cameras, to guide the choice of exposure. These tools can be used in the field to identify exposure settings which produce images with a bimodal histogram concentrated at both ends of the (DN) range. This maximises the contrast between sky and canopy while minimising saturation and the occurrence of mixed pixels. Using this method to determine optimal exposure settings, Beckschäfer et al. (2013) demonstrated that images acquired with auto-exposure overestimated gap fraction with a mean difference of 6.18%. However, the results were highly sensitive to canopy density and very low gap fraction resulted in overestimations of up to 900%. While this approach negates the need for external readings, it still requires each image to be assessed in the field and potentially re-taken, which can be time-consuming and cumbersome.

Macfarlane et al. (2014) present a further simplified field protocol whereby all images are acquired using one stop of underexposure relative to the automatic exposure below the canopy. The latter technique relies on software post-processing to alter image settings until the optimal bimodal histogram, with minimal saturation at either end, is achieved. This type of post-processing has been made possible by the advent of RAW image acquisition on high-end cameras. Images acquired in RAW format record information obtained from the camera sensor with minimal processing, maximising the number of brightness values available to represent each pixel (bit depth). Many modern digital camera settings such as gamma, contrast, white balance etc. are software manipulations applied by the onboard image processing chip. Rather than irreversibly altering the image data, RAW format captures these settings alongside the raw data, allowing changes to be made in post-processing. The advantages of RAW format image acquisition have been further explored by Hwang et al.

(2016) who used RAW images to reconstruct a sky image from cover photographs in order to better identify gap fraction under a wide range of sky conditions.

2.3.6 LI-COR LAI-2000 plant canopy analyser

The LAI-2000 is a specialised instrument for measuring LAI in a variety of canopy types. The device utilises optical sensors to obtain LAI from gap fraction as measured by canopy transmissivity (LI-COR, 2015; Stenberg et al., 1994). A detailed description of the instrument and the theory underpinning the computation of LAI from the associated optical measurements is given by Welles and Norman (1991). The key points are as follows: below-canopy light conditions are measured using five concentric light detectors. Each detector ring subtends a discrete zenith range but observes 360° in azimuth unless shielded by a view restrictor. Simultaneous measurements acquired at different zenith angles provides the observations required to solve Miller's (1967) equation for estimating LAI or leaf density based on the Poisson model. An iterative process begins with an estimate of LAI obtained using transmission (gap fraction) data covering the zenith range where the projection coefficient for canopy elements (G) is approximately equal to 0.5 (see Section 2.3.4). The relationship between projection coefficient and zenith angle can then be estimated using a regression to find the shape of an idealised curve that can be used to satisfy the requirement for knowledge of the appropriate leaf angle and projection functions (see Fig. 2.2 for example curves). This information is then used to further refine estimates of LAI and the process is repeated until convergence (Weiss et al., 2004; Welles & Norman, 1991). Rings are sensitive only to light in the blue wavelengths (320-490 nm) as light in this portion of the spectrum shows reduced scattering and transmittance from canopy elements thereby minimising the impact of these phenomena on below-canopy light readings. Below canopy measurements are then combined with concurrent (or as close as possible) measurements of sky brightness from above the canopy. The ratio between above and below readings provides a measure of canopy transmittance, or aggregate gap fraction, for each pair of rings and effective LAI is then estimated by the method described above. Using an approach similar to some HCP methods (Section 2.3.5.1), the multiple individual measurements of gap fraction from the instrument can be averaged so as to compute an approximate measure of the canopy clumping index, although the method is not as sensitive as HCP-based measures (LI-COR, 2015; Ryu et al., 2010)

This method for obtaining LAI makes several assumptions including 1) random distribution and azimuthal orientation of leaves within the canopy; 2) Foliage appears black

to the instrument (i.e. no scattering or transmission) in the blue band (320-490nm); 3) Foliage elements are small relative to the sensor. While no canopy conforms to all of these assumptions, coniferous species can seriously violate these assumptions – causing large errors in LAI estimation (LI-COR, 2015; Stenberg et al., 1994). In an evaluation of the accuracy of the LAI-2000, J. M. Chen et al. (1997) showed that within-shoot clumping and clumping at levels above the shoot each contributed 5-10% of the total error in estimating LAIt in boreal forest sites. However, these errors were dependent on stand structure, with homogenous stands producing lower errors. Mason et al. (2012) conducted a similar comparison of LAI estimates obtained from the LAI-2000 and LAIt results from destructive sampling of *P. radiata* stands. Their results confirmed the tendency of the LAI-2000 to underestimate LAIt, with underestimation of 60% observed in stands with low LAIt. When used in stands with higher LAIt, the LAI-2000 produced better estimates, but effective LAI was still 30-45% below LAIt. The study authors suggested that a single within-shoot correction factor was not appropriate for use with their results. Despite these limitations, Mason et al. (2012) could produce accurate models of LAIt (R^2=0.89) by incorporating transformed stand stocking variables in models using effective LAI from the optical instruments. This may partly reflect the fact that higher stocked stands conform more closely to the assumption of random foliage distribution by reducing the presence of large between-canopy gaps present in sparse coniferous stands. In another assessment, J. M. Chen et al. (2006) noted that dense canopies with high LAI can make LAI-2000 measurements particularly sensitive to small errors in measuring gap fraction. These errors can be exacerbated by the need to use the instrument only under diffuse sky conditions, reducing the ability to resolve small gaps at high zenith angles (Solberg et al., 2009).

Measurement with the LAI-2000 requires diffuse light conditions to minimise scattering in the blue band and to maximise the uniformity of the sky segment observed for pairs of above and below readings. In practice, this means that sampling is restricted to overcast days or the hours just after sunrise and just before sunset, and these requirements can greatly complicate sampling efforts (Solberg et al., 2009). Furthermore, when dealing with tall canopies the ‘above’ readings must instead be taken in an adjacent clearing with an unobstructed view distance of at least three times the height of the surrounding canopy. Clearings of this size are often hard to find and necessitate the use of a second calibrated unit stationed some distance away (Bréda, 2003; Solberg et al., 2009). Increasing the distance between sensors also increases the chance that they will not observe the same sky region and,

where sky brightness is not uniform, the differences will be confounded with changes in canopy transmissivity and the derived values of LAI will be in error (LI-COR, 2015).

Despite widely reported underestimation and restricted sampling conditions the value of rapid, repeatable measurements of LAI has made the LAI-2000 a common instrument choice for measuring effective LAI (Fang & Liang, 2008) and, where data are available, methods can be applied to derive values closer to LAIt (J. M. Chen et al., 2006). The advantages and shortcomings of the LAI-2000 are well documented, allowing users to plan for and use these data appropriately. Furthermore, there is a body of literature addressing important topics such as optimal sampling design for use with the instrument (Fassnacht et al., 1994; Majasalmi, Rautiainen, Stenberg, & Lukeš, 2013; Nackaerts, Coppin, Muys, & Hermy, 2000), approaches for reducing error arising from scattered light in more open canopies, sensor obstruction, and extreme canopy heterogeneity (Solberg et al., 2009; Stenberg et al., 1994).

2.3.7 A scattering correction model for LAI-2000 measurements

The requirement for LAI measurements to be conducted under uniform diffuse sky conditions poses serious logistical limits on the number and quality of measurements which can be acquired within a given period (Solberg et al., 2009). In the case of the LAI-2000, this condition is imposed primarily to avoid the influence of scattered light on gap fraction analysis (J. M. Chen et al., 2006). Incident light which is reflected or transmitted by canopy elements may be detected by the below canopy optical sensor, causing measured gap fraction to exceed the true gap fraction. In this way, scattered light leads to underestimation of LAI and clumping index and steps must be taken to minimise these effects (Kobayashi et al., 2013).

Existing approaches attempt to deal with scattering by observing light only from the blue band, where foliage scattering is reduced, and by avoiding conditions where foliage is directly illuminated by the sun, effectively limiting sampling to uniform diffuse sky conditions such as on uniform overcast days, at sunset, or at sunrise. Sampling under uniform, diffuse sky conditions has also been proposed as a way to allow the distance between above and below canopy readings to be increased where few clearings are available in the forest (LI-COR, 2015).

In practice, scattered light in the blue band cannot be assumed to be negligible in plant canopies and can cause LAI to be underestimated by up to 7.7% - even under diffuse sky conditions (Kobayashi et al., 2013). A further source of error arises from the fact that diffuse sky conditions are seldom uniform and stable in the field. Differences in the light conditions

across overcast (diffuse) skies can be substantial (Hwang et al., 2016) and can be exacerbated by shifting clouds and breaks of sunlight. Furthermore, it is often impossible to accurately observe the sky condition from below the canopy and even light precipitation on the reference sensor may go unnoticed while collecting below canopy readings under a dense canopy. These observations are supported by sky variability tests conducted using the instrument, which demonstrated that even in the best conditions, distance and time between observations can produce large errors in measured LAI (LI-COR, 2015). Sampling at sunset or sunrise on cloud-free days can produce better results, but this further restricts the sampling window. The results from a series of in-field sky variability tests conducted as part of this thesis are presented in Chapter 3.

A novel approach to this problem is proposed by Kobayashi et al. (2013). Instead of attempting to reduce or eliminate scattering, the authors utilise a one-dimensional, invertible, bi-directional, transmission model to quantify the scattered radiation reaching a sensor located below the modelled canopy. The calculated scattering correction can then be applied to gap fraction estimates obtained from the LAI-2000. The method developed by Kobayashi et al. (2013) calculates the scattering factor for a portion of the sky relative to the sun's position. This is achieved by using a simplified, invertible bidirectional transmission model that accounts for factors such as clumping, leaf reflectance, the impact of leaf angle distribution, and sun position at the time of measurement.

Kobayashi et al. (2013) used their simplified model to simulate the scattering factor observed by an optical sensor under various canopy and sky conditions. The results show scattering to be greatest in thin canopies with LAI of 1-2. Increasing canopy LAI reduces the amount of scattered light from the upper canopy reaching the ground. Simulations also revealed that observed scattering is dependent on both solar zenith angle and view angle of the sensor. In general, low solar zenith angles increased scattering in the lower portion of the canopy, which most strongly impacts gap fraction estimates taken at high zenith angles (e.g. ring 5 of the LAI-2000). High solar zenith angles produced the opposite effect, but total scattering was lower in this case, as was the error in gap fraction. Simulating an increase in the clumping index reduced the amount of scattering relative to a random canopy but estimates of clumping index from the instruments still differed from reference values. Kobayashi et al. (2013) attribute this to the increase in light penetrating the canopy without encountering scattering elements.

Kobayashi et al. (2013) also developed a practical method for adapting their theory and simulations to produce scattering corrections for data collected with the LAI-2000 instrument under clear skies. Field testing of the proposed method was conducted in a variety of canopy types where both LAIt and LAIe were well quantified. Results showed that under diffuse sky conditions LAIe was underestimated by 7.7%. Uncorrected measurements taken in sunny conditions showed increased underestimation of LAI of up to 26%. Applying the scattering correction to the clear sky data eliminated the difference between actual and measured LAIe (paired *t*-test ($p>0.05$)), and the standard deviation was reduced from 0.062 to 0.016. The field testing confirmed that changes in solar zenith and azimuth do alter the scattering effects; however, the model successfully accounted for these effects and in all cases the scatter corrected LAI-2000 estimates were not significantly different from the reference values ($p>0.05$). Application of the scattering correction model also improved estimates of clumping index obtained from LAI-2000 data using the methods of Ryu et al.(2010), but the results from the LI-COR instrument were still 30% higher than the reference values for the test site.

These results suggest that the scattering correction model is robust and can adequately deal with the impact of scattered light on gap fraction calculations, allowing accurate and unbiased measurement of effective LAI in clear sky conditions. Interestingly, the results also demonstrate that estimates obtained under 'ideal' diffuse sky conditions were biased downwards, and application of the computed scattering correction to clear sky measurements produced a better estimate of actual LAI than diffuse sky measurements.

The practical applications of this model are significant in that they allow more accurate estimates of LAI to be obtained under a broader range of sky conditions. In recognition of this LI-COR have incorporated the scattering correction model into a new version of the LAI-2000 instrument. This new instrument - the LAI-2200C - allows scattering corrections to be calculated and applied to readings taken in sunny conditions. A new protocol, described more fully in Chapter 3, has also been developed to capture the required inputs for the scattering correction, including:

- Measurements of diffuse sky radiation in the blue band (320-490 nm) from outside the canopy.
- Multiple readings to be taken with wide and narrow view restrictors to allow sky brightness to be normalised.

- Quantification of the fraction of diffuse radiation by covering the optical sensor with a uniform light diffusing panel and then exposing it to direct and indirect sunlight.
- Recording of the solar zenith and azimuth angle at the time of measurement - obtainable by reference to GPS data giving location and universal time constant.
- Measurements of leaf transmittance, ground reflectance, and leaf reflectance are also required.

In summary, the LAI-2000 is based on a robust and tested theory relating gap fraction to LAI through the Poisson model and has been validated across a broad range of canopy types. The accuracy of the original device is limited primarily by the violation of the assumptions around random foliage distribution in the canopy and the assumption that scattered light can be ignored in the blue band (Kobayashi et al., 2013; LI-COR, 2015). Previous generations of the LAI-2000 produce estimates of LAIe well below LAIt. This tendency is exaggerated in coniferous forests, where non-random leaf distribution and strong clumping effects are present. Implementation of the Kobayashi et al. (2013) scattering model, and improved methods for dealing with large-scale clumping (Ryu et al., 2010), address some of these shortcomings and greatly expand the range of conditions suitable for measurement of LAI.

However, outside of the model validation done by Kobayashi et al. (2013), very few assessments of the new instrument have been published. While the absolute accuracy of the LAI-2200C can only be determined through destructive sampling, the relative performance of the instrument is of equal interest to researchers. A large body of research has been produced using previous generations of the instrument to obtain reliable and repeatable measures of LAIe, and these values have found use in a variety of applications where LAIe can be substituted for LAIt. Within this context, the performance and limitations of the LAI-2200C remain largely unexamined. Furthermore, the changes in protocol facilitating clear sky sampling are likely to invalidate much of the literature comparing the relative performance of the LAI-2000 and other gap fraction based methods, such as hemispherical photography, which remain constrained by sky conditions.

The need for measured spectra to parameterise the scattering correction model with values for leaf reflectance and transmittance poses further uncertainty. Although a protocol is proposed for acquiring these values for flat leaf species using the LAI-2200C, and some default values for leaf reflectance and transmittance are also suggested (LI-COR, 2015), no research has addressed the impact of the spectra chosen on the performance of the scattering

correction model. Examination of this issue is particularly relevant for needle-leaved species. The small size of needles has confounded efforts to acquire accurate needle spectra for other applications. This is because a single needle provides too small a surface area for measurement by spectroradiometer (Daughtry, Biehl, & Ranson, 1989). Several methods have been proposed to overcome this; however, these often require the use of a cumbersome, custom-built needle holding apparatus. While other alternatives such as simply compacting needles together to increase surface area are known to increase multiple and forward scattering effects – polluting spectra obtained in this way (Yanez-Rausell, Schaepman, Clevers, & Malenovsky, 2014; Yanez-Rausell, Malenovsky, Clevers, & Schaepman, 2014). There is a need to assess the impact that the values chosen for leaf reflectance and transmittance have on the calculated scattering corrections. If these values are found to be important then alternative methods for obtaining accurate needle spectra will be required in order to obtain values for *P. radiata*. Furthermore, it would be useful to know if these values are stable and likely to be broadly applicable. This would allow measured spectra to be re-used to calculate the scattering correction across stands and forests within the same species.

2.3.8 Summary

In selecting a method for assessing LAI in the field it is important to consider the practical constraints of the task. Only indirect optical methods such as hemispherical photography and dedicated instruments such as the LAI-2200C are suitable for rapid and repeatable measurements across many sites. In one relevant study comparing LAI-2000 and HCP methods to destructive samples in stands of *P. radiata*, Mason et al. (2012) found that the best HCP method produced less strongly correlated LAI measurements than the LAI-2000 (R^2=0.72 vs. 0.89), although the final models also included the impact of stand density. These results must be viewed in light of the subsequent work done by Beckschäfer et al. (2013) and Macfarlane et al. (2014) who demonstrate that correct image exposure is critical to obtaining accurate LAI from HCP images. Mason et al (2012) did not have these protocols available and relied on auto-exposure to acquire images. In addition to this, the GLA and HemiView software packages used by Mason et al. (2012) do not employ methods for estimating clumping index from gap size and distribution, which can lead to significant underestimation of LAI (Chianucci & Cutini, 2012). These factors may account for the relatively poor HCP results as compared to other studies of coniferous species (e.g. J. M. Chen et al., 1997; Leblanc et al., 2005; J. M. Chen et al., 2006). Despite these limitations, Mason et al. (2012) obtained a useful model for estimating LAI from optical instruments in this forest type.

In a similar study, J. M. Chen et al. (2006) compared LAI-2000 measurements to those obtained from HCP taken in a mixed species boreal forest. The results showed that estimates from the different instruments generally agreed well – with a maximum difference of 20%. Clumping estimates extracted from HCP were within 12% of those produced by the TRAC device. This relative accuracy combined with the reduced cost, improved processing options, and archival value of the images led J. M. Chen et al. (2006) to conclude that HCP was suitable for replacing both the LAI-2000 and TRAC devices. Finally, it must be mentioned that all techniques are ultimately evaluated against destructive sampling, and this technique is not without its own limitations. Measurement via displacement, volumetric shape approximations, calculation of dry biomass ratios, and development of regression models are frequently required during destructive sampling to obtain reference LAIt values (Beets, 1977; J. M. Chen et al., 1997; Mason et al., 2012). Aside from the laborious nature of these tasks, J. M. Chen et al. (1997) suggested that these methods are themselves subject to some degree of error, and this will impact the reference values of LAIt obtained from destructive sampling.

The above review makes it apparent that no method of assessing LAIt or LAIe can be considered absolute. Rather, for a method to be useful, it must deliver consistent and repeatable estimates of either LAIe or LAIt. Methods which accomplish this allow relative changes in the measured value of LAI to be used in a variety of applications. Both HCP and the LAI-2000 family of instruments can be used to obtain such estimates. The implementation of scattering corrections to deal with full sun conditions is a significant advantage for the LAI-2200C which offers both improved accuracy and a greatly expanded range of suitable sampling conditions. However, the protocol is new and limited testing has been done to evaluate the accuracy of the instrument in comparison to previous models or to the new HCP techniques.

The advent of modern cameras, which can capture RAW images at very high resolutions, coupled with software advances, sophisticated post-processing techniques, and new methods for estimating LAI and clumping indexes have all increased the accuracy and ease of obtaining LAI from HCP. However, these techniques largely remain confined to diffuse sky conditions.

2.4 LAI from spectral vegetation indices

Passive sensors mounted on satellite or aerial platforms offer an alternative method for estimating LAI. The principle advantages of this remote sensing (RS) approach is the ability

to produce estimates across large areas with moderate temporal and spatial resolution. RS methods for estimating vegetation properties, including LAI, rely on the unique spectral signatures produced by the interaction of vegetation and electromagnetic radiation from the sun. Principally, the biophysical process of photosynthesis results in a characteristic spectral pattern whereby green vegetation reflects light at the near-infrared wavelength (700–1300 nm) while selectively absorbing a higher proportion of incident light in the visible red wavelengths (400–700 nm) (Peñuelas & Filella, 1998; Zheng & Moskal, 2009). The characteristics of this 'red-edge effect' are sensitive to vegetation properties but relatively insensitive to background effects from soil and atmospheric conditions (Broge & Leblanc, 2001). Vegetation Indices (VIs) exploit these characteristics to identify and measure plant and canopy properties. These indices have been used to successfully predict a wide range of vegetation parameters including canopy cover, canopy structure, absorption of photosynthetic radiation, biomass assessment, canopy height, and evapotranspiration (Liang & Li, 2012).

Chlorophyll pigments are a key driver of the red-edge effect. As a result, LAI is well correlated with spectral VIs and a range of methods have been developed for estimating LAI from satellite and airborne sensors (Broge & Leblanc, 2001; Zheng & Moskal, 2009). Zheng & Moskal (2009) highlight the normalised difference vegetation index, enhanced vegetation index, and reduced simple ratio as being well suited for use in estimate LAI.

The use of VIs to determine LAI is related to the gap fraction theory (Section 2.3.4) by the fact that LAI is assumed to be highly nonlinearly related to the observed reflectance. A measured increase in reflectance from vegetation is related to a reduction in canopy gap fraction and through gap probability theory is assumed to be related to an exponential increase in LAI. This implies that at high levels of LAI the VI response to marginal changes in gap fraction become very small, and this leads to issues of sensor saturation (Sellers, 1985; Sellers, Berry, Collatz, Field, & Hall, 1992). While some of the highlighted VI methods rely on developing statistical relationships between the index values and measured values of LAI across a narrow range, still others attempt to relate increasing reflectance directly to gap fraction and LAI (Liang & Li, 2012). LAI from VIs may be true or effective, depending on the measured value used in the model and the inclusion of correction factors. The generic term LAI is used to deal with this ambiguity in the following discussion.

2.4.1 Vegetation indices related to LAI

2.4.1.1 Normalised difference vegetation index

The normalised difference vegetation index (NDVI) is a well-established and widely used index for vegetation assessment and was originally developed to take advantage of emerging space-borne sensors to monitor and observe cropland and grass plains (Asrar, Fuchs, Kanemasu, & Hatfield, 1984; Tucker, 1979). NDVI has been shown to be useful for retrieving LAI in forested areas as well (J. M. Chen & Cihlar, 1996). An advantage of NDVI is that it only requires measurements in two spectral bands (Fang & Liang, 2008):

$$\mathrm{NDVI} = \frac{(\rho_{\mathrm{NIR}} - \rho_{\mathrm{RED}})}{(\rho_{\mathrm{NIR}} + \rho_{\mathrm{RED}})} \qquad 2.11$$

Where ρ_{NIR} (841–876 nm) and ρ_{RED} (620–670 nm) are the spectral reflectance values for the near-infra red and red wavelengths. NDVI has been used to estimate LAI with varying success. J. M. Chen & Cihlar (1996) achieved models with R^2 values ranging from 0.38 to 0.66. The varied results of this study highlighted the sensitivity of NDVI to background conditions. Both the forest canopy and background vegetation contribute to observed reflectance in the relevant wavelengths. Imagery acquired when the understory is reduced by seasonal changes or canopy closure produces NDVI values more strongly related to the measured LAI of the forest (J. M. Chen & Cihlar, 1996). The sensitivity of NDVI to scene composition can create scaling problems and in some situations a nonlinear, asymptotic relationship between forest LAI and NDVI, meaning that LAI cannot be retrieved above certain thresholds (Mu, Heinsch, Zhao, & Running, 2007; Stenberg, Rautiainen, Manninen, Voipio, & Smolander, 2004). Curran et al. (1992) demonstrated the use of NDVI to estimate and monitor LAI changes in a plantation of slash pine (*Pinus elliottii* Englem.). Regression model predicting LAI from NDVI were developed at three different dates. The impact of seasonal changes caused the relationship to vary greatly (R^2=0.35, 0.75 and 0.86). Nonetheless, the authors could make predictions with a root mean square error equal to 0.74 LAI, and the effects of fertiliser application on LAI were discernible in the data. Curran et al. (1992) attributed some of the variability in model performance to plots with rapid understory growth and hence low contrast between ground and canopy. Plots with poor contrast caused inflation in the NDVI values, leading to overestimation of canopy LAI. In less homogeneous forests, estimation of LAI from NDVI has been less successful. Stenberg et al. (2004) reviewed several studies using NDVI to estimate LAI across a range of different forest types. The review highlighted that NDVI-LAI relationships are site specific and do not translate

well to different forest types. In the same study, Stenberg et al. (2004) developed NDVI-LAI relationships for a mixed species conifer forest in Finland. The relationship using NDVI was tested against alternative VIs, namely: simple ratio and reduced simple ratio. NDVI performed poorly (R^2=0.55) compared to the reduced simple ratio (R^2=0.63). Based on these findings, Stenberg et al. (2004) concluded that NDVI-LAI estimation was site-specific and limited by poor sensitivity and suggested that the use of alternate VIs should be investigated. Another review of VIs by Song (2013) noted that NDVI sensitivity appears to vary between conifer and broadleaf forest and saturation effects appeared most evident where LAI exceeds 3~5. The specificity of NDVI-LAI relationships, combined with the strong impact of background reflectance, and spectral saturation limits, greatly limits the usefulness of NDVI in many forest types.

2.4.1.2 Enhanced vegetation index

The enhanced vegetation index (EVI) was developed in an attempt to overcome some of the limitations of NDVI and to facilitate delivery of new data products derived from the NASA MODIS space-borne sensor. EVI provides improved sensitivity to vegetation while minimising atmospheric interference and the impact of background vegetation that interfere with NDVI and related VIs (Huete et al., 2002). EVI achieves this by incorporating reflectance from the blue portion of the spectrum as:

$$\mathrm{EVI} = \mathrm{G}\left(\frac{(\rho_{NIR} - \rho_{RED})}{(\rho_{NIR} + \mathrm{C1}\ \mathrm{x}\ \rho_{RED} - \mathrm{C2}\ \mathrm{x}\ \rho_{BLUE} + \mathrm{L})}\right) \qquad 2.12$$

Where *G* is the gain factor for EVI – set at a constant of 2.5, ρ_{BLUE} is the reflectance in the blue band (459-479 nm), *C1* and *C2* are coefficients relating to corrections for aerosol influence that are applied to the red band, and *L* is an adjustment to account for band-related differences in canopy and background vegetation reflectance (Huete et al., 2002; Mu et al., 2007). Results from studies evaluating the performance of EVI have been mixed. In a validation study of MODIS NDVI and EVI products, Huete et al. (2002) concluded that the use of the non-saturated NIR band to derive EVI offered increased dynamic range in high biomass areas and EVI values were judged to offer a smoother, more defined seasonal profile when compared to other VIs. The impact of these properties on LAI prediction was not examined. In another study, substitution of EVI-based LAI estimates in place of those derived from NDVI produced a marked improvement in a global evapotranspiration model developed by Mu et al. (2007). In contrast, Soudani et al. (2006) calculated EVI-based

estimates of LAI from a range of sensor platforms and found EVI to produce results similar to other VIs - concluding that EVI did not offer any advantage.

The performance of EVI is impacted by reliance on the blue band, which suffers from interference and high signal-to-noise ratios. This frequently reduces the number of clear images available suitable for analysis (Huete et al., 2002; Zheng & Moskal, 2009). The low spatial resolution of common EVI-based products (1 km for MODIS LAI products) is of little value to plantation forest managers who require much finer resolutions. However, the MODIS products based on EVI already include a global LAI map incorporating sophisticated radiative transfer models that attempt to capture the nonlinear relationship between spectral reflectance and LAI (Yang et al., 2006). Re-implementation of products using higher resolution data sources is not practical, nor is this approach supported by evidence that improved resolution would improve the usefulness of EVI-based LAI estimates. Moreover, the requirements for blue-band information and derivation of complex parameters make EVI of little use to forest managers looking for rapid and repeatable estimates of LAI.

2.4.1.3 Other image-based approaches

While NDVI and EVI are among the most widely used VIs for vegetation and LAI assessment, several alternative approaches have been demonstrated. The reduced simple ratio (RSR) is a modification of the simple ratio (SR) (ρ_{NIR}/ρ_{RED}) introduced by Brown et al. (2000). The original SR was found to be strongly correlated with LAI, in some cases surpassing other VIs in terms of accuracy and sensitivity (J. M. Chen & Cihlar, 1996). However, the SR index curves developed are strongly dependent on background reflectance and canopy closure in the source data. Therefore, shortwave infrared reflectance (SWIR) values are introduced in order to reduce the impact of varied canopy background (Brown et al., 2000). Application of RSR methods to RS-LAI models in one study increased the R^2 from 0.55 to 0.75 (Cohen et al., 2003). In another study, the introduction of RSR techniques produced the highest correlation with field measured LAI values across a range of biomes (Yang et al., 2006). In stands of spruce and jack pine, the introduction of RSR improved LAI models by 15% and 30% respectively (Brown et al., 2000; Zheng & Moskal, 2009). Overall, RSR appears to offer some improvement on RS and NDVI, providing enhanced sensitivity to changes in LAI, with reduced impact from canopy background. Significantly, RSR has been shown to perform equally well in deciduous and coniferous forests, removing the need for complex image delineation in mixed forest scenes (Y. Wang et al., 2004; Zheng & Moskal, 2009). Nonetheless, few studies have validated the use of RSR in high LAI coniferous

forests, and the index requires specialised bands not often available from high-resolution commercial sensors.

Textural analysis of imagery for estimation of LAI has also shown promise as an alternative to VIs. These metrics examine the spatial relationship between pixels by deriving statistical measures from a grey-level co-occurrence matrix. Use of textural metrics from high-resolution satellite imagery has been found to produce improved estimates of the spatial variation in LAI than spectral-based estimates in a mixed natural forest in Florida (Pu & Cheng, 2015).

2.4.2 Summary

RS data is widely available from a range of different platforms. Progress has been made in developing a range of VIs which may be used to develop models of LAI across large areas. RS data suffers some drawbacks. Atmospheric correction and image processing can be complex, and factors such as cloud cover can limit the availability of these data. Overcoming these limitations by using multiple platforms is confounded by the impact of different sensors, which can cause large differences in index values (Soudani et al., 2006). Resolution issues remain an obstacle for accurate LAI estimation. At present, there are only a limited number of satellite sensors with pixel sizes less than a few meters. Indeed, sensors on common platforms such as MODIS and Landsat have pixel sizes of 1 km and 30 m respectively, at this scale a single pixel may represent multiple trees or differing surface types. Perhaps the greatest limitation in using RS to derive LAI is signal saturation in areas of dense foliage due to the nonlinear relationship between gap fraction, estimated by changes in aggregate canopy reflectance, and LAI. While MODIS EVI products go some way to overcoming this using radiative transfer models, the low resolution (1 km) of these products is restrictive (Song, 2013). Furthermore, few studies have demonstrated reliable, accurate LAI estimation for coniferous forests using VIs or textural metrics. Instead, researchers have increasingly turned to active RS technologies that offer improved ability to estimate gap fraction, LAI, and other canopy properties across a range of forest types with few of the limitations associated with passive optical sensors.

2.5 LAI estimation from lidar

All the methods for LAI measurement discussed so far rely on passive optical sensors to measure gap fraction and estimate LAI, usually via inversion of the Poisson model (Section

2.3.4). Measurements of gap fraction can also be achieved using active methods such as light detection and ranging (lidar). Lidar scanners may use either pulse or waveform energy from laser light to range targets using time-of-flight, and, frequently, record some measure of the energy returned. The accuracy of timing in modern systems allows the distance to a reflecting object to be calculated with a high level of precision (Zheng & Moskal, 2009). Lidar systems have the advantage of capturing three-dimensional information while being less sensitive to atmospheric interference, spectral saturation, and resolution issues than passive sensor technologies (Harding & Carabajal, 2005; Zheng & Moskal, 2009). Lidar scanning of forests may be conducted with terrestrial lidar scanners from below the canopy (Danson, Hetherington, Morsdorf, Koetz, & Allgower, 2007), from aircraft-mounted sensors (Lefsky et al., 1999), or even from space-borne platforms such as the GLAS instrument carried aboard the ICESat satellite (Harding & Carabajal, 2005). Lidar sensors may be broadly divided into waveform and pulsed systems. Waveform lidar sensors record a near-complete record of the returned energy from the emitted laser beam, allowing detailed information about the reflecting surface(s), such as the various elements in forest canopies, to be extracted. Waveform sensors have the advantage of very fine range resolution between reflecting targets and the interaction between light and canopy elements in the path of the beam can reveal detailed information on the structural arrangement and properties of the canopy (Anderson, Hancock, Disney, & Gaston, 2016; Armston et al., 2013). These advantages come at a significant cost in terms of the data volume produced by the sensor and the complexity of the processing required to extract meaningful information about canopy architecture from changes in reflected energy (Anderson et al., 2016). In contrast, discrete lidar sensors offer a simpler means of ranging canopy elements by emitting discrete pulses of laser light and recording the time-of-flight for pulses reflected by canopy elements. Scanners range from units that record only a single return per emitted pulse to those with the capability to range up to 5 or more discrete returns from a single pulse. Discrete systems have the disadvantage that signal digitisation limits often introduce a minimum distance below which subsequent returns cannot be discerned. This reduces the information content but simplifies the processing and data volume issues encountered with waveform lidar (Anderson et al., 2016; Wulder et al., 2012).

The ability of lidar to range reflected returns from the canopy, penetrate through gaps in the canopy, and, in the case of airborne lidar, to retrieve information about the underlying terrain has been very valuable for the study and management of forest ecosystems with

applications ranging from measurement of canopy height, canopy cover, forest biomass, wood volume, stem density, species classification, and many other applications (Coops et al., 2007; Leeuwen & Nieuwenhuis, 2010; Magnussen & Boudewyn, 1998; Økland & Næsset, 2002). In New Zealand's *P. radiata* plantation forests, lidar data has been used to estimate forest yield information (Dash et al., 2015), perform individual tree counting (Pont, Kimberley, Brownlie, Sabatia, & Watt, 2015), develop national models of stand volume (P. J. Watt & Watt, 2013), and to develop predictive models for Site Index (M. S. Watt, Dash, Bhandari, & Watt, 2015). In the context of New Zealand, the technology is widely valued by the forest industry and has seen increasing usage for a range of management operations (Morgenroth & Visser, 2013).

The application of these different sensor types and platforms for retrieval of LAI is discussed in the following sections. Throughout the remainder of this thesis, the term airborne laser scanning (ALS) is used to refer to discrete lidar captured from airborne scanners.

2.5.1 Terrestrial lidar and LAI

Terrestrial laser scanning lidar (TLS) has been widely used to assess forest canopy LAI using both waveform and discrete sensors (Jupp et al., 2009; Zheng & Moskal, 2012). One early approach relied on the use of an elementary non-scanning terrestrial laser rangefinder to estimate the vertical distribution of foliage by recording the heights to the lowest intercepting canopy elements above numerous sampling locations within forest plots (Radtke & Bolstad, 2001). The height profiles from the rangefinder data were used to estimate LAI based on an adaptation of the point quadrat method for estimating LAI from the number of foliage contacts observed when a probe is inserted through the canopy (Jonckheere et al., 2004; Wilson, 1959). Although the results showed no significant correlation with LAI measured from litter traps, this approach presents an alternative to the more common approaches to measuring gap fraction using active, scanning lidar instruments.

Scanning TLS sensors allow measurements over nearly the entire hemisphere to record both the angular direction and time of emission for discrete pulses or waveforms (Zheng & Moskal, 2009). Emitted energy that does not generate a return may be interpreted as either a gap or, in the case of discrete sensors, a region of the canopy with reflectance below the pulse triggering energy threshold of the sensor (Danson et al., 2007), while canopy areas that generate a return can be accurately located and ranged. Gap probability may then be applied to these 3-dimensional scans to infer LAI. One approach infers gap fraction by comparing the

number of expected pulses based on the scanner's configuration to the actual number of returned pulses from discrete lidar. This method has been used to construct two-dimensional (2-D) projections of the three-dimensional (3-D) point cloud to generate hemispherical scenes of canopy gap fraction similar to those collected by HCP, with results showing strong agreement with gap fraction estimated from actual hemispherical photographs (Danson et al., 2007). Larger studies have confirmed the viability of the 2-D approach, with TLS reconstructions explaining 89% of the variation in LAI from hemispherical photos (Zheng, Moskal, & Kim, 2013). A single hemispherical scan behaves as a point source of light rather than parallel beams of radiation as with solar radiation and can suffer from occlusion; furthermore, limited scanner range can lead to incomplete coverage (Danson et al., 2007; Zheng & Moskal, 2009). Scanning of the canopy in layers from several different locations is often adopted to avoid occlusion and achieve even coverage and has been shown to significantly improve representation of the canopy after co-registration of the scans (Hosoi & Omasa, 2006, 2007; Zheng et al., 2013). Projection of TLS point clouds to 2-D images discards considerable information about canopy structure. To reduce this information loss, voxelization of co-registered point clouds has been proposed as an alternative approach to extract gap fraction and LAI as well as to obtain properties unavailable from simple 2-D projections such as leaf area density profiles and clumping index (Hosoi & Omasa, 2006, 2007; Huang & Pretzsch, 2010; Li et al., 2016). In the voxelization approach, the point cloud is divided into 3-D pixels (voxels) and these form the basis for identifying canopy elements and gaps based on the distribution or absence of points within these voxels. Slicing of the point cloud voxels into layers allows the foliage density to be estimated accurately based on the interceptions (points) recorded through the slices (Hosoi & Omasa, 2006, 2007; Zheng & Moskal, 2012). Gap fraction can be identified from the profile of empty voxels within the canopy layers. This process is computationally intensive and means that the minimum gap size detectable is a function of the voxel dimensions used. Theoretically, smaller voxels would allow smaller gaps to be resolved as empty pixels, lowering the implied LAI (Li et al., 2016). TLS is also useful for retrieving LAI from individual trees (Moorthy, Miller, Hu, Chen, & Li, 2008) both in isolation and in stands (Huang & Pretzsch, 2010). Validation of the single tree LAI methods using carefully measured individual trees showed strong agreement (R^2 = 0.98, RMSE = 0.26) (Moorthy et al., 2008). Sophisticated computational geometry tools have also been developed to allow retrieval of LAD from voxelized point clouds taken of mature isolated trees. (Béland, Widlowski, & Fournier, 2014). These methods have been

validated using data collected in the leaf-off season, with results showing that this approach was also sensitive to voxel size and occlusion effects (Béland, Baldocchi, Widlowski, Fournier, & Verstraete, 2014).

Methods to retrieve the ratio of woody to photosynthetic elements using TLS have also been demonstrated (Zheng & Moskal, 2012), offering the potential to isolate true LAI - a task that is still not easily achieved using other methods (Woodgate et al., 2016). The voxelization approach has also been shown to allow extraction of extinction coefficient (*K*, Section 2.3.4) (Zheng & Moskal, 2012). In this approach, the projected area is computed using a method defined by the number of points in a voxel. For voxels with a larger number or returns, the ratio of the area of 2-D to 3-D convex hulls fitted to the points was used to estimate the projection coefficient (*G*) of the 'shape' within the voxels. The estimated *G* function value was then related to *K* using an approach similar to that outlined in Section 2.3.4, where the *G* function of the voxels in a layer normal to a chosen angle was used to determine the extinction coefficient for incoming light.

In summary, discrete return TLS has shown strong promise as a tool for retrieving LAI along with other canopy properties that are not easily recovered from traditional methods such as 3-D structural information, single tree LAI, and separation of woody material from photosynthetic elements. However, shadowing of elements necessitates multiple scans and retrieval of gap fraction from point cloud data often requires the use of voxelization to identify canopy gaps, and this process impacts the minimum size of gaps that can be detected. TLS methods are evolving and current limitations should be viewed in the context of the limitations of other indirect LAI methods such as hemispherical photography where the selection of a threshold to separate sky and canopy pixels (Section 2.3.5.2) has been shown to have a greater impact on measured gap fraction (and hence LAI) than errors arising from the properties and processing of discrete TLS (Hancock, Lewis, Foster, Disney, & Muller, 2012). Persistent limitation of discrete TLS that are likely to remain challenging relate instead to the fact that discrete return data by its nature provides only an incomplete survey of canopy structure and cannot easily range multiple targets within the canopy. It is for these reasons that waveform lidar has been proposed as an alternative technology that may produce superior estimates of gap fraction and LAI (Anderson et al., 2016).

2.5.2 Waveform terrestrial lidar

Waveform lidar measures and records the interaction between canopy elements and a near continuous beam of laser light as the scanner surveys the canopy. The distance to canopy

elements is determined by recording phase shifts in the returned energy. Where attenuation is incomplete, the system can range multiple successive targets accurately without the 'dead time' that impacts pulse-based discrete TLS, potentially providing precise and detailed descriptions of the entire canopy profile (Anderson et al., 2016; Hilker et al., 2010). A range of waveform instruments adapted from the surveying industry has been used to collect waveform data for use in various forestry research applications (Dassot, Constant, & Fournier, 2011). For retrieval of gap fraction and LAI, the experimental Echidna® class of instruments are among the most important and widely used full waveform TLS systems (Dassot et al., 2011; Douglas et al., 2012; Jupp et al., 2009). The Echidna system and the prototype Echidna Validation Instrument (EVI) were both developed by the Australian Commonwealth Scientific and Industrial Research Organisation (CSIRO). Echidna scans the entire upper hemisphere to near 130° zenith and 180° azimuth range using a 1064 nm continuous laser light source, providing full-waveform data with a high signal to noise ratio for the entire scan region (Jupp et al., 2009). Unlike discrete TLS, gap fraction can be directly estimated from Echidna data without the need for estimating the outgoing number of returns or voxelization of recorded points. This is achieved by transforming the energy reflected by canopy elements to an apparent reflectance value using a model of the returned power expected from a large diffuse target at a similar range. In this way, the Echidna measures gap probability across the entire hemisphere, with most studies then proceeding to extract LAI at either 1 radian or by integrating gap fraction across a range of zenith angles to minimise the impact of unknown LAD (see Section 2.3.4) (Jupp et al., 2009; F. Zhao et al., 2011, 2012). The fine-scale (7.5 cm between peaks) 3-D data on gap probability captured by Echidna allows gap sizes to be analysed to distinguish gaps within canopies from those between canopies – allowing the element clumping index to be calculated using the same approach employed for analysis of hemispherical images (J. M. Chen et al., 1997; F. Zhao et al., 2012). Because Echidna uses waveform data, the gap fraction and clumping index can be retrieved out to the maximum range of the instrument which is partially dependent on the density of the canopy. A second-generation device, the Dual Wavelength Echidna Lidar (DWEL) is under development. DWEL adds a second laser light source at 1548 nm which shows increased absorption by foliage due to the higher water content of leaves and allows foliage elements to be separated from woody elements in the canopy (Douglas et al., 2012). A similar system, Salford Advanced Laser Canopy Analyser (SALCA) has also recently been developed and

preliminary results have highlighted the significant challenges that must be overcome to ensure accurate system design to co-register the data from two beams (Danson et al., 2014).

In summary, both discrete and waveform TLS scanners have been validated as tools for measuring gap fraction, LAI and, in some studies, extinction coefficient and separation of woody and photosynthetic elements. Data processing is much more complex than other instruments for measuring LAI, especially in the case of waveform TLS. However, these evolving methods may offer improvements in accuracy, measurement of isolated or individual trees, and no special requirements for sky conditions during measurement. Despite these advantages, TLS is only practical for surveying small area of forest and large-scale assessment of LAI depends on airborne sensors to survey large areas.

2.5.3 Waveform satellite lidar

Waveform sensors carried by aircraft and satellites have been widely used to study forests, including retrieval of gap fraction and LAI (Tang et al., 2014). The operation of these instruments is similar to waveform TLS scanners in that a nearly-complete waveform is captured instead of a series of discrete returns, but in this case, the instruments view the canopy from above and the waveform represents the impact of the vertical vegetation profile to the ground (Armston et al., 2013). The Geoscience Laser Altimeter System (GLAS) on the NASA Ice, Cloud and land Elevation Satellite (ICESat) has captured millions of waveforms covering a significant portion of the earth's surface, including many forested areas (Schutz, Zwally, Shuman, Hancock, & DiMarzio, 2005; X. Wang et al., 2011). The laser system onboard emits infrared radiation to capture surface elevation. Where the waveform is captured over forested areas, the peaks and attenuation of the signal can be used to retrieve structural attributes such as canopy height (Popescu, Zhao, Neuenschwander, & Lin, 2011; Xing, de Gier, Zhang, & Wang, 2010). A common method for retrieving LAI from GLAS data reverses the common gap penetration probability theory, reasoning that because laser energy can only penetrate to the ground through gaps the energy returned from the vertical canopy profile is the opposite of gap probability i.e. represents the reflectance of all plant elements once ground reflectance is isolated (Tang et al., 2012). The cumulative laser energy returned for a known ratio of ground and canopy reflectance is then used to calculate the canopy closure implied by the observed laser profile. Once the implied gap fraction is computed and assumptions are made regarding the LAD (a spherical distribution is commonly assumed) then LAI can be retrieved from GLAS data, potentially over very large areas (Tang et al., 2012, 2014). LAI and other parameters estimated from GLAS data require

complex pre-processing steps to decompose the waveform and accurately separate ground and canopy energy. Manipulation of these waveforms is complex and the data are prone to interference from atmospheric effects, complex terrain, and highly heterogeneous vegetation (Tang et al., 2014). At 70 m, the footprint (the ground area covered by the beam) and hence approximate resolution of GLAS waveforms is relatively coarse in comparison to other data sources for estimating LAI such as Landsat imagery (30 m resolution); however, GLAS has the advantage of not showing saturation in areas of high LAI such as dense forests (Tang et al., 2012). Planned space-based waveform laser sensors such as the Global Ecosystems Dynamics Investigation Lidar (GEDI) will provide significantly increased coverage at a much finer spatial resolution (25 m) and unlike ICESAT/ GLAS the GEDI instrument is specifically targeted towards the study of terrestrial biomes such as forests (Dubayah et al., 2014) and may offer new means to estimate LAI over large areas using similar methods based on canopy closure. Others have argued that a reduction in footprint size for future space-borne waveform lidar sensors such as GLAS may offer the only practical and cost-effective means of obtaining LAI estimates for major terrestrial biomes where traditional spectral methods fail due to saturation (Lefsky et al., 1999; Lefsky, Cohen, Parker, & Harding, 2002; Rosette et al., 2013).

2.5.4 Waveform airborne lidar

Early investigations into forestry applications of airborne waveform lidar such as that done by Lefsky et al. (1999) explored the potential for the three-dimensional profile captured by waveform sensors as a means of estimating canopy structure and LAI in high biomass forests, where existing RS techniques largely fail. To test this theory, they attempted to extract LAI and other canopy measurements for a Douglas-fir/western hemlock (*Pseudotsuga menziesii* (Mirb.) */Tsuga heterophylla* (Raf.)) forest using full-waveform lidar data from NASA's airborne SLICER sensor. The sensor supplements lidar waveform data with positional data from aircraft flight systems, thereby allowing precise geo-referencing of the reflected energy profile with ground plot information (Lefsky et al., 1999). To obtain estimates of LAI the authors first divided the surveyed area into a matrix of cells with a diameter equal to the lidar beam footprint of 10 m, with a vertical profile based on the classification of each complete wavelength (each 1 m high). Key metrics from these canopy volume measurements were used in a stepwise regression to develop a model for LAI as determined from allometric relationships with sapwood cross-sectional area. The model performed well (adjusted R^2=0.75), and three of the derived canopy volume metrics were

included in the final model. Notably, this volume by height approach could detect the shifting pattern of vertical LAI distribution between old-growth and young forests (see Section 2.2.2 for a description of this process). This early approach suffered from several drawbacks. Firstly, the LAI values used to develop the model were derived from allometric models between sapwood and leaf biomass, which were in turn derived from models of sapwood and DBH. As discussed in Section 2.3.3, this approach frequently under-predicts LAI and the relationships vary between stands. In addition, the approach was not able to link gap probability theory with measures of LAI and so would require re-calibration for new sensors or forest types. Nonetheless, the work was pioneering and demonstrated the utility of waveform lidar for forest studies. Subsequent efforts have sought to build on the use of airborne waveform sensors. For example, measurements from the Laser Vegetation Imaging Sensor (LVIS) airborne waveform scanner have shown moderate agreement (R^2=0.63) with LAI measurements obtained from destructive sampling (Tang et al., 2012). Other studies have used LVIS data to retrieve LAI using an approach based on estimating canopy closure (as the opposite of gap fraction) from waveform energy profiles that would later be adapted to underpin the GLAS-based LAI retrieval methods described above (Tang et al., 2012, 2014). As with many full-waveform platforms, the footprint size was quite large (10 m) and this has the effect of lowering the effective resolution of the platform and increasing the potential for non-canopy elements to be included in waveform data.

Until recently, even airborne waveform lidar has largely been confined to research applications and has been characterised by large footprint size and limited choice of sensors (Richardson, Moskal, & Kim, 2009; Wulder et al., 2012). Recent developments in technology have seen small-footprint waveform lidar sensors become more widely available for use in forestry. These sensors perform in a similar way to other waveform systems by digitising the full signal returned from canopy and ground elements; however, the beam divergence is reduced, reducing the footprint area. Gap probability has been successfully retrieved from small-footprint waveform sensors using an approach similar to that employed for large-footprint waveform sensors (Armston et al., 2013). In this approach, the waveform was decomposed to separate canopy and ground energy and calibrate the waveform data to a model of reflectance. Once this was achieved the ratio of apparent energy reflected from vegetation and ground elements was used to compute gap fraction as the opposite of canopy closure. Small-footprint estimates of gap fraction using this approach were within 5% of ground truth estimates (Armston et al., 2013). Furthermore, this approach applied to small-

footprint waveform data appears to be relatively insensitive to aircraft altitude and may be broadly applicable without the need for re-calibration for use with new sensors or forest types (Armston et al., 2013; X. T. Chen et al., 2014). If these results are confirmed to be broadly applicable, the lack of a need for local calibration will offer significant advantages over discrete lidar based methods (Section 2.5.5). However, waveform processing benefits from access to raw data, which is not always available. Moreover, discrete lidar sensors have advanced rapidly in technological capabilities and their general utility for a range of forestry-related applications has seen them eclipse waveform sensors in terms of cost, availability, range of processing tools, and development of methods (Anderson et al., 2016; Armston et al., 2013; X. T. Chen et al., 2014; Wulder et al., 2012)

2.5.5 Discrete lidar sensors and methods

The rapid advances in discrete lidar sensor technology have seen increases in the pulse frequency, reduced dead time, increased precision, and lower costs for acquisition and for these reasons discrete lidar has superseded waveform lidar in many commercial and research applications (Armston et al., 2013; Coops et al., 2007; Wulder et al., 2012). The availability of discrete lidar data has led many researchers to investigate using these data to estimate forest LAI. A proliferation of methods and approaches has resulted from these efforts. To understand these approaches, it is worth reviewing the technical characteristics of these discrete lidar platforms.

Discrete lidar systems of the type used in forestry are based on a sensor package that records the interval between emission and return of discrete light pulses. Where a pulse is only partially absorbed by complex features such as vegetation, several returns may be reflected towards the sensor. Early sensors discarded this information, recording only the first or last return but modern variants frequently record many returns per pulse, with the number of possible returns depending largely on the intensity threshold for triggering a return by the receiver, the initial pulse power, and the height and complexity of the vegetation (Lim, Treitz, Wulder, St-Onge, & Flood, 2003; Wulder et al., 2012). The elapsed time between pulse generation and return allows the range to be accurately calculated for each return. Lidar sensor packages are frequently mounted on board light aircraft, helicopters or even unmanned aerial systems to conduct airborne laser scanning surveys (ALS). Information streams from high-precision GPS receivers and the aircraft's inertial measurement unit (IMU) (which records pitch, roll, and yaw) are combined with the lidar data using precise time referencing. In this way, recorded laser returns are converted into accurately geo-referenced 3-D

representations of the scanned surface in the form of a point cloud (Wulder et al., 2012). The technical details behind the integration of these data streams to produce these point clouds are beyond the scope of this review, detailed explanations can instead be found in Wehr & Lohr (1999) and Baltsavias (1999).

The popularity of discrete lidar systems has led to a proliferation of commercial sensor packages for conducting ALS. The characteristics and configurations of these packages can vary greatly, and these differences can significantly alter the results obtained from lidar data (Rombouts, Ferguson, & Leech, 2010). Wulder et al. (2012) highlight some of the most important campaign and sensor characteristics which are known to impact lidar-derived products and these are summarised below:

- ***Maximum number of returns per pulse***: The ability to record multiple returns is particularly useful in forestry settings, where small gaps in the canopy allow some pulses to penetrate deeper into the canopy or to the ground. These additional returns can aid in the identification of the ground surface elevation and characterisation of the gap fraction of the canopy. Multiple return ALS units typically record between 3-8 returns per pulse. However, the number of returns possible is dependent on the emitted energy and the intensity threshold used to classify a return (Lim et al., 2003; McGaughey, Andersen, & Reutebuch, 2006).

- ***Footprint size*****:** Lidar pulses strike the ground as circular beams, diverging from the point laser source to the reflecting surface. The divergence is measured in milliradians (1 mrad = 1/1000 of a radian). The size of the lidar beam at reflectance is referred to as the footprint size. Sensor footprint depends on a combination of divergence and distance to the target. For example, a sensor footprint may be expressed as 0.25 m increase in diameter per 1000 m of altitude, which would indicate a divergence of 0.25 mrad (Leeuwen & Nieuwenhuis, 2010; Wulder et al., 2012). Lim et al. (2003) identify typical values for discrete lidar footprints of between 0.2–0.9 m, whereas full waveform sensors may be anywhere up to 70 m.

- ***Swath width, scan angle, and scan frequency*****:** ALS systems utilise oscillating or rotating mirrors to distribute pulses across a range of angles perpendicular to the flight path. The angle of the pulse from the nadir direction is termed the scan angle. The combination of maximum scan angle, beam divergence, and flight altitude determine the cross-track width on the ground covered by a complete oscillation, this is the

swath width in meters. In topographic applications, high scan angles are well tolerated; however, in forestry applications, a high scan angle implies an increased chance of hitting canopy elements before striking the ground. Simulations have demonstrated that high scan angles can adversely impact lidar estimates of canopy properties (Disney et al., 2010; Holmgren, Nilsson, & Olsson, 2003). A maximum scan angle of between 10–15° is recommended for forestry applications (McGaughey et al., 2006; Wulder et al., 2012). Aircraft platforms must maintain a minimum speed during surveys, as such the scan frequency (number of oscillations per second in Hz) becomes an important factor, with higher values producing desirable increases in pulse density on the ground.

- ***Pulse frequency and sample rate*:** Pulse frequency (Hz) refers to the number of pulses emitted per second and is an important factor in determining the final number of pulses per unit area on the ground. Higher frequencies allow for greater sampling coverage from higher altitudes. However, higher frequency sensors generally deliver lower powered pulses, resulting in less canopy penetration and reduced ability to generate clear ground returns (Chasmer, Hopkinson, Smith, & Treitz, 2006). The utility of higher pulse frequencies is further reduced by limitations on the maximum number of return pulses that a sensor can record per second. This sample rate determines the minimum distance that can be measured between multiple returns of the same pulse. Although the delay in processing a return signal may be only fractions of a second, this may translate into a significant 'dead-time' of several meters (Chasmer et al., 2006). In forestry settings, this dead time may lead to misclassification of intermediate returns as ground returns or to ground returns that are not captured during the dead time (K. Zhao & Popescu, 2009).

2.5.6 Lidar campaigns for forestry

The summary of key lidar variables represents only a handful of sensor and survey variables which must be decided on. The complex interactions between variables present a challenge to those seeking lidar data for forestry applications. While the field is still evolving, and many topics still require further research, a set of general best practices for gathering useful lidar data has emerged (Wulder et al., 2012).

Many of these recommendations and guidelines highlight the importance of obtaining a target final pulse density (Jakubowski, Guo, & Kelly, 2013; McGaughey et al., 2006). This

variable represents the average footprint count per unit area (pls/m^2) and should not be confused with return density (which accounts for multiple returns per pulse). In effect, the pulse density is a measure of lidar spatial resolution and is frequently used as a measurement to compare different data sets (Gatziolis & Andersen, 2008).

As a result of early experiments in pulse density for terrain mapping, an assumption developed that increasing pulse density would facilitate increasingly accurate estimates of forest parameters (Jakubowski et al., 2013; Lovell, Jupp, Culvenor, & Coops, 2003). However, in many forestry applications, this relationship has not always held true, and a more nuanced relationship between resolution and accuracy has emerged. Yu et al. (2004) demonstrated that varying both footprint size and pulse density had relatively little impact on estimates of stocking and tree height. A more thorough treatment of the effects of pulse density by Jakubowski et al. (2013) determined that metrics including tree height, basal area, DBH, and understory height remained relatively accurate at pulse densities as low as 1 pls/m^2. Findings from the same research showed a divergence in the benefits of higher pulse density depending on the nature of the metric. Cover based metrics such as tree density, canopy cover, and shrub cover benefitted significantly from higher pulse densities. Height and DBH related estimates showed an asymptotic relationship with pulse density, whereby additional pulses beyond 1 pls/m^2 resulted in minimal accuracy improvements. In another study, Rombouts et al. (2010) were able to increase altitude and reduce point density by a factor of 10 and still produce consistent estimates of predicted timber volume. These requirements are in contrast to variables such as individual tree delineation, which generally requires a minimum of 4 pls/m^2, while also requiring scan angles below 12–14° to avoid increased multi-path error (Gatziolis & Andersen, 2008).

This has important implications for efforts to produce estimates of LAI and other novel variables from lidar data. A strong relationship exists between acquisition costs, pulse density, and total area covered (Jakubowski et al., 2013). As such, any increase in point density required to estimate new variables will increase the cost of data acquisition, and this cost must be weighed against the value of these new variables. The optimal lidar parameters (including pulse density) required to achieve accurate estimates of LAI are complicated by the variety of algorithms and ground sampling techniques used to obtain estimates to date (Morsdorf, Frey, Meier, Itten, & Allgöwer, 2008). An examination of the topic by Morsdorf et al. (2008) found that reduced point density from 10 pls/m^2 to around 5 pls/m^2 due to increased flight altitude caused LAI to be overestimated by around 0.2. The authors theorise

that this change can be attributed to increased footprint size rather than changes in pulse density.

The uncertainty around optimal pulse density for LAI estimation creates additional uncertainty when translating methods developed in other settings and forest types. In the context of this study, the acquisition will be dictated by the needs of the commercial forestry operator. Lidar data acquisition costs are cited as a major obstacle for New Zealand forest management companies (Morgenroth & Visser, 2013) and current campaigns are strongly focused on obtaining a specific level of accuracy for the lowest cost.

2.6 Overview of approaches for ALS-LAI estimation

Despite the complexity of discrete lidar campaigns, the range of forestry applications for this technology continues to increase. The pioneering work by Lefsky et al. (1999) demonstrating the potential of full waveform lidar to overcome saturation issues has led to several efforts to obtain LAI estimates using discrete lidar sensors. Topographical applications for discrete lidar led to the rapid advancement of the sensor technology, greatly helping these efforts (Lefsky et al., 2002). Riaño et al. (2004) combined a topographic discrete lidar system with newly available high precision ground GPS receivers to accurately overfly test plots in oak and pine forests. Ground estimates of LAI were derived from hemispherical photographs taken along transects within the plots. The authors processed the lidar data to calculate descriptive statistics including variables such as percentile heights representing the height above the ground below which a given percentage of returns falls. In addition to this, the percentage of canopy returns was calculated, this was motivated by previous success using similar metrics to estimate fractional leaf area above a given height (Magnussen & Boudewyn, 1998). Riaño et al. (2004) found percentage canopy hits to be strongly correlated with LAI for both forest types. Another key finding from this study related to the impact of plot radius. By aggregating ground samples outwards from the plot centre, the authors determined that plot sizes of between 7.5-12.5m radii were optimal for estimating LAI. This study demonstrated that even simple metrics from first and last return data can be useful for estimating complex attributes such as LAI. Indeed, the authors were able to generate low-resolution maps of LAI for large areas, validating the long theorised utility of lidar data for this purpose (Lefsky et al., 1999, 2002). One criticism of this approach is that it relies on empirical relationships, implying that for each new area or species new

relationships between ground sampling and lidar metrics must be re-developed (Roberts et al., 2005).

2.6.1 Linking theory to lidar metrics

Several studies have addressed the use of discrete lidar to estimate LAI in different forest types. To adapt these methods for use in New Zealand's *P. radiata* forests a comprehensive review of the literature was required. This process highlighted several key questions that have remained unanswered in the context of New Zealand and in the field of ALS-LAI estimation more generally. The review identified two major approaches for estimating LAI from lidar in the literature. The first approach attempts to link lidar to gap probability theory by using ratio-based metrics as a proxy for measuring canopy gaps and relate these metrics to LAI through the Poisson model using the methods outlined in Section 2.3.4. The second major approach attempts to develop empirical links between LAI and various lidar metrics without direct links to gap probability theory. In the theory based approach, several different metrics have been proposed as proxies for gap fraction, while in the empirical approach it was apparent that a very large number of metrics have been linked to LAI in the literature, including recent work using complex voxelized metrics. Furthermore, both theoretical and empirical approaches appeared to be sensitive to choices such as the selection of lidar plot radius from which to extract and link metrics to LAI and the height threshold to be used when computing ratio-based metrics as a proxy for canopy gap fraction. A dedicated software tool had to be developed to address these issues in sufficient detail to achieve the thesis objectives. The results from the literature review surveying lidar-LAI metrics accompanies the description of the software tools and ALS-LAI methodology presented in Chapter 4. To avoid duplication, this section of the literature review focusses instead on providing a broader introduction to the main approaches and results that have made ALS-LAI estimation an appealing approach and to identify and frame the key questions addressed in Chapter 4.

Early approaches to estimating LAI from lidar followed a similar methodology used to estimate other forest variables. In short, this approach uses field measurements of LAI and a range of standard descriptive lidar metrics, such as percentile heights and descriptive statistics, from the point cloud coincident with field plots to develop empirical models of LAI (e.g. Riaño et al., 2004). While effective, many researchers have reasoned that empirical approaches are strongly limited by site specificity and the need to calibrate models and have instead pursued the development of physically based approaches. In an attempt to directly link lidar measurements and LAI, Roberts et al. (2005) conducted a study to evaluate a new

approach to estimating LAI from canopy attributes. In their study, lidar was utilised to estimate stem and crown dimensions of individual trees in a *P. taeda* trial site. Destructive sampling of a limited number of trees was used to develop a model of LAI from stem and crown dimensions and this relationship was applied to the lidar estimates of the same crown properties. The results were mixed, with crown dimensions proving difficult to extract in some stands. However, in certain evenly spaced stands estimates of LAI were within 0.1 of measured LAI. Overall, the approach did not provide a means of estimating individual tree LAI without again resorting to empirical relationships between lidar metrics and LAI measurements.

Morsdorf et al. (2006) also attempted to address the issues of relying on empirical predictive variables by instead developing and evaluating physically meaningful predictors. To achieve this, Morsdorf et al. (2006) relied on a simplified contact frequency equation. The contact frequency is the opposite of the gap probability (Section 2.3.4) and the approach of Morsdorf et al. (2006) adapted this to relate LAI to the probability that a leaf element lies in the path of a lidar beam penetrating the canopy at given zenith and azimuth angles. Contact frequency using needle probes inserted through the canopy has been validated as a means of measuring LAI and it has the advantage of being independent of assumptions relating to leaf distribution, shape, and size (Weiss et al., 2004). Using this approach, Morsdorf et al. (2006) derived an equation to estimate LAI from lidar as:

$$LAI = \frac{\sum FE}{\sum LE + SE} \qquad 2.13$$

Where *FE* is the first return, *LE* is the last return, and *SE* represents a pulse with a single return. These metrics were limited to canopy elements by applying a height threshold of 1.25 m to exclude understory and ground returns. The lidar data contained only first and last pulses acquired over a pine dominated forest in Switzerland. Ground measurement of LAI was accomplished using HCP images processed using the GLA software package. The results from a regression analysis demonstrated moderate agreement (R^2=0.69) between the novel lidar LAI metrics and HCP estimates. The result was strongly dependent on the choice of plot diameter from which lidar data were extracted, with a 15-m diameter proving to be optimal. This study highlighted important issues for ALS-LAI estimation also identified by Riaño et al. (2004). In particular, the question of selecting an appropriate plot size when the view distance of the instrumentation (in this case a hemispherical camera) are unclear. In addition, the further observation was made that viewing geometry of the camera at higher zenith angles

(i.e. close to the horizon) was well above typical lidar scan angles, resulting in different regions of the canopy being sampled by the respective sensors. While Morsdorf et al. (2006) provided insight into new metrics with a theoretical link to LAI, they were not able to completely eliminate the need for site and sensor specific corrections and the optimum radius (fixed at ~ 15 m) differed from that observed by Riaño et al. (2004) (7.5–12.5 m or approximately one-times canopy height in the plot).

The difficulty in formulating direct theoretical links between LAI and lidar data has led to a proliferation of alternate methods for linking LAI and lidar. Griffin, Popescu, & Zhao (2008) approached the problem by using discrete lidar based data to identify the percentage cover and to divide the canopy profile into 'height bins'. Regression analysis showed that the height bins alone produced estimates close to HCP measurements of LAI (R^2=0.78). Indeed, in this study, the lidar-only models outperformed similar models using NDVI estimates for the same region. The strength of this result is also remarkable for the fact that the study area included a mix of plantation forest and natural forest containing a broad range of species.

Another approach developed by Hopkinson & Chasmer (2007a) reasoned that gap fraction theory could be utilised in combination with lidar data to estimate LAI by application of the Beer-Lambert law (see Section 2.3.4). Their approach to estimating gap fraction relied on the use of discrete lidar scanners capable of recording intensity information from each lidar return. Using this information, they could reconstruct a profile of the vertical pulse power. Gap fraction measurements were acquired using HCP techniques at ground locations within a mixed-species temperate forest. The results showed that the measured gap fraction was strongly correlated (R^2=0.92) with lidar power distribution ratio metrics calculated from the reconstructed pulse intensity data. Hopkinson & Chasmer (2007a) concluded that lidar data alone may be suitable for estimating canopy transmissivity without the need for ground calibration. However, this assertion must be tempered with the observation that, where available, intensity data from discrete sensors is not usually standardised or calibrated (K. Zhao & Popescu, 2009), and campaign differences have the potential to impact methods based on intensity derived metrics. The technique developed by Hopkinson & Chasmer (2007a) for estimating LAI and other forest properties have been refined and replicated in at least one other mixed species forest (Morrison, Hopkinson, Chasmer, & Kljun, 2011). However, other attempts to replicate the use of intensity based metrics to retrieve gap fraction were less successful (K. Zhao & Popescu, 2009). In addition, a comprehensive evaluation of radiometric properties of intensity data from discrete lidar by Kaasalainen et al. (2011)

demonstrated that large variability exists between sensors. The study concluded that calibration between differing flights and instruments is essential before intensity data can be reliably compared. Although conceptually appealing, the use of intensity based metrics is not yet well validated for LAI estimation. Furthermore, comparisons between intensity metrics and other classes of metrics that do not require calibration are lacking.

One promising, physically-linked approach for estimating LAI from lidar has been the proposed use of a proxy for pulse penetration (*P*) that can be linked to light penetration through the Beer-Lambert law (Solberg et al., 2009). The penetration proxy is computed as:

$$P = \frac{N_{go} + 0.5\left(N_{gF} + N_{gL}\right)}{N_o + 0.5(N_F + N_L)} \quad 2.14$$

Where N_{go} and N_o respectively denote the count of pulses with only one return below a height threshold and in total. N_{gF} and N_F are, respectively, the counts of first returns from pulses with multiple echoes below a height threshold and in total. While N_{gL} and N_L give the count of last returns from multiple echo pulses below a height threshold and the total number of last returns, respectively. This equation has the benefit of providing a lidar metric that quantifies the amount of penetration through the canopy while accounting for differences in total pulse density per unit area, essentially providing a measure of canopy gap probability from the lidar data. The weighting factor of 0.5 was chosen arbitrarily to account for the fact that a second return is conditional on a first return and the multiplier equally weights pulses with a single return and those with multiple returns. LAI can be estimated from the penetration proxy *P* by fitting an intercept-less model (Korhonen, Korpela, Heiskanen, & Maltamo, 2011) that takes the form:

$$LAI = \beta(-\ln(1 - P)) \quad 2.15$$

Where the slope coefficient (β) can conveniently be estimated from *in situ* measurements of LAI and then the computed values of *P* for any new area can be used with this value to predict effective LAI from the penetration rate of lidar in that new area. This approach is appealing because it is directly linked to LAI theory through the Beer-Lambert law (Section 2.3.4), where the gap fraction is estimated by measuring lidar penetration (1-*P*, Eq. 2.11) and the effective extinction coefficient *K* for the inversion of the Poisson model (Eq. 2.5, Section 2.3.4) to obtain LAI from gap fraction is derived empirically as the slope of the regression between the measured LAI values and *P*, the lidar proxy for gap fraction. This approach has been successfully used to estimate LAI in several coniferous forests (Härkönen, Tokola, Packalén, Korhonen, & Mäkelä, 2013; Korhonen et al., 2011; Solberg et al., 2009). However,

the performance of this model has not been compared to the many other ALS-derived proxies for gap fraction proposed in the literature, nor has it been compared to empirical estimation. While some efforts have been made to identify the optimum plot radius for use with this metric (Solberg et al., 2009), the impact of height threshold in combination with radius and the arbitrarily chosen weighting factor has not been tested.

2.6.2 Evaluating optimal lidar metrics and plot parameters

The number of studies attempting to develop theoretical links between LAI and lidar has led to the development of many new lidar metrics. The resulting proliferation of metrics available for use in models predicting LAI led Zhao & Popescu (2009) to review and compare the performance of several of these metrics in a study estimating LAI from lidar collected in a mixed pine and hardwood forest in East Texas. The list of metrics included commonly used height metrics (e.g. mean height of all returns, percentiles etc.) and a selection of penetration metrics, which were computed as the ratio of returns or pulses above and below a chosen height threshold. The results demonstrated that penetration metrics outperformed all other metrics. The best penetration metric was based on the total number of returns, and the use of all returns was a feature common to many of the best performing penetration metrics. The final form of the best predictive penetration metric was:

$$\frac{Nin + Nground}{Ntotal} \qquad 2.16$$

Where *Nin* is the number of inside canopy returns, and *Nground* is the number of ground returns and *Ntotal* is the total number of returns (a maximum of two per pulse). The results showed strong agreement between penetration metrics and LAI (R^2=0.84). Height metrics also showed strong agreement, albeit not as good as those using penetration metrics (R^2=0.72). These results were among the first to compare different classes of lidar metrics and highlighted that metric choice was important to ALS-LAI estimation. As with the methods of Solberg at al. (2009), these penetration metrics are sensitive to the gap fraction of the canopy, with increased ALS penetration reflecting increased gap frequency and size within the forest canopy. This property can be connected to the gap probability theory for measuring LAI presented in Section 2.3.4. However, the penetration (or ratio) based metrics required selection of a height threshold to decide, for example, what counts as below or in-canopy returns in Eq. 2.16. There is no formal agreement on height threshold in the literature, with most studies choosing to use the camera height or measurement conventions (e.g. DBH) as a threshold for calculation of lidar metrics (Jensen et al., 2008; Morsdorf, 2006; Riaño et

al., 2004). Moreover, as noted earlier, the choice of plot size for ALS-LAI assessment is equally uncertain. Zhao & Popescu (2009) attempted to address these questions by varying height thresholds and plot size independently. Their findings indicated that penetration metrics were sensitive to the choice of height threshold, with the optimal value for their study found to be 3.6 m. Their results also showed an increase in model accuracy as plot size rose to the optimal radius of 25 m, beyond which the impact of radius diminished. In another study estimating LAI from lidar in a temperate-boreal forest site, Solberg et al. (2009) concluded that variable radius plots based on dominant tree height were better than fixed radius plots, with plot radius equal to 0.75 times tree height producing the best results in that study.

The work by Zhao and Popescu (2009) represents a valuable assessment of the optimal combination of lidar metrics, plot radius, and height threshold for ratio metrics. The results clearly demonstrate that simple penetration metrics that form a proxy for measuring the canopy gap fraction are more closely related to canopy LAI when combined with the correct choice of plot size and height threshold. The authors were also able to generate a large-scale LAI map and demonstrate the superiority of ALS-based LAI measurements over NDVI spectral estimates for the same area. However, the study did not evaluate the use of a variable plot radius and height threshold and plot radius were optimised sequentially rather than testing all combinations of the two parameters. To date, no work has simultaneously addressed the optimum combination of lidar metrics, fixed or variable plot radius, and height threshold. Furthermore, a number of new metrics for the prediction of LAI from lidar have recently been proposed, including some with tentative links to the Beer-Lambert law (e.g. Jensen et al., 2011; Korhonen et al., 2011; Peduzzi et al., 2012; Pope & Treitz, 2013). Zhao and Popescu (2009) also observed that the challenges of determining the optimum method for estimating LAI from lidar calls for the use of newer statistical learning approaches. Successful estimation of LAI from lidar in *P. radiata* will require these questions to be addressed to develop robust models predicting LAI from ALS data. Furthermore, a simultaneous comparison of these factors could provide insight into the best approach for other forest types, as well as a much-needed assessment of the proposed physically-linked models for estimating LAI from lidar against empirically derived ones.

2.6.3 Evaluating the impact of forest type on ALS-LAI models

Many of the studies examined so far have largely been conducted in natural forests with a mixture of hardwoods and softwoods. None have dealt with New Zealand's specific forest

conditions, where single species plantation forestry is common. The nature of highly stocked stands of relatively homogeneous trees, and the silvicultural treatments applied such as pruning and thinning are all known to impact LAI (Beets et al., 2011; Mason et al., 2012; Raison & Myers, 1992). It is conceivable that these properties and management decisions could significantly impact any relationship between LAI and lidar or cause previously successful approaches for ALS-LAI estimation to be unsuitable altogether.

Peduzzi et al. (2012) provide one example demonstrating that ALS-LAI estimation is worth exploring in plantation forestry settings. The goal of their study was to develop a method to provide a large-scale assessment of LAI in a plantation forest. This was motivated by the close link between LAI and important attributes for management such as forest productivity, site utilisation, fertiliser impact, and resource availability.

In reviewing the previous literature, Peduzzi et al. (2012) noted that the most successful attempts to derive LAI from lidar were conducted in mixed species forests, especially temperate forests. Whereas the handful of studies conducted in pure pine stands generally produced weaker relationships. This tendency, combined with the intensive management activities would seem to suggest reduced performance of ALS-based LAI estimation in plantation forestry settings. Peduzzi et al. (2012) tested these assumptions by attempting to use ALS data to estimate LAI in a *P. taeda* plantation in the USA. The study locations included stands of varying ages and densities, as well as a variety of silvicultural treatments including fertilisation, thinning, irrigation, and mixed treatment stands. Ground measurements were taken at 109 plot locations using the LI-COR LAI-2000 described in Section 2.3.6, while lidar data was acquired using a multiple return sensor. A selection of lidar metrics were calculated and tested in a linear regression model. Good agreement was found (R^2=0.83) from a linear regression between *in situ* LAI and selected lidar metrics. All models trialled included a lidar-based penetration index (LPI) calculated as:

$$LPI = \frac{Gpulses}{(Gpulses + Apulses)} \qquad 2.17$$

Where *Gpulses* is the ground return count and *Apulses* represents all pulses. The LPI is remarkable for being very similar in approach to the metrics based on ratios of returns shown in Eq. 2.13-2.16 and once again reflects a measure of canopy gap fraction derived from the penetration of lidar through the canopy. The work by Peduzzi et al. (2012) provides evidence that despite the intensive management practices used in some coniferous plantations, the techniques for estimating LAI from lidar remain applicable. Of note is the fact that silvicultural treatments such fertiliser response showed some correlation with the value of

lidar-derived metrics, hinting at a possible means of detecting treatment response from lidar-based LAI estimates. These responses were not strong enough to be included in the final model but with further refinement, it may be possible to detect and monitor silvicultural treatments which impact LA such as fertilisation, thinning and pruning.

2.6.4 Potential applications of ALS-LAI estimation in New Zealand forestry

New Zealand's commercial forestry sector is centred around 1.5 million hectares of *P. radiata* plantation forest. The estate is primarily managed for timber production, with a range of intensive silvicultural treatments such as pruning, thinning, and fertilisation frequently employed (MPI, 2012). Large-scale measurement of LAI in these forests is of interest to forest managers and scientists, especially where LAI measurements may improve forecasts obtained from a new generation of growth models utilising physiological inputs (Mason et al., 2012). Routine assessment of LAI in commercial plantation forests from remote sensing data could also be valuable for silvicultural scheduling and monitoring. For example, LAI could be used to identify areas which may benefit from fertilisation. LAI is also closely linked to net primary production and hence serves as a link to forest health and productivity (Pope & Treitz, 2013).

Despite the many advantages of obtaining large-scale LAI estimates, little work has been conducted in New Zealand's plantation forests on using lidar to obtain these estimates. Indeed, a review of the literature highlighted only one study demonstrating the use of lidar to obtain LAI. This study was conducted by Beets et al. (2011) on a stand of 9-year-old *P. radiata* in New Zealand's North Island. A total of 50 trees from 10 plots were destructively sampled to derive accurate measurements of LAI. Lidar data acquired over the same area were then used to derive models of LAI. The study used the approach of developing empirical relationships between measured LAI and various lidar metrics (as described in Section 2.6.1). The best model accounted for 88% of the variation in LAI. Once again, some of the most useful metrics had links to canopy gap fraction. In this case, simple metrics such as cover percentage - computed as the number of returns above a threshold divided by total returns – and a height percentile were the two most powerful predictors of LAI. All models utilising these variables performed well but the choice of threshold height for both metrics showed a significant effect. Interestingly, Beets et al. (2011) found the optimal threshold to be 0.5 m, with higher thresholds producing weaker models. This is in contrast to other findings where higher thresholds improved model performance (K. Zhao & Popescu, 2009). The primary goal of the study was to evaluate the utility of lidar as a tool for a national

carbon monitoring program in New Zealand. As such, few of the questions highlighted in the literature were examined in the context of New Zealand's plantation forest type. The limitations of this study included:

1) The study relied entirely on destructive sampling of small stands containing a single age class. For ALS-LAI techniques to be useful, non-destructive *in situ* LAI measurement techniques such as HCP or the LAI-2000 will need to be evaluated across a range of forest conditions.

2) The impacts of silvicultural treatments and heterogeneous stand conditions and ages in *P. radiata* forests remain unexamined.

3) The impact of different plot parameters such as radius and height threshold were not fully examined.

4) Alternative metrics proposed in the literature, including those intended to form a proxy for gap fraction (see Section 2.6.1), were not evaluated, and the study relied only on those metrics available from common lidar processing software programs.

5) A comprehensive trial of the best combination of the above techniques and newer methods for model development has yet to be carried out in *P. radiata* forests.

2.7 Conclusion

This review demonstrates that LAI can be reliably obtained from lidar data in a range of forest types. At the present time, empirical approaches appear to provide the best means of estimating LAI from lidar. The primary drawback of these approaches is that each successful model is linked to the site and sensor, requiring re-calibration for each new campaign. Newer metrics linking the Beer-Lambert law to lidar penetration appear to offer improvements on empirical methods but these methods have not been compared. Typically, studies estimating LAI from lidar choose to test only a few metrics and a limited number of plot parameters – if these are altered at all. A detailed examination of the optimum combination of lidar metrics, plot parameters, and modelling approaches is required to develop insight into the best methods for estimating LAI from lidar and to evaluate the relative importance of new metrics with closer links to LAI theory. New Zealand's large areas of managed forests could benefit greatly from an accurate and reliable means of estimating LAI from lidar, but the previously

identified questions must be addressed before this can be achieved. This represents a significant gap in the literature which will be addressed by this thesis.

For these questions to be addressed, it will be critical to collect a large number of LAI measurements covering a range of different stand conditions using non-destructive means. Moreover, collection of these measurements should be attempted in the shortest amount of time possible to avoid seasonal impact on LAI. The advent of a scattering correction model for the LAI-2200C offers one opportunity to obtain the required measurements. This instrument also offers repeatable and inexpensive measurements, making it suitable for general use by commercial forest managers. Although the previous generation of the instrument (suitable for use only under diffuse sky) has been repeatedly compared to LAI from destructive sampling, no comparison of measurements from the new instrument has been made. While a comparison to LAI from destructive sampling would be valuable, a comparison between measurements taken with the old instrument and the new will also be valuable. This would provide information as to whether application of the scattering correction model, and the spectral values the model depends on, drive significant differences in LAI. Large differences would potentially limit LAI measurement to only diffuse or clear skies with no opportunity to pool measurements. Furthermore, the LAI-2000 is well known to underestimate LAI in coniferous forests (J. M. Chen et al., 1997; Mason et al., 2012). Therefore, a comparison of measurements with and without the scattering correction model could still provide insight into instrument performance beyond comparability of measurements. Higher LAI values may indicate improved performance and would suggest the advent of the scattering correction model offers improvements beyond an expanded range of sampling conditions.

Success in these areas would enable the rapid estimation of LAI across New Zealand's plantation estate, this would open a new area of research exploiting the strong and demonstrable link between LAI, site quality, and silvicultural management. Furthermore, the process of identifying the best methods for ALS-LAI estimation would offer an opportunity to provide much-needed insight into the choice of lidar metrics, plot parameters, and modelling approaches for ALS-based estimation of LAI more generally.

2.8 Research questions

The over-arching goal of this thesis is to develop methods for estimating LAI from lidar data in New Zealand's planted *P. radiata* forests. The review of the literature identified

several areas that require investigation in order for this objective to be achieved. These questions are grouped together in two main themes. Firstly, there is a need to validate new instrumentation to facilitate the collection of a large number of *in situ* LAI measurements in a short amount of time (to minimise seasonal effects on LAI). The instrument validation also calls for collection of accurate needle spectra using methods suitable for use with needle-leaved species. The specific questions addressed for this part of the thesis are:

(1) To compare in-situ LAI measurements taken with the new LAI-2200C instrument under clear sky conditions to measurements acquired using the traditional approach of sampling only under diffuse skies. If results are comparable, the instrument will be selected for use in in the second part of the thesis. This study will provide the first in-situ comparison of the scattering correction model in a coniferous forest.

(2) To evaluate the impact of the values chosen for needle reflectance and transmittance on the output of the scattering correction model and to determine to what degree these values impact agreement between LAI measurements taken under clear and diffuse sky conditions. The results of this work will provide the first assessment of this topic.

(3) To test emerging methods proposed to allow collection of accurate reflectance and transmittance spectra from needle leaf species by spectroradiometer. These methods have only recently been proposed and this thesis will evaluate them as a potentially useful means of collecting the spectral data required for the scattering correction model. If successful, the thesis will be expanded to include collection and measurement of a large number of *P. radiata* needle spectra using a spectroradiometer. This work will also address the question of whether needle spectra are stable across the vertical profile of the canopy and the amount of variability observed between individual trees. The results will provide the first demonstration of these methods for collecting needle spectra for use in the scattering correction model. And will provide the first assessment of the stability of laboratory measured *P. radiata* needle spectra at different positions in the canopy and between individual trees.

The second part of this thesis addresses the best method for estimating LAI from lidar. As very little work has been conducted in this forest type, many of the open research questions in

the broader field of ALS-LAI estimation must be addressed in order to obtain robust results. The specific questions addressed in this thesis are:

(4) To test the relative and absolute importance of the many different lidar metrics proposed or used to estimate LAI from lidar data in the wider literature. This question cannot be answered using existing software tools and will require the development of a dedicated software tool capable of computing a wide range of metrics from raw lidar data. These results will form the first comprehensive comparison of the many LAI-related metrics including standard metrics frequently used in empirical studies, complex sub-plot metrics recently linked to LAI, and ratio-based metrics that relate lidar penetration rates to canopy gap fraction and hence to the theory underpinning measurement of LAI using gap probability theory.

(5) To identify the optimum plot parameters for the estimation of LAI from ALS data. To accomplish this, the thesis will address the optimum choice of plot radius when extracting lidar data to compute metrics. For ratio metrics, this thesis will also seek to identify the optimum height threshold at which ratio metrics should be constructed. This assessment will include both fixed radii, set at increments from plot centre, and the use of variable plot radii based on the height of trees within each plot. For the choice of height threshold, the study will include testing of fixed height thresholds and the novel concept of setting the height threshold as a percentage of maximum canopy height in each plot. Importantly, the software tool for (4) will allow all combinations of height threshold, plot radius, and lidar metric to be evaluated simultaneously. The exploration of the combined effects of the major factors known to impact ALS-LAI estimation will be novel in the literature, as will the software tool developed for this purpose.

(6) To test the use of new modelling approaches capable of handling the high-dimensional data produced by (4) and (5). Nearly all of the ALS-LAI research to-date has relied on simple linear regression techniques. In order to provide a robust assessment of a large number of possible models from the different permutations of lidar metrics and plot parameters, it will be necessary to explore alternative modelling approaches. The methods used in this thesis will include modern statistical learning techniques as well as linear modelling methods adapted to

handle high-dimensional problems. The results of this work will represent the first use of these techniques for ALS-LAI estimation and will also produce robust measures of prediction error from the identified 'best' models.

The results from the completed thesis will provide an indication of the suitability of lidar as a tool for obtaining large-scale estimates of LAI in New Zealand's *P. radiata* forests and identification of the best methods for achieving these estimates. In doing so, this thesis will address many questions of broader relevance such as the performance of the LAI-2200C and the impact of lidar metrics, plot parameters, and modelling approaches on ALS-LAI estimation more generally. It is hoped that this work will provide the foundation for large-scale ALS-LAI estimation to realise the many benefits this information offers to scientists and commercial forest managers.

Chapter 3 - Instrument Validation

Preface

Chapter 3 addresses research questions 1-3 (see Section 2.8) by presenting the results from a validation of new instrumentation for measuring LAI in a planted forest of *Pinus radiata*. The contents of this chapter have been published as:

Pearse GD, Watt MS, Morgenroth J. *Comparison of optical LAI measurements under diffuse and clear skies after correcting for scattered radiation.* Agricultural and Forest Meteorology. 2016 May 1;221:61–70.

3.1 Abstract

Leaf area index (LAI) is a forest canopy variable that is closely related to forest growth and health. The LAI-2000 Plant Canopy Analyzer is widely used for indirect measurement of LAI; however, use of the instrument is limited to diffuse sky conditions, greatly restricting sampling. A new bidirectional transmission model allows measurements to be obtained under clear sky conditions. This is accomplished by calculating a correction factor to reduce the impact of scattered light from canopy elements on gap fraction estimates. In this study, we evaluate this technique by contrasting LAI measurements taken under diffuse and clear skies in a *Pinus radiata* D. Don plantation. We also evaluate the importance of obtaining accurate needle optical properties to parameterise the scattering correction model. Clear sky LAI estimates calculated with (a) measured optical values of *P. radiata* needles, (b) default values from the instrument software, and (c) maximum published values were compared to diffuse sky LAI estimates. Agreement was strongest where measured optical properties were used (R^2=0.87), with the relationship weakening under the default (R^2=0.78), and maximum value (R^2=0.67) scenarios. Under these three scenarios average clear sky LAI exceeded diffuse sky LAI by 16%, 17%, and 22% respectively. The disagreement was due in part to erroneous measurements from the outer sensor ring under diffuse skies. With these data removed agreement improved markedly under all scenarios (R^2=0.94, 0.89, and 0.75, respectively), and the mean differences under each scenario declined to 8%, 9%, and 15% respectively. Measurement of LAI under clear skies appeared to reduce error in the outer ring, greatly reduced logistical constraints, and reduced errors associated with sky variability.

3.2 Introduction

Leaf area index (LAI) is defined as one half the total leaf surface area per unit ground area (Jonckheere et al., 2004). In forest ecosystems LAI is a key variable in a range of processes including: gas and energy exchange, water and nutrient cycling, canopy health and primary production (Bréda, 2003). For forest managers, LAI is valuable for use in hybrid growth models (Mason et al., 2012) and as a tool for assessing the impact of management practices such as fertilisation (Carlyle, 1998; Peduzzi et al., 2012).

Despite its fundamental importance to forest managers and scientists, LAI usage has been limited by the difficulty of obtaining rapid and accurate measurements. In deciduous forests litter traps can provide accurate estimates of LAI, but in evergreen forests direct measurement relies on destructive sampling of representative trees (J. M. Chen et al., 1997). Although this approach provides accurate measurements of LAI, the process is labour intensive and costly (Beets et al., 2011; Küßner & Mosandl, 2000; Mason et al., 2012).

A variety of methods have been developed that allow indirect measurement of effective LAI (*Le*), which includes all light blocking elements (hereafter referred to as LAI), to be assessed using optical instrumentation. Hemispherical canopy photography (HCP) and the LAI-2000 (LI-COR Biosciences Inc., Lincoln, NE, USA) are two of the most widely used methods, and the accuracy of both has benefited from ongoing improvements in theory and technique (Macfarlane et al., 2014; Ryu et al., 2010; Woodgate, Jones, et al., 2015). Despite these improvements, both instruments suffer from limitations that make measurement of LAI challenging in forest canopies. In the case of HCP, accurate estimation of LAI requires correct classification of canopy and sky elements in order to calculate the gap fraction. This constrains image acquisition to diffuse sky conditions where the contrast between sky and foliage is greatest, and requires careful attention to image exposure and post processing (Macfarlane et al., 2014; Zhang et al., 2005).

The LAI-2000, and the newer LAI-2200, have been widely used to obtain indirect measurements of LAI for several decades (e.g. (J. M. Chen et al., 2006; Stenberg et al., 1994; Welles & Cohen, 1996). The instrument measures sky brightness in the blue band (320–490 nm) using five concentric light sensor rings centred at zenith angles of: 7°, 22°, 38°, 52°, and 68°. Canopy transmittance can be calculated by comparing measurements taken above and below a plant canopy, and it is then possible to estimate gap fraction, LAI, mean foliage orientation, and apparent canopy clumping (LI-COR, 2015). Estimation of these variables relies on the assumption that multiple scattering of solar radiation by canopy elements is

minimal in the blue band. Measurements taken under clear skies can seriously violate this assumption, and scattered light reaching the below canopy sensor can cause LAI to be underestimated by up to 26% (Kobayashi et al., 2013; Leblanc & Chen, 2001). To minimise the impact of scattered light, LAI measurement is restricted to diffuse sky conditions. However, the impact of scattered light is not completely eliminated, and measurements under diffuse conditions have been observed to underestimate LAI by up to 8% due to scattering (Kobayashi et al., 2013). Finally, in tall canopies suitable sampling conditions are often further constrained by the need to acquire above canopy readings in clearings some distance away from below canopy measurements (Solberg et al., 2009). Under these circumstances differences in sky brightness will be confounded with canopy transmission. Therefore, a large expanse of uniformly diffuse sky is required to minimise potential error in LAI introduced by variations in sky brightness between locations (LI-COR, 2015).

A new bidirectional transmission model proposed by Kobayashi et al. (2013) quantifies the impact of scattered light on gap fraction estimates obtained from the LAI-2200. The Kobayashi et al. (2013) model (hereafter the Kobayashi model) has been implemented as a software-based scattering correction model for LAI-2200 data, and is included with the latest iteration of the instrument - the LAI-2200C. The basic principle of operation remains the same with some additional features and protocols that are briefly outlined here. Given solar zenith, azimuth, and prevailing sky conditions the Kobayashi model predicts the impact of scattered light on gap fraction measurements obtained across the view zenith range of the LAI-2200C sensor located below a simplified one-dimensional canopy. To implement the model, a GPS receiver in the LAI-2200C records accurate time and position data to reconstruct solar position at the time of measurement.

The Kobayashi model requires parameterisation with measurements of diffuse sky radiance, fraction of diffuse light in the blue band, and leaf optical properties. The sky variables can be measured using the LAI-2200C (Kobayashi et al., 2013; LI-COR, 2015). However, obtaining leaf optical properties is more challenging. Although Kobayashi et al. (2013) demonstrate a method for obtaining these values in broadleaf species using the LAI-2200C, the technique is cumbersome when applied to needle leaf species. This method requires obstruction of a small view hole close to the size of a single needle, followed by arrangement of needles to cover a large diffuse panel. These species also pose a challenge when measured with a spectroradiometer, and published values can vary depending on the protocol employed (Yanez-Rausell, Schaepman, et al., 2014). As such, the accuracy of the

LAI-2200C method for needle leaved species is unclear. Where accurate measurements are available from published results, reflectance measurements may not cover the blue band used by the LAI-2200, and data for transmittance are often absent.

The scattering correction model promises to greatly expand the range of conditions under which LAI can be measured using the LAI-2200C, removing a major obstacle to measurement of LAI at larger scales. However, the expanded range of sampling conditions raises questions about the comparability of diffuse measurements and scatter corrected clear sky measurements. In-situ validation of the Kobayashi model was limited to a well characterised oak-grass savanna woodland, and revealed differences between diffuse and scatter corrected clear sky LAI (Kobayashi et al., 2013). Comparisons of in-situ measurements obtained from coniferous forests are lacking at present.

In this study, we aim to evaluate the agreement between LAI measurements obtained using the LAI-2200C under clear and diffuse sky conditions. This was accomplished using repeated measurements from 21 plots located in an intensively managed *Pinus radiata* D. Don forest under ideal sky conditions. We also examined the effectiveness of the scattering correction model in improving data collected from the error prone outer ring. This is of interest as the outermost ring observes the largest portion of the hemisphere, but valuable canopy information is often lost due to scattered light or gap fraction saturation (Gower et al., 1999; Kobayashi et al., 2013; Leblanc & Chen, 2001). Finally, we present needle spectra obtained from *P. radiata* needles using a new method for measuring small leaved species with a spectroradiometer (Noda, Motohka, Murakami, Muraoka, & Nasahara, 2013). These data were combined with default optical properties suggested by the LAI-2200C software, and published values measured using older protocols to form three needle optical property scenarios. The impact of each scenario on the calculated scattering corrections and the agreement between clear and diffuse sky LAI was examined.

3.3 Materials and methods

3.3.1 The forest plots

Data were acquired from Kaingaroa forest which is located in the Central North Island of New Zealand (38.67S; 176.46E). Kaingaroa is New Zealand's largest contiguous plantation covering around 180,000 ha. The majority of the forest occupies the pumice plateau within the Central North Island and has generally flat topography. Sample plots were restricted to

stands of *P. radiata* which cover 92% of the total forested area. Individual stands are typically homogenous in terms of age, silvicultural treatment, and stand density.

3.3.2 Plot selection and layout

Permanent sample plots (PSPs) are maintained throughout Kaingaroa forest, and a subset of these plots were chosen for the study. PSP locations were determined using a systematic sampling approach where the nodes of a grid with random origin and orientation form plot centres. Within the forest, the plot centre for each 600 m^2 circular plot was located using a Trimble Geo6000 XH GNSS (Trimble Navigation Ltd., Sunnyvale, CA, USA).

In tall forest canopies, the size and location of clearings available for a reference sensor to collect open sky readings can constrain measurement protocol and accuracy (see Section 3.3.3). To address this, we used satellite imagery to identify clearings within the forest that satisfied the following criteria: (1) unobstructed view of the sky across a wide azimuth, (2) at least 200 m x 200 m in size, (3) vegetation less than 3.5 m tall.

PSPs adjacent to suitable clearings were selected for measurement. In total, 21 plots covering a wide range of stand densities (200 – 917 stems ha^{-1}) were selected (Table 3.1). Estimates of stand height ranged from 17 m to 39 m (mean of 18 m), while stand ages ranged from 10 to 26 (mean and median of 18). The LAI measurements were conducted in early spring (September – October, 2014), with the time between diffuse and clear sky measurements of any plot minimised to avoid seasonal fluctuations in LAI. With the exception of plot 18, all plots were on relatively flat terrain, and the average straight-line distance to a clearing was 1.1 km. Some plots contained large tree ferns (*Cyathea* spp. and *Dicksonia* spp.), but these did not obscure canopy views from measurement locations.

3.3.3 Measurement of LAI with the LAI-2200C

The study was conducted using a pair of LAI-2200C sensors. Accurate measurement of canopy transmission requires simultaneous measurements of sky brightness to be taken above (A readings) and below (B readings) the canopy, while viewing the same region of sky (LI-COR, 2015). The height of the canopy in our study required all A readings to be obtained using a sensor located in one of the identified clearings. The sensors were matched using the recommended method and synchronised to GPS time at the start of each day. The reference sensor was placed on a levelled 3.5 m tripod and set to obtain A readings every 20 seconds. All clearings provided unobstructed views of the sky, but 180° view caps were fitted to both sensors to exclude the sun and operator from view. The gradient in plot 18 (14%) necessitated

the use of a 90° view cap, and additional measurements (n=25) were taken to compensate for the reduced canopy views.

Table 3.1. Summary of plot data and LAI measurements obtained under diffuse and clear skies using the LAI-2200C. Scattering corrections for clear values were calculated using measured optical properties (Table 3.2). Diffuse measurements were taken under sunset (SST) or uniform overcast skies (UOC). Clear plots with non-monotonic distributions of mean tilt angle (MTA) indicated invalid outer ring data, all overcast plots had invalid outer ring data. Masked LAI values excluded the outer ring data. SEL gives the standard error of LAI. Unmasked clear sky LAI is calculated as: scatter error + uncorrected LAI.

		Diffuse Sky Measurements				Clear Sky Measurements						
Plot	Stems ha^{-1}	Sky condition	LAI	SEL	Masked LAI	LAI	SEL	Scatter error	Valid MTA	Masked LAI	Solar zenith angle	Solar azimuth angle
1	367	UOC	2.09	0.04	2.04	2.48	0.03	0.69	Y	2.20	40	45
2	483	SST	3.26	0.05	3.27	4.16	0.03	1.30	Y	3.65	50	59
3	450	SST	4.38	0.05	4.52	4.95	0.04	0.70	Y	4.85	67	289
4	350	UOC	3.32	0.05	3.42	4.32	0.03	1.10	Y	3.89	57	300
5	467	SST	4.58	0.08	4.72	5.18	0.06	1.30	N	5.18	42	329
6	500	SST	4.02	0.06	4.10	4.43	0.07	1.60	Y	4.12	33	338
7	533	UOC	4.96	0.11	5.36	5.46	0.09	0.59	N	5.60	61	287
8	367	UOC	3.70	0.07	3.87	4.74	0.04	1.40	Y	4.52	43	313
9	417	UOC	4.40	0.05	4.64	4.94	0.05	0.50	N	4.85	78	288
10	600	UOC	4.91	0.08	5.31	5.62	0.09	1.50	N	5.85	40	15
11	367	SST	4.93	0.08	5.11	5.21	0.08	0.38	N	5.25	79	272
12	483	UOC	4.16	0.11	4.40	4.99	0.09	1.30	N	4.90	46	40
13	917	UOC	3.60	0.11	3.77	4.43	0.21	0.96	Y	4.19	57	313
14	467	UOC	3.24	0.07	3.35	3.98	0.08	1.40	Y	3.42	46	343
15	400	UOC	3.67	0.10	4.37	3.61	0.11	0.38	Y	4.35	38	360
16	383	UOC	4.27	0.05	4.49	5.23	0.05	1.50	N	5.26	44	35
17	550	SST	5.57	0.07	5.86	6.00	0.06	0.93	N	6.42	44	325
18	417	UOC	4.34	0.06	4.63	4.93	0.04	1.00	Y	4.81	44	9
19	283	UOC	4.13	0.08	4.41	5.08	0.06	1.00	N	5.03	49	312
20	200	SST	3.98	0.04	4.23	4.18	0.05	0.35	N	4.37	71	286
21	483	UOC	3.25	0.04	3.37	3.50	0.03	0.21	Y	3.43	79	268

The plot layout was adapted from other studies utilising previous generations of the instrument within circular plots (Law et al., 2008; Solberg et al., 2009, 2006). Marker pegs were laid at plot centre and at a distance of 3 m away in each cardinal direction, with a further 3 pegs located randomly up to 4 m away from the plot centre. An additional 10 measurements were taken at unmarked locations within the bounds of the plot (total n=18). These extra samples provided different views of the canopy in order to improve measurement accuracy and reduce standard error of LAI (SEL) (LI-COR, 2015).

The same view direction was used for both diffuse and clear sky measurements, with only one plot requiring a large change in direction, and in this case we reversed the view direction to preserve any impact from tree rows.

The sky properties required by the scattering correction model were measured shortly after completing each clear sky plot using the sequence described in the instrument manual (LI-COR, 2015). A 270° view cap was used to obtain the final 'wide sky' reading for this sequence, except for plot 18 where a 180° view cap was used.

3.3.4 Sky conditions during sampling

The two sensor arrangement is sensitive to differences in sky condition between sensor locations. Fast moving clouds or changes in sky brightness between the two locations can pollute measurements of canopy transmittance. Therefore, we took measurements only under ideal clear and diffuse sky conditions as defined in the LAI-2200C manual.

Clear sky measurements required regular adjustments to the reference sensor's orientation to ensure the sun was kept slightly out of the field of view. Using a 180° view cap, the relative azimuth of the sun was then just over 90°. With the sun in this position the normalised sky radiance observed across the LAI-2200C's five sensors is stable for different solar zenith angles (Kobayashi et al., 2013). This solar position also reduces potential differences between the radiation path length predicted by the scattering correction model, and the actual path length from canopy gaps to the LAI-2200C (LI-COR, 2015). Diffuse measurements were obtained at sunset or under uniformly overcast skies. For overcast skies the reference sensor was orientated to view the region of sky that appeared most stable. At sunset the sensor always viewed a cloud free isotropic portion of the sky. Patchiness of clouds, precipitation, and swirling clouds greatly reduced the number of suitable overcast days, and sunset conditions were relied upon for many diffuse measurements (Table 3.1).

Apparent LAI was used as a measure of sky variability over time. These values were computed in the instrument software using a process of substitution, whereby the first

reference sensor 'A' reading collected during plot measurement was paired with subsequent A readings collected at increasing time intervals. Paired records were treated as 'above' and 'below' canopy readings, and the resulting LAI values represent the potential measurement error arising solely from changes in sky brightness over time (LI-COR, 2015). Reference sensor data from plots measured close to sunset were excluded from analysis due to the rapid changes in sky brightness. Twenty minutes of suitable reference sensor data were available from the remaining plots, with a measurement interval of 20 seconds. Measurements were pooled by sky condition, and the mean and standard deviation of apparent LAI at each 20 second interval was calculated.

3.3.5 Obtaining needle optical properties

The scattering correction model requires values for leaf reflectance, leaf transmittance, and ground reflectance in the blue band. Kobayashi et al. (2013) noted non-negligible contributions to scattered light from snow covered forest floors. In our plots the canopy floor was always covered by forest litter or vegetation. As such, we retained the default ground reflectance value of 0.05. Few published values for *P. radiata* needle reflectance could be found, and no data were found for transmittance (Table 3.2).

Table 3.2. Summary of candidate values for *Pinus radiata* needle reflectance and transmittance in the blue band. Scattering corrections were calculated using values from the measured, defaults, and maximum scenarios. *Where no data were available the default transmittance of 0.01 was substituted.

	Optical Scenario	Reflectance		Transmittance	
Source		Blue Band	Average	Blue Band	Average
Measured Spectra	Measured	370-490	0.033	390-490	0.023
FV2200 Defaults	Defaults	320-490	0.05	320-490	0.01
Trotter and Hosking (1998)	Maximum	445-455	0.066	N/A	N/A*
Coops and Stone (2005)	N/A	400-490	0.03	N/A	N/A

Spectra presented in Coops and Stone (2005) were obtained from unhealthy *P. radiata* specimens growing in Australia. The presented spectra had to be extrapolated to cover the full LAI-2200C blue band. Values from Trotter and Hosking (1998) were taken from sick and healthy *P. radiata* trees in Waikato, New Zealand. However, their methods differed significantly from established measurement protocols for needle leaved species (Yanez-Rausell, Schaepman, et al., 2014), and blue band reflectance was twice the value from Coops

and Stone (2005). To resolve the uncertainty around needle reflectance, and to obtain data for transmittance, we measured the spectra of healthy *P. radiata* needles.

3.3.6 Collection of needle samples

Needle samples were collected from 10 randomly selected trees within a single stand during January 2015. The chosen stand contained LAI plot 2, and the stand age (17) was close to the mean and median age (18) for all LAI plots, and was judged to be typical of the plot conditions in the main study.

Because solar zenith angle alters the relative influence of upper and lower canopy elements on scattered light (Kobayashi et al., 2013), and needle optical properties can vary within the canopy (Carter & Knapp, 2001), we tested the impact of canopy position on needle reflectance and transmittance. A shotgun was used to collect two branches from the live portion of the lower crown, and two from the more sun exposed upper crown. Sampling was conducted on a cloudy day after a period of rain, and samples were quickly transported to the laboratory. All samples were placed in large plastic bags, along with wet cloths, and stored at 4° C. All measurements were completed within 72 hours of sample collection.

3.4 Measurement of needle spectra by spectroradiometer

Needle spectra were measured using an ASD FieldSpec Pro Jr spectroradiometer connected to an ASD RTS-3ZC integrating sphere (Analytical Spectral Devices Inc., Boulder, CO, USA), measuring radiation between 350 nm and 2500 nm. Optical properties are challenging to measure in needle leaved species due to their size, and accurate measurement necessitates an increase in the illuminable area (Yanez-Rausell, Schaepman, et al., 2014). This is usually achieved by arranging several needles in a grid, maintaining small air gaps to reduce multiple scattering between adjacent needles, and then placing the grid on the sample port of an integrating sphere (Daughtry et al., 1989). However, additional steps are then required to calculate the gap fraction of the array (Yanez-Rausell, Schaepman, et al., 2014). We followed the protocol described by Noda et al. (2013) for small leaves. In this method gap fraction for reflectance and transmittance are measured separately, and without the need for post-hoc analysis of each needle array. This is achieved by measuring the reflectance of the array with gaps vacant, and then with a diffuse medium, with known optical properties, placed behind the array to occupy the gaps. Gap fraction is calculated by subtraction and used to correct

reflectance measured from the array. Gap fraction for transmittance is calculated from the change in flux when the array is placed in front of the light source.

The steps described by Noda et al. (2013) for measuring transmittance with the LI-1800 integrating sphere (LI-COR Biosciences Inc., Lincoln, NE, USA) were adapted for use with the ASD RTS-3ZC. We used registration marks on the sphere and sample slides to reduce the error associated with sample misplacement between measurements (Yanez-Rausell, Schaepman, et al., 2014).

We validated our modifications in the same manner as Noda et al. (2013) by measuring whole leaves of *Pittosporum eugenioides* (A. Cunn.), and then cutting the measured area into 2 mm strips to be re-measured as an array. The obtained spectra (not shown) agreed closely.

Healthy needles from the same shoot were plucked from each branch and arranged adaxial side up 1.5 – 2 mm apart on the sample slide. Measurements of abaxial and adaxial reflectance were taken first, before reconfiguring the integrating sphere to measure adaxial and abaxial transmittance. Laboratory filter paper was used as the diffuse material to fill array gaps, and a calibrated zenith standard (Analytical Spectral Devices Inc., Boulder, CO, USA, reflectance = 99%) was used as the reflectance reference where required.

The impact of canopy position on needle reflectance and transmittance in the blue band was evaluated using a mixed effects regression model with tree number specified as a random effect and canopy position as a fixed effect. The random effect was introduced to account for the fact that branch samples were not independent, with four branches collected from each tree. In coniferous forests the relative contribution of adaxial and abaxial sides to scattered light cannot be easily separated. Therefore, we pooled spectra from both sides of all samples to calculate an overall mean and standard deviation for reflectance and transmittance.

3.5 Analyses

The LAI-2200C data were processed using the FV2200 software package (version 2.1.1, LI-COR Biosciences Inc., Lincoln, NE, USA). The B records were paired with closest in time A records from the reference sensor to calculate LAI. The impact of needle optical properties on the scattering correction model was assessed by calculating scattering corrections for clear sky LAI measurements using the three needle optical property scenarios defined in Table 3.2, namely (1) measured values from our spectra, (2) default values suggested by FV2200, and (3) the maximum reflectance value found in the literature. Transmittance was not available for scenario 3 so the value from scenario 2 was used instead. The values from Coops and

Stone (2005) were not included in a separate scenario as they were close to the measured values. These scenarios reflected the data available for *P. radiata*, and are typical of the choices other users of the LAI-2200C may face.

The solar position, measurement time, sky condition, and needle optical properties from each of the three scenarios were input into FV2200 to calculate the scattering corrections for clear sky LAI.

Ordinary least squares regression was used to estimate the relationship between clear sky LAI estimates from each needle optical property scenario and the corresponding diffuse sky LAI measurements. The underlying model assumptions of normality, homogeneity of variance, and lack of bias were checked through examination of model residuals. Potentially influential points were investigated by assessing influence and leverage on the fitted models. Natural log, square root, and power transformations of the dependent and independent variables were also trialled. Mason et al. (2012) compared optical estimates of LAI to values obtained from destructive sampling. The authors demonstrated that stand density was a significant variable in the best model predicting LAI from optical measurements. Following Mason et al. (2012) we applied a scaled-power transformation ($\lambda = 0.08$) to measurements of stand density and tested this variable alone and in combination with the best predictive variable.

Without reference to directly measured LAI, measures of agreement, such as the coefficient of determination (R^2), may show strong agreement between diffuse and clear sky LAI, regardless of any systematic differences across the range of LAI values. Bland-Altman contrasts have the advantage of illustrating both bias and precision across the range of measurements (Bland & Altman, 1986). We constructed Bland-Altman plots to evaluate agreement between diffuse and clear sky LAI measurements for each needle optical property scenario.

All analyses were repeated with the outer sensor ring masked from analysis. This ring is sensitive to the impact of scattered light, even under diffuse sky conditions, and it is frequently excluded from analysis of LAI-2000 and LAI-2200 data (Leblanc & Chen, 2001; Peduzzi et al., 2012; Solberg et al., 2009). Diagnostics were carried out by examining the mean plot contact number for each sensor ring. The contact number is defined as the probability that a beam penetrating through the canopy will contact a foliar element (Weiss et al., 2004) and is calculated as the mean of the logarithm of each ring's transmittance divided by path length through the canopy (LI-COR, 2015). The change in MTA and LAI implied by

the contact number at increasing view zenith angles can be compared with theoretical assumptions to identify invalid readings from the outer ring (LI-COR, 2015; Solberg et al., 2009).

All statistical analysis was conducted using R statistical software (R Core Team, 2015). The mixed effects model was implemented using the nlme package for R (Pinheiro, Bates, DebRoy, Sarkar, & R Core Team, 2015).

3.6 Results

3.6.1 Sky variability

The mean apparent LAI induced by changes in sky brightness was greatly reduced under clear skies (Fig. 3.1), and remained stable across the 20 minute interval. By contrast, the mean apparent LAI from overcast data started higher and increased greatly in magnitude and variability with increasing time from the first reading.

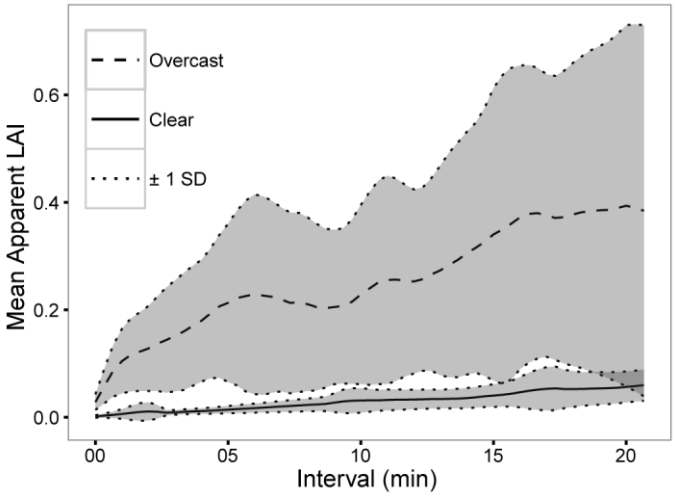

Fig. 3.1. Mean apparent LAI calculated from above canopy (A) readings collected at 20 s intervals in an open clearing during plot measurement. Values indicate the potential error in LAI arising solely from changes in sky brightness over time. Values were obtained by computing LAI using A readings from time = 0 with all A readings at time > 0 substituted in place of below canopy readings. Data from 12 measurements periods were pooled by sky condition, and the mean and standard deviation were calculated at each interval.

3.6.2 Needle optical property scenarios

The mean reflectance and transmittance calculated from 80 measured spectra (adaxial and abaxial values from 40 samples) are shown in Fig. 3.2. The difference between reflectance and transmittance represents absorption by the needles.

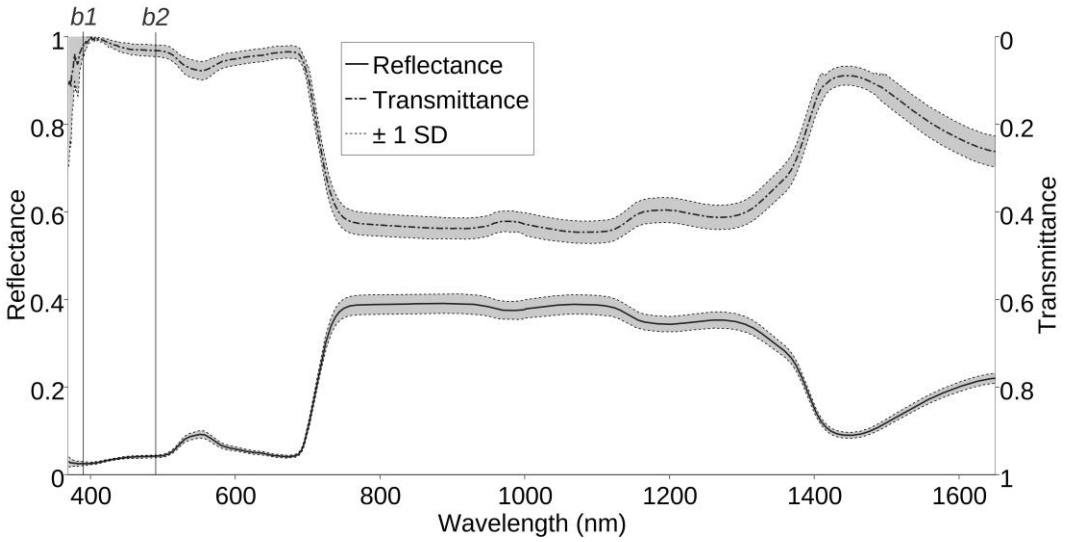

Fig. 3.2. Mean reflectance and transmittance spectra of *Pinus radiata* needles. Shaded regions around each trace indicate ±1 standard deviation from the mean. Adaxial and abaxial measurements from 40 samples were pooled. Needle absorbance is represented by the gap between reflectance and transmittance. Blue band was defined as 370-490 nm for reflectance (left extent to *b*2, and as 390-490 nm (*b*1 to *b*2) for transmittance.

Gap fraction, calculated from adaxial and abaxial measurements of the same sample slide, had an estimated mean difference of 1.4% (paired t-test, P <0.001), indicating that sample placement on the integrating sphere was reliably achieved, and corrections for vacant space were consistent within samples. Overall, needle transmittance exhibited greater variability than reflectance, especially between 350–390 nm (Fig. 3.2). Examination of the data in this region showed many invalid readings (negative values) for transmittance, and fairly high levels of instrument noise. Therefore, the blue band for transmittance was truncated to the stable region between 390–490 nm (Fig. 3.2, *b1-b2*). Reflectance values were stable above 370 nm, and the blue band for reflectance was defined as 370-490 nm (Fig. 3.2 left extent to *b2*). The mean reflectance and transmittance within the re-defined blue bands was calculated for each sample.

Canopy position had no significant effect on the mean value of needle reflectance (P=0.11) or transmittance (P=0.15) for samples collected from the upper and lower crown. Pooling adaxial and abaxial readings for the 40 samples, the overall mean reflectance was 0.033. This value was lower than both the software defaults (0.05), and the maximum value of 0.066 obtained from Trotter and Hosking (1998), but close to the extrapolated value of 0.03 from Coops and Stone (2005) (Table 3.2). The overall mean transmittance was 0.023.

This value was more than twice the default transmittance (0.01) used by FV2200. To address the loss of transmittance data below 390 nm, we compared the mean, median, modal value, and a weighted mean favouring lower wavelengths. All values were similar, and with no other data available we chose to retain the mean transmittance for use in the measured scenario.

3.6.3 Comparison of diffuse and clear sky LAI

Clear sky LAI values obtained using the 'measured', 'default', and 'maximum' needle optical property scenarios (Table 3.2) are shown alongside the corresponding diffuse sky LAI values in Table 3.1. LAI values recalculated to mask data from the outer sensor ring are presented alongside the unmasked values. Plot 13 had notably higher SEL (standard error LAI), due to detritus on the innermost ring at the end of clear sky sampling, and the last measurement was dropped. The SEL values for the remaining plots were low, and appeared similar across sky conditions.

Comparison of the unmasked measurements showed strong agreement between diffuse and clear sky LAI under the three optical scenarios (Fig. 3.3). The correlation was greatest for the measured scenario with R^2=0.87 and RMSE of 0.29. The relationship weakened with increasing values for needle reflectance in the default and maximum scenarios.

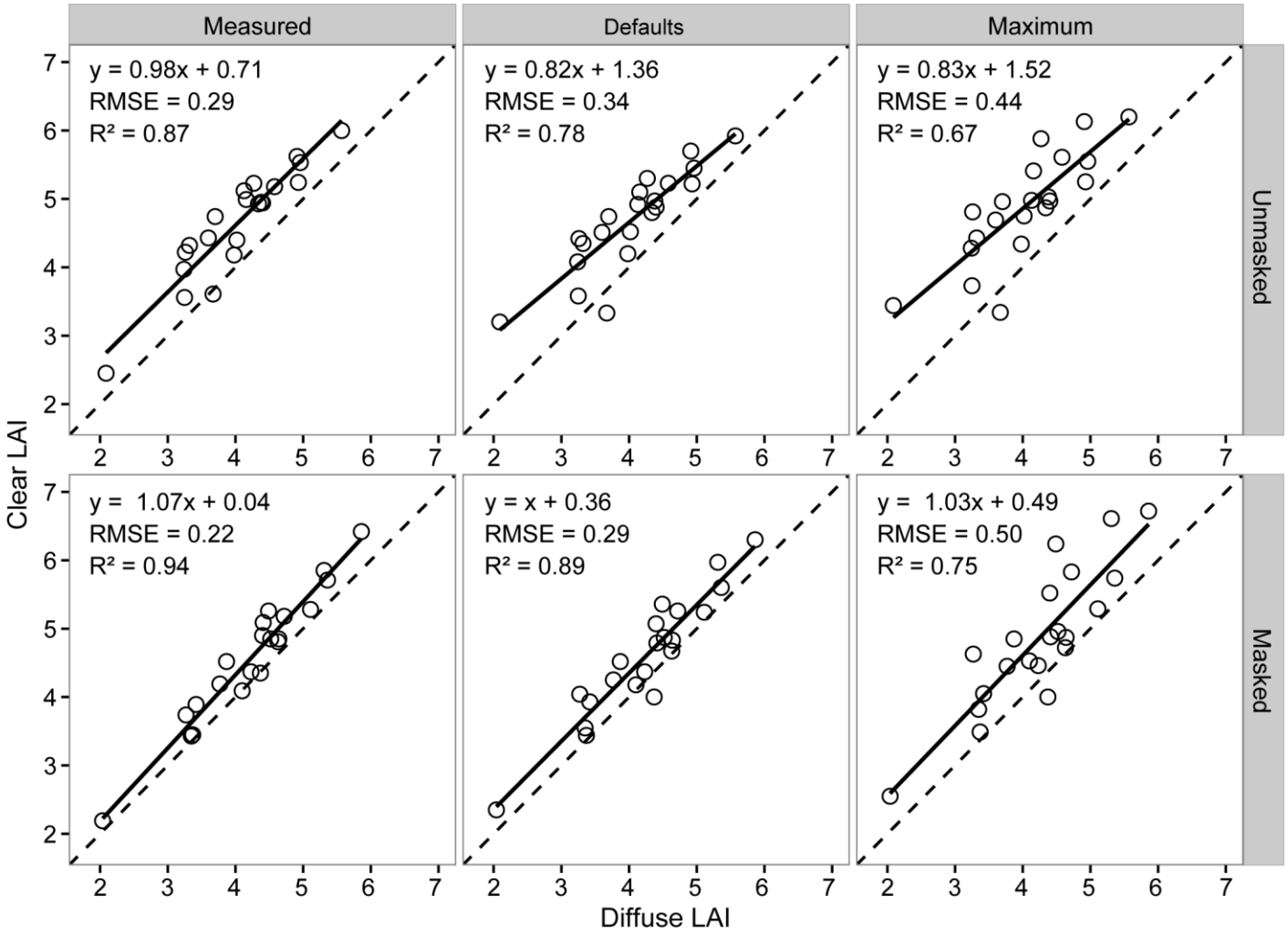

Fig. 3.3. Comparison of LAI measurements obtained under clear and diffuse sky conditions using the LAI-2200C. Clear sky estimates were calculated using three needle optical property scenarios (Table 3.2). Lines of best fit (solid) are shown along with lines of identity (dashed). Upper panels (unmasked) show comparisons including data from the error prone outer sensor ring, while lower panels (masked) show the same comparisons with these data omitted.

Repeating the analysis with the outer ring masked improved agreement under all scenarios, and the measured scenario in particular showed very strong agreement between diffuse and clear sky values with R^2=0.94 and RMSE of 0.22. A plot of model residuals against fitted values (Fig. 3.4) showed no evidence of bias or serious outliers, and the highest Cook's distance observed in the best model was 0.09. Transformations of the dependent and independent variable did not reduce residual variance, and in some cases introduced outliers with high leverage on the fitted model. The addition of the scaled-power-transformed stand density variable did not significantly improve the best model (ANOVA P=0.86). Residuals from the unmasked models showed higher variability, especially for the default values optical scenario, but none had sufficient leverage or influence (largest Cook's D=0.3) on the model to justify exclusion.

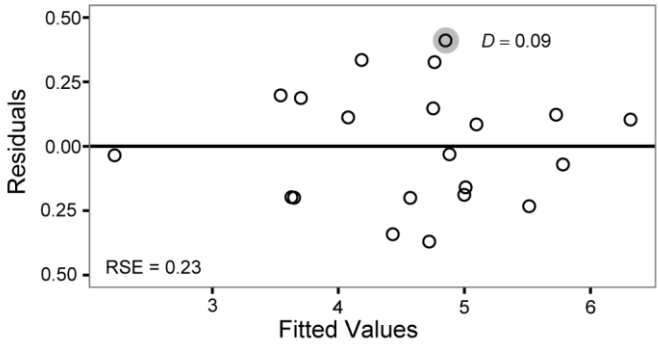

Fig. 3.4. Plot of residuals from the best model comparing masked clear sky LAI obtained using measured spectra against masked diffuse sky LAI. The residual with the highest Cook's distance is circled in grey. RSE is the residual standard error for the model.

3.6.4 Bland-Altman contrasts

While clear and overcast values of LAI generally agreed under all scenarios, none of the lines of best fit lie along the line of equivalency between measurements (Fig. 3.3, dashed). With the exception of plot 15, clear sky LAI exceeded diffuse sky LAI for all plots, under all three optical scenarios.

Bland-Altman contrasts (Fig. 3.5) illustrate the degree of agreement for each pair of measurements by optical scenario, and outer ring masking condition. The dashed lines are equivalent to a paired t-test for the difference between means, with associated 95% confidence intervals (CI). The difference between means was significant for all comparisons (all P values < 0.001).

No comparison showed unbiased agreement, with all estimated mean differences exceeding zero. The unmasked comparisons showed poorer agreement, with higher estimated mean differences, and wider CIs. In the case of the measured scenario the 95% CI excluded 0. Comparisons using masked data improved agreement, but the general spread of the differences, as well as the estimated mean difference for each comparison, still reflected a tendency for clear sky LAI to exceed diffuse sky LAI.

Overall, the differences generally appeared stable across the range of LAI values. The exceptions were the unmasked ‘defaults’, and both the masked and unmasked ‘maximum’ scenarios, where differences appeared greater at the extremes.

Average unmasked clear sky LAI under the measured, default, and maximum optical scenarios exceeded unmasked diffuse sky measurements by 16%, 17%, and 22% respectively. Masking the outer ring reduced these differences to 8%, 9% and 15% respectively.

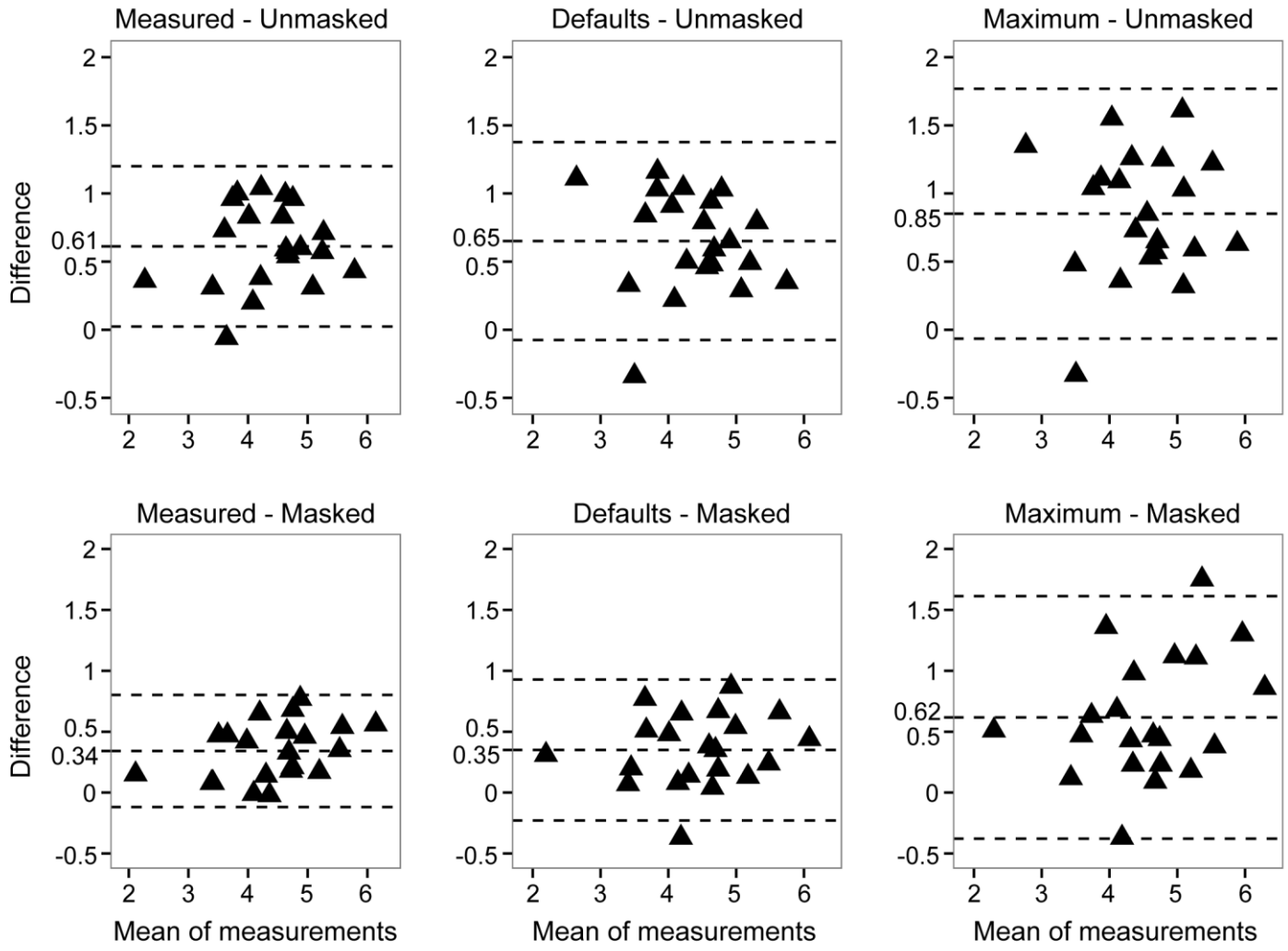

Fig. 3.5. Bland-Altman plots contrasting diffuse and clear LAI measurements by needle optical property scenario, and repeated with the outer sensor ring of the LAI-2200C masked. Plots show measurement difference (clear-diffuse) against mean of measurements. Dashed lines show estimated true difference of the means with associated 95% confidence interval. Measurements in perfect agreement would scatter around $Y = 0$ with no bias across the range.

3.6.5 Differences in instrument error

For all unmasked diffuse measurements the outer ring showed contact numbers close to zero, and the implied foliage mean tilt angle (MTA) contradicted the expected monotonic change in canopy MTA with increasing view zenith angle (Lang, 1986). Therefore, wherever MTA was non-monotonic the outer ring data were considered invalid (Table 3.1). The outer sensor has the widest view angle, and these data carry a higher weighting in FV2200. Consequently, the erroneously low LAI from the outer ring data biased total LAI downwards in most diffuse sky plots. Masking the erroneous data, and the reweighting of the remaining rings, tended to increase total LAI in these plots.

Application of the scattering corrections to clear sky data, especially using the measured scenario, increased the number of plots with monotonic changes in MTA. In the remaining non-monotonic plots, the MTA and LAI estimates were still improved, and were generally close to estimates from the fourth ring. As such, masking the outer ring from clear sky LAI measurements led to a negligible decrease in plot LAI (-1.7% on average).

3.7 Discussion

Our results demonstrate that clear sky LAI estimates obtained using the LAI-2200C agree strongly with those obtained under diffuse sky conditions, especially when the outer ring is masked, and measured needle spectra are used to calculate the scattering correction. In addition, the need for masking outer ring data arose from erroneous readings under diffuse skies, with strong indications that clear sky measurements produced useable data from all sensor rings.

The ability to measure LAI under clear skies removes a major logistical constraint to the number and frequency of LAI measurements possible in forest ecosystems (Leblanc & Chen, 2001; Mason et al., 2012; Solberg et al., 2009). In our study the number of suitable clear days far exceeded the number of uniform overcast days, and only the inclusion of sunset plots kept the study duration reasonably short.

Clear skies were more stable than overcast sky conditions, and were observed to be isotropic over large distances. This was reflected in the greatly reduced magnitude and variability of the apparent LAI calculated from clear sky A records (Fig. 3.1). With access to two sensors the time difference between A and B readings never exceeded 20 seconds in our

study. However, our findings suggest measurement of LAI under clear skies can reduce error when a single sensor is available, or where the distance between sensors is large.

Our results demonstrated strong agreement between LAI measurements obtained under diffuse and clear sky conditions. Although clear sky LAI measurements exceeded those obtained under diffuse conditions, the magnitude of the difference was strongly impacted by the needle optical properties used to parameterise the scattering correction model. This result has important implications for situations where data are collected under different sky conditions.

Using the default needle reflectance and transmittance suggested by FV2200 resulted in good agreement between LAI measurements obtained under clear and diffuse sky conditions, but the residuals from the regression model were quite large. Relying on poorer quality data such as those in our 'maximum' scenario – where reflectance was twice the measured value – produced a much weaker relationship between diffuse and clear sky measurements. Direct comparisons or pooling of these data would have introduced substantial bias. By contrast, use of the measured needle spectra greatly reduced the magnitude of the differences, and the regression analysis based on these data showed lower residual error. Removing the outer ring from analysis further improved agreement and residual error; however, there was still evidence of bias across the range of LAI values. Although stable, this bias would impact pooled data taken under different sky conditions.

Prior to the advent of the scattering correction model, few applications required accurate measurement of leaf reflectance and transmittance in the blue band. This fact, combined with the difficulty of obtaining accurate spectra for needle leaved species, helps to explain the paucity of published data for *P. radiata* needles. Those seeking to calculate scattering corrections for LAI-2200C data obtained from other needle leaved species are likely to face similar challenges.

The method described by Noda et al. (2013) provided a simple and efficient means of obtaining needle spectra. In contrast to our study, Noda et al. (2013) did not report high levels of noise for measurements of transmittance from *Pinus densiflora* needles. One potential source of error may be forward-scattered light from the ridged side of the needles (Zarco-Tejada et al., 2004), but we observed high levels of noise in both adaxial and abaxial measurements. A more likely explanation lies with the configuration of the RTS-3ZC integrating sphere for use with the method of Noda et al. (2013). Transmittance measurements require reconfiguration of the integrating sphere, with a change in beam path

length. Ideally, the collimated light source should be refocused to provide optimal illumination of the sample. In our study this was not practical due to the large number of samples to be measured before the onset of desiccation. It is likely that the observed variability is largely attributable to the reduced illumination of samples in transmittance mode.

Despite apparent differences in needle colour, size, and branch order, the variability of spectra remained low, especially for reflectance. This suggests that the values we obtained may be broadly applicable for use in the scattering correction model when dealing with this species.

In our data, the diffuse sky measurements from the first four rings produced monotonic values of MTA; however, the outer ring showed a markedly lower MTA, and the definite integral from rings 4 to 5 implied a canopy with dramatically declining LAI at higher zenith angles. In plantation forests with dense homogenous stands and deep canopies it is unlikely that LAI is reduced at these angles. In other studies, this has been attributed to scattered light present under diffuse skies (Leblanc & Chen, 2001; Solberg et al., 2009), or to gap fraction saturation when LAI is high (~6) (Gower et al., 1999). Because our diffuse plots contained both sunset and overcast measurement we were able to develop some insight into the relative contribution of these two factors.

Kobayashi et al. (2013) showed that even under diffuse skies all LAI-2200 measurements taken with the sun above the horizon are affected by scattered light. The impact of scattered light was greatest on the outer ring, and erectophile foliage exacerbated this effect. However, when measurements were conducted with high solar zenith angles (84−86°) the reported impact on LAI was small (LAI + 0.05−0.06). In our study, all sunset measurements (Table 3.1) coincided with a solar zenith of 90° and the impact of scattering could be expected to be minimal. Furthermore, according to the simulations conducted by Kobayashi et al. (2013), scattered light at sunset in canopies with LAI close to that of our plots (3-5) would most affect the inner rings of the instrument. Despite these facts, all sunset plots in our data had low, non-monotonic, contact numbers from the outer sensor ring. This suggests that the presence of scattered light could not fully account for the low contact numbers.

We hypothesise that outer ring errors in our data resulted from a combination of scattered light and gap fraction saturation. Measurements conducted in the last minutes of twilight may have reduced scattered light at the expense of resolving small gaps in the canopy at high

zenith angles. Conversely, measurements conducted under brighter overcast skies may have reduced gap fraction saturation, but suffered from additional scattered light in the outer ring.

The clear sky measurements provide additional support for our conclusions. Without scattering corrections the outer ring of the LAI-2200C sensor is strongly impacted by scattered light during clear sky measurement (Leblanc & Chen, 2001), and would be expected to produce low contact numbers. It is significant that application of the 'measured' scenario scattering correction to clear sky LAI data produced monotonic MTA values in 11 plots (Table 3.1). In the remaining non-monotonic plots, it is plausible that the scattered light entering the fifth ring exceeded the model predictions. Our plots had a combination of erectophile foliage, high LAI, and poor estimates of apparent clumping (due to the wide view caps), all of which impact actual and predicted scattered light (Kobayashi et al., 2013). Notwithstanding these canopy specific issues, our results indicate that measurement under clear skies addresses both gap fraction resolution at high zenith angles, and the presence of scattered light, thereby allowing canopy information to be obtained from all sensor rings.

Without reference to direct measurements of LAI, our data cannot be used to provide an indication of the absolute accuracy of clear sky LAI estimates. To date, in-situ validation of the LAI-2200C has been limited. Kobayashi et al. (2013) found in-situ measurements taken with the instrument under diffuse sky conditions to be 7.7% lower than total canopy LAI for a well characterised oak-grass savanna woodland. While this value is close to the smallest difference we observed between measurements taken under diffuse and clear sky conditions, this does not imply that our optical estimates accurately reflect true LAI. Indeed, our data did not account for the presence of woody material in the instrument's field of view, or the effect of foliar clumping at the level of the shoot. Corrections to account for these factors have been shown to be necessary in order to obtain accurate values of true LAI from optical LAI measurements taken under coniferous canopies (J. M. Chen et al., 1997). Destructive sampling of coniferous species to determine if measurements obtained under clear sky conditions offer improved estimates of true LAI would be of significant value, especially if efforts were made to collect and apply the aforementioned correction factors.

3.8 Conclusions

The results of our study demonstrate that LAI measurements taken using the LAI-2200C under clear skies, and corrected for scattered light, agree well with, but exceed those taken under diffuse skies. The degree of agreement is improved when the outer ring is masked,

largely because diffuse conditions and dense canopies appear to create serious errors in data from the outer ring. In contrast, scatter corrected clear sky measurements generally produced useable outer ring data. The scattering correction model is sensitive to the choice of needle optical properties. Agreement was acceptable when the software default optical values were used, but measured optical properties produced the strongest agreement between diffuse and clear skies, with the smallest estimated mean difference. The ability to obtain LAI measurements under clear skies makes routine measurements of LAI from a large number of plots a realistic objective.

3.9 Acknowledgements

The authors would like to thank Timberlands Ltd. for access to forest plots and associated data, as well as Dr H. Noda at the University of Tsukuba, Japan and Andrew Dunningham at Scion, Rotorua for their help with the spectroscopic analysis. Jon Welles at LI-COR, Nebraska also provided helpful advice. This research was supported by the Growing Confidence in Forestry's Future (GCFF) research program administered by Scion New Zealand Forest Research Institute Ltd. The corresponding author received additional support from the Canterbury Scholarship Award funded by the University of Canterbury, Christchurch.

Chapter 4 - Estimating LAI from Lidar

Preface

Chapter 4 addresses research questions 4-6 (see Section 2.8) by presenting the results from a study examining the optimal combination of lidar metrics, plot parameters, and modelling approaches to develop a method for accurately estimating LAI from ALS data in *Pinus radiata* forests. These results are presented in the form of a manuscript submitted for publication as:

Pearse GD, Morgenroth J., Watt MS., Dash JP. *Determining optimal plot parameters, metric selection, and modelling approaches for estimation of leaf area index from airborne discrete-return lidar.* Manuscript submitted for publication.

The manuscript presented here may differ substantially from any published version as a result of peer-review and editorial processes.

4.1 Abstract

Estimation of forest leaf area index (LAI) from airborne laser scanning (ALS) offers improved accuracy but study specificity has led to a proliferation of approaches. Our goal was to develop ALS-LAI models for stands of *Pinus radiata* D. Don in New Zealand. To achieve this, we addressed the following methodological questions: (1) Identification of important covariates from an extensive list of lidar metrics with empirical or theoretical links to LAI. (2) Evaluation of the impact of lidar plot radius on metric importance and model accuracy by trialling fixed radii and radii based on mean top height (MTH). (3) For ratio metrics, which depend on the selection of a height threshold (HT), identification of the optimum fixed HT and to evaluate the use of a novel variable HT set as a percentage of canopy height (CH). Custom lidar processing software was used to evaluate all combinations of metric, radius, and HT. For model development, we used: (a) elastic net linear regression for regularisation and variable selection, (b) random forests (RF) to explore potential nonlinear relationships and to provide insight into variable importance through use of conditional importance scores, and (c) semi-physical models based on the Beer-Lambert law and fitted using a proxy for ALS pulse penetration. Field observations of LAI (n=135) were acquired using the LAI-2200C with minimal seasonal influence. Elastic net models using variable radius plots performed best with the lowest RMSE=0.57 LAI at radius=100% of MTH and HT=20% of CH. Models with low RMSE often had radii in the range of canopy height - supporting theoretical links to instrument view distance. The best fixed radius model (RMSE=0.64) was located at radius=20 m and HT=20% of CH. RF results showed little evidence for nonlinear relationships (lowest RMSE=0.64). Both elastic net and RF showed: (1) Using field plot radius (14 m) and instrument height (HT=1.4 m) produced weak models; (2) RMSE generally decreased with increasing radius; (3) above radius=16 m, HT had a greater influence on model RMSE and, for elastic net, model sparsity; (4) Nearly all of the frequently selected variables in elastic net models were ratio metrics quantifying canopy gap fraction, and many of these were also assigned high RF conditional importance scores. Semi-physical models showed good agreement with field measurements of LAI (RMSE=0.72). This approach may offer a means of estimating LAI without calibration by inverting the Poisson model using gap fraction from lidar and an empirical projection coefficient.

4.2 Introduction

Leaf area index (LAI) in coniferous forests is defined as one-half the total green leaf surface area per unit ground area (J. M. Chen et al., 1997). Forest LAI is a key ecophysiological parameter with close links to canopy light use, water interception, and a range of biochemical and ecosystem processes (Bréda, 2008). Managers of forests used for production values face increasing pressure to lift output per unit area as resource pressures increase. Precision management approaches are increasingly being sought to achieve this objective. LAI is a good candidate for fine-scale information that may be used to target and monitor silvicultural treatments. Measurable increases in LAI can be obtained with site treatments such as fertilisation or irrigation (Brix & Mitchell, 1983; Raison & Myers, 1992). Defoliating events such as insect attack can also be identified through changes in LAI (Solberg et al., 2006).

4.2.1 Remote sensing of LAI

Despite the importance of LAI in forest ecosystems, difficulties in measurement have limited the range of practical applications. *In-situ* measurement of LAI over large areas of forest is labour intensive, and forest LAI shows high levels of spatiotemporal variation (Bréda, 2003). Measurements must usually be obtained by optical instruments. In practice, plant area index is measured, which includes all light blocking canopy elements (Woodgate, Jones, et al., 2015). Techniques based on spectral indices such as the normalised difference vegetation index (NDVI), the simple ratio (SR), and the reduced simple ratio (RSR) derived from multispectral imagery have shown promise for large-scale LAI estimation (Stenberg et al., 2004). However, sensor saturation in areas of high LAI, interference from background vegetation, canopy gap distribution, and processing difficulties frequently reduce the accuracy of spectral-LAI estimates, restricting the usefulness of these approaches (Carlson & Ripley, 1997; Jensen et al., 2011; Turner, Cohen, Kennedy, Fassnacht, & Briggs, 1999).

Airborne discrete laser scanning (ALS or airborne lidar) has emerged as a valuable tool for large-scale assessment of LAI in forested areas where spectral methods may be unsuitable. Strong relationships (R^2=0.78) have been found between *in situ* measurements of LAI and ALS data from intensively managed pine plantations, and correlations were observed between the values of lidar metrics and stand silvicultural treatments (Peduzzi et al., 2012). Similar strong relationships between LAI and ALS data have been observed in a range of natural and mixed forest types (Jensen et al., 2008; Morsdorf et al., 2006; Riaño et al.,

2004). The strength of ALS-LAI relationships has facilitated detection and monitoring of insect attack in a Norwegian Scots pine (*Pinus sylvestris* L.) forest (Solberg et al., 2006) and large-scale mapping of LAI. For example, Solberg et al. (2009) found a strong relationship between LAI and a semi-physical ALS-based proxy (R^2=0.92–0.93) and used the relationship to map LAI over a large area dominated by Norway spruce (*Picea abies* L.). The improved accuracy of ALS-LAI estimates has also facilitated the validation of large-scale spectral-LAI data products. For example, aggregation of superior ALS-LAI estimates facilitated identification of important deficiencies in GLOBCARBON LAI products (K. Zhao & Popescu, 2009) and overestimation of LAI in some MODIS products (Jensen et al., 2011).

4.2.2 Development of ALS-LAI models

The development of ALS-LAI models discussed so far can be broadly divided into empirical and theoretical approaches. The empirical approach uses, for example, subset regression to develop models of *in situ* LAI from lidar metrics (e.g. Griffin et al., 2008; Jensen et al., 2011, 2008; Peduzzi et al., 2012; Pope & Treitz, 2013). In the theoretical approach, parallels are drawn between optical LAI measurements, obtained by application of the Beer-Lambert law to measurements of light extinction through the canopy (Jonckheere et al., 2004), and the penetration rate of lidar pulses through the canopy. This is usually achieved by constructing a metric from ALS data sensitive to the penetration of laser pulses to levels within the canopy (e.g. Hopkinson & Chasmer, 2007b; Korhonen et al., 2011; Morsdorf et al., 2006; Solberg et al., 2009, 2006). Although the form of these models may vary, all require common methodological decisions in order to establish predictive relationships, and these decisions can have significant impacts on model performance (Riaño et al., 2004; Richardson et al., 2009; K. Zhao & Popescu, 2009).

First, lidar data coincident with *in situ* LAI measurements must be extracted to compute lidar metrics. A common choice is to set the lidar plot radius equal to that used to collect field plot data (e.g. Jensen et al., 2008; Peduzzi et al., 2012). However, the optical instruments used to acquire *in situ* LAI measurements may view canopy elements beyond field plot boundaries, and ALS-LAI models have been shown to improve with increasing plot radii, often reaching maximum agreement at radii in excess of the defined field plots (e.g. Morsdorf et al., 2006; Richardson et al., 2009; K. Zhao & Popescu, 2009). An alternative is to define lidar plot radius as some multiple of canopy height (e.g. Riaño et al., 2004; Solberg et al., 2009). This approach is supported by the optical theory underpinning common LAI instruments where maximum view distance can, in part, be determined by canopy height (LI-

COR, 2015). The choice of variable radius is not clear, with reported optimum values ranging from 75% of canopy height (Solberg et al., 2009) to 100% of canopy height (Riaño et al., 2004)

After extraction, the lidar data must be described so as to capture the underlying canopy properties related to light penetration, and hence LAI. A wide range of metrics have been used to estimate LAI, including standard descriptive metrics such as height percentiles, descriptive statistics, and distributional statistics for return elevations (e.g. Beets et al., 2011; Jensen et al., 2008; Pope & Treitz, 2013). An important class of metrics for ALS-LAI relate to the penetration of the laser beam through the canopy, and metrics of this type have been widely used in the development of ALS-LAI models (Morsdorf et al., 2006; Peduzzi et al., 2012; Solberg et al., 2009, 2006). The use of these metrics is also supported by theoretical links to the Beer-Lambert law relating extinction of light through the canopy to gap fraction, LAI, and related properties (Leblanc et al., 2005). However, physical differences between ALS pulses and solar radiation, such as footprint size and campaign effects on pulse energy dispersion make these models semi-physical at best (K. Zhao & Popescu, 2009). Alternative approaches seek to use these distinctive properties of ALS pulses by exploiting intensity data from returning lidar pulses as a more direct analogue of solar radiation absorption through the canopy (Hopkinson & Chasmer, 2007b, 2009).

A common feature of penetration related metrics is the selection of a height threshold (HT) around which ratios of intensity sums or return counts are computed. The value used for the HT is frequently set at instrument or field measurement height (Peduzzi et al., 2012; Solberg et al., 2009). Where alternatives have been trialled ALS-LAI models strongly benefited from increased HTs, with the optimum HT found to be well above instrument height (K. Zhao & Popescu, 2009). Numerous ratio metrics have been highlighted in previous ALS-LAI studies but a comparison of more than a few ratio metrics has not been done. In addition, the optimum choice of height threshold has only been examined for a small subset of these metrics.

More sophisticated metrics attempt to increase information content by considering the distribution of returns at the sub-plot level. For example, lidar analogues to ecological complexity indexes, stratified crown closure indices, and stratified measures of mean canopy closure computed from sub-pixels within the plot have all been found to be useful in the development of ALS-LAI models (Griffin et al., 2008; Pope & Treitz, 2013). Theoretically, metrics based on sub-pixels may be able to capture additional information, but their

performance has not been tested against the many alternative metrics used for ALS-LAI estimation.

The final methodological choice requires selection of a modelling approach for ALS-LAI estimation. As mentioned, subset regression has been frequently used. For pulse penetration metrics, it is common for a linear relationship to be sought between LAI and a single log-transformed penetration metric, often using regression forced through the origin in order to adhere more closely to LAI theory and produce intuitive results (Korhonen et al., 2011; Solberg et al., 2009). Zhao and Popescu (2009) caution that the correct choice of model form for ALS-LAI is not yet well defined, and must be determined in each case by the modeller. The authors strongly recommended exploration of modern non-parametric statistical learning approaches for ALS-LAI estimation.

4.2.3 Study objectives

Our primary objective was to develop ALS-LAI models for stands of pure *Pinus radiata* D. Don in New Zealand. Our secondary objective was to examine the methodological questions previously highlighted, namely: (1) To assess the impact of lidar plot radius on ALS-LAI estimates by evaluating models constructed using data from a range of fixed radii, and using variable radii based on canopy height. (2) For those metrics where an HT must be specified, we sought to identify the impact of this choice by constructing these metrics using a wide range of fixed and variable HTs. (3) To identify those lidar metrics most closely related to LAI by comparing an extensive list of metrics previously proposed or used in the construction of ALS-LAI models. (4) To trial the use of modelling approaches capable of handling the large number of candidate variables alongside simpler semi-physical models. A key aim of our study was to address the need for an integrated assessment of these choices in order to test for interactions between lidar plot radius and height threshold on metric choice and modelling approach on the accuracy of LAI estimates.

4.3 Materials

4.3.1 The forest

The study was conducted in Kaingaroa forest located on New Zealand's North Island (Fig. 4.1). The forested area covers approximately 180,000 ha, and 90% of this is planted *P. radiata*. Stands are usually even-aged, and silvicultural treatments such as pruning of lower branches, thinning, and disease control are frequently employed. Understory vegetation

varies with stand condition and canopy closure. Younger stands frequently contain grasses, gorse (*Ulex europaeus* L.), and broom (*Cytisus scoparius* L.) to around 1 m. In more mature stands tall tree ferns (*Cyathea spp.* and *Dicksonia spp.)* are observed more frequently. The density of these tree ferns varies from isolated individuals to dense groves in some places. These ferns frequently grow to over 10 m tall and exhibit large fronds with individual blades often exceeding 3 m in length. Blackberry (*Rubus fruticosus* L. agg.) is pervasive on the forest floor, frequently reaching very high densities, but stems seldom exceed 1.5 m in height.

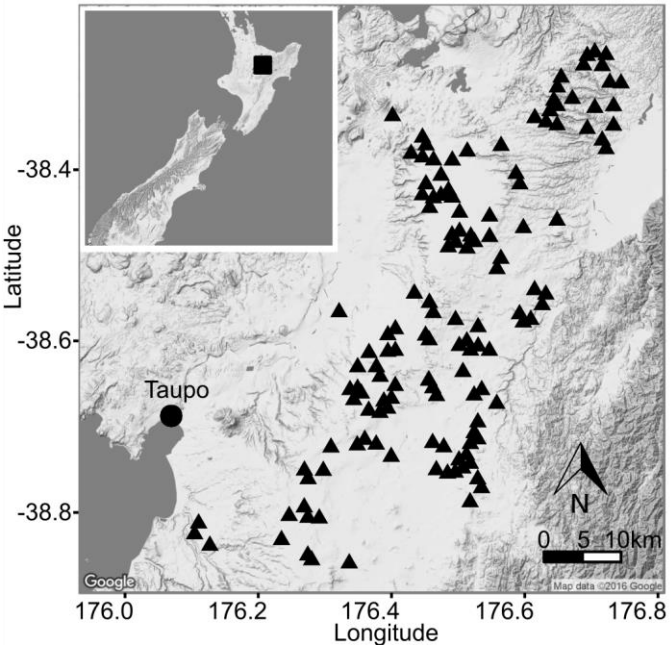

Fig. 4.1. Geographic location of Kaingaroa forest, New Zealand. Triangles show the location of LAI plots.

4.3.2 Inventory and LAI plots

A total of 500 inventory plots were established across Kaingaroa in preparation for the acquisition of forest-wide airborne lidar. Plots were located at the intersections of a grid with a randomised orientation and start point overlaid onto the study forest. Plot centres were located using a Trimble Geo6000 XH GNSS (Trimble Navigation Ltd., Sunnyvale, CA, USA), and slope adjusted plot radius of approximately 14 m (0.06 ha) was used when collecting inventory data. Inventory measurements included diameter at breast height (DBH=1.4 m in New Zealand) and heights of selected well-formed stems. The heights of unmeasured trees were predicted using a regression model between DBH and height fitted for each plot. These data were used to compute mean top height (MTH) for all plots. MTH is defined as the average height of the 100 largest diameter trees per hectare. In New Zealand, MTH is widely used to compute the Site Index measure of stand productivity and can be

estimated from lidar data (M. S. Watt et al., 2015). For our study, we identified a subset of plots from stands aged greater than 10 to ensure canopy closure. LAI field work was constrained to the time period between lidar acquisition in the autumn (March 2014) and the expected onset of needle extension in spring (September 2014). Plots were selected for inclusion in the study at random without replacement. However, lack of suitable location for a reference sensor (see 4.3.3), harvesting operations, or poor access occasionally necessitated substitutions to be made in a few instances. In total, LAI measurements were acquired in 135 plots. Table 4.1 provides summary statistics for the measured plots.

Table 4.1. Summary statistics including standard deviation (SD) for measured plots (*n*=135). SE LAI gives the standard error of LAI.

Variable	Min	Max	Mean	Median	SD
Age class (years)	10	36	19.1	17.8	5.7
Stand density (stems / ha)	166.7	916.7	413.9	400.0	131.1
Mean top height (m)	13.8	42.8	19.2	29.5	7.1
LAI	1.36	6.69	4.01	4.02	1.01
SE LAI	0.03	0.27	0.12	0.11	0.05

4.3.3 LAI measurements

Hemispherical canopy photography (HCP) (J. M. Chen, Black, & Adams, 1991) and the LAI-2000/LAI-2200 (LI-COR Biosciences Inc., Lincoln, NE, USA) are frequently used to collect *in situ* LAI measurements for ALS-LAI studies (e.g. Morsdorf et al., 2006; Jensen et al., 2008). Both instruments require the collection of measurements under diffuse sky conditions i.e. sunset, sunrise, or uniform overcast skies. This greatly constrains the number of measurements obtainable in a given period, and violation of these assumptions can cause underestimation of LAI (Solberg et al., 2009). To overcome this, we chose to use the LI-COR LAI-2200C, which represents an update of the LAI-2000/LAI-2200. This iteration allows LAI measurements to be collected under both diffuse and clear sky conditions. The principle of operation remains the same – the instrument uses five concentric rings centred at zenith angles of 7°, 22°, 38°, 52°, and 68° observing below canopy radiation levels in the blue band (320–490 nm). These data are combined with above canopy readings to compute an estimate of gap fraction (transmittance) from each sensor ring. LAI is then obtained by inversion of the Beer-Lambert law (LI-COR, 2015). Clear sky measurements are achieved through the use of a scattering correction model (Kobayashi et al., 2013). This model reduces the influence of scattered radiation from canopy elements on the instrument's estimates of gap fraction, which would usually cause underestimates of LAI. In total 58 plots were measured using the clear

sky method and 77 plots were measured either at sunset or under diffuse overcast skies. To minimise differences due to sky condition we applied the method of Pearse, Watt, and Morgenroth (2016) who showed strong agreement between clear and diffuse sky measurements in the same forest (8% mean difference, R^2=0.94) when the outer ring was masked from analysis and measured needle spectra were used to compute the scattering correction.

All measurements were collected using a pair of LAI-2200C sensors, with the reference sensor located in the closest suitable clearing. Sky condition and size of available clearings necessitated the use of 90° or 180° view caps to restrict both sensors' field of view. Clear sky measurements required the following additional steps: (1) the view direction for both sensors kept the sun slightly behind the sensors field of view in order to reduce differences between observed gap fraction and values predicted by the one-dimensional scattering correction model, (2) hemispherical sky light intensity was measured from an isotropic, cloud free, region of sky with a view cap 90° larger than that used in the plots, and (3) the fraction of diffuse radiation was measured directly after (2) by fitting a halon 'diffuser' cap to the instrument (Kobayashi et al., 2013; LI-COR, 2015).

In the forest, plot layout was adapted from similar studies using the LAI-2200C in coniferous forests (Majasalmi, Rautiainen, Stenberg, & Rita, 2012; Solberg et al., 2009) to suit the existing inventory plot layout. LAI measurements were collected at plot centre and at 3 m in each cardinal direction. To compensate for differences in the fraction of canopy observed, and to ensure low standard error of LAI, additional measurements were collected at random within the plot to achieve a total of n=18 or n=25 for the 180° and 90° view caps respectively. These data were combined with GPS records of measurement time and location to compute the scatter corrected LAI values (LI-COR, 2015). LAI data are summarised in Table 4.1.

4.3.4 Lidar data

Discrete aerial lidar data were acquired between January and March 2014 using an Optech ALTM 3100EA Pegasus scanner. The lidar system collected data at 100 kHz, with a maximum scan angle of 12° off nadir, and approximate swath overlap of 25%. The sensor recorded a maximum of 4 returns per pulse, with an average density of 11.5 points m^{-2} achieved over the area. Initial processing was conducted by the supplier. Ground and other return types were classified using Terrasolid TerraScan (Terrasolid Ltd., Helsinki, Finland), followed by manual reclassification where required. We conducted secondary processing to

remove moderate levels of high and low noise using a filtering algorithm. Following this, return elevation values were height normalised using a digital terrain model (DTM) constructed from ground classified points.

4.4 Methods

4.4.1 Lidar metrics

Based on an extensive review of the literature we assembled a comprehensive list of metrics with theoretical or empirical links to LAI. We observed a common approach in the ALS-LAI literature whereby the set of metrics available from lidar processing software such as FUSION (McGaughey, 2015) and LAStools (Rapidlasso GmbH, Germany) are combined with more complex or theoretically motivated metrics to form the basis for model development (e.g. Jensen et al., 2011, 2008; Peduzzi et al., 2012; Pope & Treitz, 2013). While heuristic clues are sometimes used to guide the process of variable selection (K. Zhao & Popescu, 2009), the list of metrics found to be useful showed great variability regardless of the theoretical linkages. Therefore, we expanded our list of metrics to include most of those available from the aforementioned software tools. A secondary motivation for including these metrics comes from the fact that they are relatively easy and efficient to compute, making them appealing candidates for large-scale ALS-LAI assessment.

To establish the optimal plot parameters for constructing these metrics we divided metrics into those impacted only by plot radius (height metrics), and those impacted by plot radius and selection of an HT (ratio metrics). A third class was introduced to account for metrics that fell outside of these conditions, such as those based on sub-plot analysis (complex metrics). Details and descriptions of the metrics in these classes are provided in the following sections. We adopt the terminology shown in Table 4.2 to describe lidar returns according to the LAS 1.4 properties *number of returns* and *return number* (Graham, 2012) attached to each return.

Table 4.2. Lidar terminology describing returns according to the LAS properties: *return number* and *number of returns*. Subscripts A and B are added in Tables 4.3-4.5 to denote returns with heights above and below a chosen height threshold HT.

Type abbreviation	Returns	Return number	Number of returns
AR	All returns	1, 2, 3, 4	1, 2, 3, 4
SR	Single returns	1	1
FMR	First of many returns	1	> 1
FR (=SR+FMR)	First returns	1	1, 2, 3, 4
INR	Intermediate returns	2, 3, 4	> return number
LR (=SR+LMR)	Last returns	=number of returns	1, 2, 3, 4
LMR	Last of many returns	=number of returns	2, 3, 4

4.4.1.1 Height metrics

Metrics in this class are impacted only by the choice of plot radius defining which returns are included. The full list of height metrics assembled for our study is given in Table 4.3, and additional details and rationale are provided for the following metrics:

(1) For canopy density metrics based on specified heights (Næsset, 2002) we used no minimum height threshold and set the maximum height to the value of the 99.9th percentile to guard against unobserved high noise.

(2) Pearson's second skewness coefficient (PMedSkew) was included on the basis that this statistic offers a standardised description of the distance between the mean and median (Doane & Seward, 2011), which may reflect canopy openness.

(3) The mode was nearly always 0 at any radius when ground returns were included, so a vegetation mode (VegMode) was computed from all returns above 0.5 m. The mode was determined as the mid-point of the bin with the highest return count from a histogram with 0.5 m wide bins.

We initially included the approach by Jensen et al. (2008) of calculating the difference between canopy-only percentiles (using returns above DBH) and percentiles using all returns (e.g. the 50th percentile minus the 40th percentile). However, the number of permutations was high and values showed high intercorrelation. These metrics were screened according to the methods outlined in Section 4.4.3 to exclude permutations with excessive intercorrelation.

Table 4.3. Summary of height metrics calculated using data extracted from plots with variable and fixed radii (see 4.4.2) and trialled in models of LAI from ALS data. Raw return intensity values are denoted by *int* and return counts are denoted by *num*. All other metrics were computed from the normalised return heights in metres. Lidar terminology is described in Table 4.2. Sources including FUSION or LAStools indicate metrics available as standard outputs from software tools of the same name.

Metric / variable name	Sources	Name in source	Metric details	Notes
AAD	FUSION	Absolute average deviation	AAD of AR	Defined as per McGaughey (2015).
ADMedian	FUSION	Median absolute deviation from the median	MADmedian of AR	Defined as per McGaughey (2015).
ADMode	FUSION	Median absolute deviation from the mode	MADmode of AR	Defined as per McGaughey (2015), but using VegMode
Canopy densities: b(10, 20, 25, 30, 40,…, 90, 95, 99)	Næsset et al. (2002), Peduzzi et al. (2012), LAStools	Canopy densities (bincentiles)	bx = *num* AR_B / *num* AR Where HT = p99.9(x/100)	See 4.4.1.1 for further details. Note irregular cut-offs.
CanopyRR	FUSION	Canopy relief ratio	(Mean – Min) / (Max – Min) of AR	
Cube Mean	FUSION	Cubic mean	M_3 of AR	Defined as per McGaughey (2015).
CV	FUSION, LAStools, Pope and Treitz (2013)	Coefficient of variation	MeanZ / STDev of AR	Precursors: MeanZ, STDev
FR_All	Pope and Treitz (2013)	DA	FR / AR	
Imean	Peduzzi et al. (2012), FUSION	Int mean / Imean	Mean *int* of AR	Raw intensity values used
IQR	FUSION	Interquartile range	p75 – p25 of AR	Precursors: p75, p25
Kurtosis	FUSION, LAStools	Kurtosis	Kurtosis of AR	Defined as per McGaughey (2015).
Lmom_CV	FUSION	L-moment coefficient of variation	τ_2 of AR	Defined as per Hosking (1990)
Lmom_Kurtosis	FUSION	L-moment kurtosis	τ_4 of AR	Defined as per Hosking (1990)
Lmom_Skew	FUSION	L-moment skew	τ_3 of AR	Defined as per Hosking (1990)
Lmom1-Lmom4	FUSION	L-moments (L1, L2, L3, L4)	(λ_1, λ_2, λ_3, λ_4) of AR	Defined as per Hosking (1990)
MeanZ	FUSION, LAStools	Mean	Mean of AR	
MeanZFirst	Zhao and Popescu (2009)	*H*sr + fr	Mean of FR	FR = SR + FMR
Percentiles: p(10, 20, 25, 30,…, 90, 95, 99, 99.9)	Beets et al. (2011), FUSION, LAStools, Peduzzi et al. (2012)	Height percentiles / quantiles	Height percentiles of AR	Defined as per McGaughey (2015).

Table 4.3 continued

Metric / variable name	Sources	Name in source	Metric details	Notes
PMedSkew	Novel	Pearson's second skewness coefficient	3(Mean – Median) / σ of AR	See 4.4.1.1 for details
Product percentiles: (p30-p20, p50-p40, p60-p50)	Jensen et al. (2008)	Percentile differences	p*i* – p*j* of AR, where i > j	See 4.4.1.1 for details
QuadMean	FUSION, LAStools	Quadratic mean	M_2 of FR	Defined as per McGaughey (2015).
Skew	FUSION, LAStools	Skewness	Skewness of AR	Defined as per McGaughey (2015).
STDev	FUSION, LAStools	Standard deviation	SD of AR	
VegMode	FUSION	Mode	Mode of AR_A, HT = 0.5 m	See 4.4.1.1 for details

4.4.1.2 Ratio metrics

We used a narrow definition of ratio metrics as any metric where the calculated ratio depends on the choice of height threshold (HT) and plot radius. This excludes related metrics such as the canopy relief ratio and the ratio of first returns to all returns (CanopyRR, FR_all Table 4.3) that compute ratios but are invariant to changes in HT. This limited definition allowed us to address the uncertainty surrounding the choice of optimum HT for metrics of this type and to assess changes in metric importance within and between classes in response to HT. In contrast to height metrics, only a few ratio metrics were standard outputs from lidar processing software with the majority originating from previous ALS-LAI studies. Conceptually, these metrics offer a link between the penetration of laser pulses through the canopy and physical factors influencing LAI such as canopy density, canopy length, and fraction of cover. However, the exact form of these metrics is not clear and a large number have been used in ALS-LAI studies (see Table 4.4). Several of these metrics required adaptation to suit our study. For example, the metrics proposed by Zhao and Popescu (2009) and Morsdorf et al. (2006) are based on two returns per pulse, where we had a maximum of four returns per pulse. Wherever adaptation was required we attempted to retain the conceptual link between LAI and ratio metrics. Details of the ratio metrics utilised in our study are provided in Table 4.4. The majority of these metrics count returns by type above or below the HT; however, the following metrics deviated from this pattern or required special consideration:

(1) Several metrics utilised the mean height of all returns as an HT. We substituted a vegetation mean (VegMean, Table 4.4) calculated as the mean height of all returns above the chosen HT. This allowed the VegMean to vary with HT and made the dependent metrics more sensitive to the location of returns within the crown by excluding ground returns and, at higher HTs, understory and lower canopy returns.

(2) Similarly, the percentage of first returns above the mode was modified to use the vegetation mode (VegMode, Table 4.4) computed from returns above the HT. In practice, the mode was generally insensitive to changes in HT once ground returns were excluded. Nonetheless, we included this value because of an observed association between the location of the vegetation mode and mid-crown height (Peduzzi et al., 2012).

(3) The intensity based ratio metrics of Hopkinson and Chasmer (2009) (IR, IR_BL, Table 4.4) were included for their ability to link absorption of pulse power by canopy elements to fraction of cover, which is closely related to LAI.

(4) The LAI proxy (MLP, Table 4.4) proposed by Morsdorf et al. (2006) depends only on canopy returns and must be adjusted for the fraction of cover (fCover) within the scene. Morsdorf et al. (2006) used HCP estimates of fCover from 0–10° zenith angle. We opted to use the mean gap fraction from the first two rings of the LAI-2200C. This was to account for the wider scan angle of our lidar data (0–12° vs 0–7.15°) and because in strongly clumped canopy types the inner ring alone (centred at 7°) is known to provide poor estimates of gap fraction (Solberg et al., 2009). Following the method proposed by Morsdorf et al. (2006), we developed a regression model predicting fCover using lidar data. Canopy cover (CCov, Table 4.4) at radius=12 m and HT=1.4 m (instrument height) provided the best estimate of fCover as measured by rings 1 and 2 of the LAI-2200C. Predicted values for scenes computed with larger radii were used to adjust corresponding values of MLP.

(5) Penetration metrics used by Zhao and Popescu (2009) were adapted for use with multiple return lidar while attempting to retain the link with canopy penetration (ZP metrics, Table 4.4). Where required, we substituted the number of first returns (FR) as a proxy for the number of pulses. Inspection of several plots showed split pulses across the lidar trap had a negligible impact on estimated number of pulses.

(6) Solberg's Cover Index (SCI, Table 4.4) assigns a lower weighting (λ) to intermediate returns. Solberg et al. (2009) used λ=0.5 but suggested this value may be tuned. We computed SCI at λ=(0.1, 0.2, …, 0.9). The resulting metrics were highly correlated (lowest r=0.97), but all showed similar correlations to LAI. We opted to use the suggested weighting of 0.5 to reduce dimensionality and metric inter-correlation during model development.

Table 4.4. Summary of ratio metrics computed at a range of plot radii and height thresholds (HT) (see 4.4.2) and used to develop ALS-LAI models. VegMean and VegMode were precursor metrics only. Intensity metrics IR and IR_BL used raw intensity values. All other metrics used counts of returns by type and position relative to the HT as defined in Table 4.2. Sources including FUSION or LAStools indicate metrics available as standard outputs from software tools of the same name. Subscripts A and B are added to denote returns with heights above and below a chosen height threshold HT.

Metric / variable name	Sources	Name in source	Metric details	Notes
CCov	FUSION, LAStools, Beets et al. (2011), Morsdorf et al. (2006)	Canopy cover, FCLidar(FR)	FRA / FR	Equivalent to FCI (Korhonen et al., 2011) when FRA = SRA + FMRA
CDens	FUSION, LAStools, Riaño et al. (2004), Hopkinson and Chasmer (2009)	Canopy density, FCLidar(RR)	ARA / AR	
FaZ_All	Pope and Treitz (2013)	DV	FRA / AR	
IR	Hopkinson and Chasmer (2007b, 2009)	Intensity ratio		
IR_BL	Hopkinson and Chasmer (2007b, 2009)	Beer's law intensity ratio	$1-\left(\frac{\left(\frac{\sum \mathrm{SR_B}}{\sum \mathrm{AR}}\right)+\sqrt{\frac{\sum \mathrm{LR_B}}{\sum \mathrm{AR}}}}{\left(\frac{\sum \mathrm{FR}+\sum \mathrm{SR}}{\sum \mathrm{AR}}\right)+\sqrt{\frac{\sum \mathrm{INR}+\sum LR}{\sum AR}}}\right)$	
LCI	Korhonen et al. (2011)	Last echo cover index	LRA / LR	
lnSD	Solberg et al. (2006), Richardson et al. (2009)	ln(Na/Nb), -ln(Rg/Rt)	-ln(FRB / FR)	
MLP	Morsdorf et al. (2006)	N LAI, canopy	FRA / LRA	Canopy returns only
NaMean_First	Adapted from FUSION	Num above VegMean as % of first	ARA / FR, HT=VegMean	
NaMode_First	Adapted from FUSION	Num above VegMode as % of first	ARA / FR, HT=VegMode	See Section 4.4.1.1 for VegMode
NaZ_First	FUSION	Num above HT as % of first	ARA / FR	
nLAI	Morsdorf et al. (2006)	N LAI, scene	MLP fCover	fCover described in Section 4.4.1.2
PAaVegMean	Adapted from FUSION	% all above VegMean	ARA / AR, HT=VegMean	See Section 4.4.1.2 for details.

Table 4.4 continued

Metric / variable name	Sources	Name in source	Metric details	Notes
PAaVegMode	Adapted from FUSION	% all above VegMode	ARA / AR, HT=VegMode	See Section 4.4.1.1 for VegMode
PFaVegMean	Adapted from FUSION	% first above VegMean	FRA / FR, HT=VegMean	See Section 4.4.1.2 for details.
PFaVegMode	Adapted from FUSION	% first above VegMode	FRA / FR, HT=VegMode	See Section 4.4.1.1 for VegMode
SCI	Solberg et al. (2009), Korhonen et al. (2011), Heiskanen et al. (2015)	P, SCI	SRB + λ (FMRB + LMRB) / SR + λ (FMR + LMR)	λ=0.5, see Section 4.4.1.2
VegMean		Mean height of returns above HT	Mean height of AR ≥ HT	See Section 4.4.2 for HT values.
VegMode		Modal height of returns above HT	Modal height of AR ≥ HT	Mode described in Table 4.3. See Section 4.4.2 for HT values.
ZP_Rg_p	Zhao and Popescu (2009)	r grd / pulse	ARB / FR	FR proxy for pulses.
ZP_Rig_p	Zhao and Popescu (2009)	r in+grd / pulse	(INRA + ARB) / FR	FR proxy for pulses.
ZP_Rig_t	Zhao and Popescu (2009)	r in+grd / total	(INRA + ARB) / AR	
ZP_Rsrg_p	Zhao and Popescu (2009)	r sr^grd / pulse	SRB / FR	FR proxy for pulses.
ZP_Rsrg_t	Zhao and Popescu (2009)	r sr^grd / total	SRB / AR	

4.4.1.3 Complex metrics

The metrics shown in Table 4.5 are not available as standard outputs and most require more complex point cloud processing or estimation of additional parameters. The definition and construction of these metrics were implemented as follows:

(1) Pope and Treitz (2013) estimated canopy closure above height *z* (cc_z, Table 4.5) by dividing the plot into regular size sub-pixels and counting the number that contained returns ≥ *z* as a proportion of all pixels. The correct value for *z* and the pixel size must be determined empirically. We chose a finer grid of 1 x 1 m pixels (2.5 m in the original study) to compensate for the higher return density of our lidar and calculated the canopy closure at a range of heights. Our method trialled plots with larger perimeters; therefore, we adopted a stricter boundary condition whereby only sub-pixels with a centre on or within the perimeter were processed.

(2) Peduzzi et al. (2012) found crown density slice metrics to be useful in ALS-LAI models. These metrics were derived from equally sized slices (height bins) taken around the modal value of vegetation returns (above 1 m in their study). We adapted this concept as follows: (1) VegMode (Table 4.3) height was taken as the mid-point of a central 1 m bin (CD0, Table 4.5), with 5 x 1 m bins defined either side. (2) Points within each bin were used to compute a range of statistics (CD metrics, Table 4.5). We did not have data to identify a strong correlation between mid-crown height and the mode (Peduzzi et al., 2012). Instead, VegMode was most strongly correlated with the 30th percentile, suggesting the bulk of returns were centred lower in our study. As a result, the lowest three slices (CD-3, CD-4, CD-5, Table 4.5) frequently contained no or few returns and were excluded from analysis.

(3) The laser penetration index (LPI, Table 4.5) is computed from the ratio of ground to total points (Barilotti, Turco, & Alberti, 2006). Peduzzi et al. (2012) adapted LPI to successfully predict LAI in planted forests similar to our study site. Under their definition (Table 4.5) LPI does not change with HT and so was not included as a ratio metric. Ground returns were a very small fraction of first returns in our data. Therefore, we counted any returns classed as ground.

(4) The mean free path (MFP) of successive lidar returns (MFP, Table 4.5) has been used as a proxy for foliage density and for ALS-LAI estimation (K. Zhao & Popescu, 2009). The minimum MFP is constrained by the ‘dead time’ that limits the sensor’s

ability to record subsequent returns. However, a high density of canopy elements should reduce the average distance between successive returns. We treated SRs as pulses with MFP=0 and used GPS times from other returns used to reconstruct pulses, exclude stray pulses originating outside the plot, and compute MFP between successive returns within the canopy (returns > 2 m).

(5) Griffin et al. (2008) found the voxel-based metrics proposed by Popescu and Zhao (2008) to be useful for ALS-LAI estimation. In this approach, the plot is divided into sub-pixels (2.5 x 2.5 m in Griffin et al. (2008)), with further division along the vertical axis according to the number of height bins *HB.* The number of returns in each voxel is divided by the sum of all returns within the same vertical column and the percentage canopy cover (PCC metrics, Table 4.5) is given by:

$$PCClidar_{LB-UB} = \sum_{LB}^{UB} HB_n \qquad 4.1$$

Where HB*n* denotes each bin located between the lower (LB) and upper (UB) bin numbers. We used the same bin definitions and summed PCC from LB = bin 5 to UB = bin 11 (Table 4.5). As with VCI (d), we refined the sub-pixel size to 1 x 1 m and calculated the plot mean average *PCClidar* from sub-pixels meeting the same boundary conditions.

(6) The vertical complexity index (VCI) (Van Ewijk, 2015) has been proposed as a lidar specific adaptation of ecological diversity indices with links to canopy structural properties and LAI (Pope & Treitz, 2013). After dividing the point cloud equally along the vertical axis into *HB* height bins VCI is then computed as:

$$VCI = \frac{-\sum_{i=1}^{HB}\left(p_i(\ln(p_i))\right)}{\ln(HB)} \qquad 4.2$$

Where $p_i$is the number of returns within each height bin as a proportion of the total number of returns. The number of bins must be determined empirically and has a significant impact on VCI (Van Ewijk, 2015). We calculated VCI using bins of height= 0.5, 1, …,3 m with the number of bins dependent on a maximum height fixed according to the tallest plots in the study area.

Table 4.5. Summary of additional metrics computed at a range of plot radii and included in the development of ALS-LAI models. Where permutations of a variable were trialled, new variable names were formed from the base variable name and values.

Metric / variable name	Sources	Name in source	Metric details	Notes
CC_zh h = 3, 6, …, 15 m	Pope and Treitz (2013)	Crown closure ≥ X (ccX)	Number of 1 x 1 m sub-plot pixels containing returns with height ≥ h / Total pixels	See Section 4.4.1.3 for detailed description
CDh h = -2, -1, …, 5 m CDh_cv CDh_sd CDh_kurt CDh_skew CDh_prop	Peduzzi et al. (2012)	Canopy density (CD) slices	Statistics computed from height values of returns in 8 1 m slices CDi around VegMode. cv = coefficient of variation, sd = standard deviation, kurt = kurtosis, skew = skewness, prop = proportion of all returns in slice.	CD-3,-4,-5 dropped – see Section 4.4.1.3 for details
LPI	Barilotti et al. (2006), Peduzzi et al. (2012)	Laser penetration index	AR Ground / FR	Ground = class 2, see Section 4.4.1.3
MFP, ln(MFP)	Zhao and Popescu (2009)	lfree	Mean distance between consecutive returns in the plot.	See Section 4.4.1.3 for details
Pcc_nLB_nUB Z bin edges=[0, 0.5, 1, 1.5, 2, 5, 10, 15, 20, 25, 30, >30]	Popescu and Zhao (2008), Griffin et al. (2008).	Percentage canopy cover (PCClidar)	Returns in 1 x 1 x Z bins as a fraction of total returns in the column. Summed from LB to UB. Last bin full open.	See Section 4.4.1.3 for detailed description
VCI_h h = 0.5, 1, …,3 m	Van Ewijk (2015), Pope and Treitz (2013)	Vertical complexity index	VCI defined in equation (4.1) h = bin width, HB = (0-max canopy height) / h	Max canopy height from plots

4.4.2 Plot parameters and lidar processing

To identify the optimum choice of plot radius and, where applicable, height threshold at which to construct lidar metrics we followed an approach similar to Zhao and Popescu (2009). Lidar data were extracted at a range of fixed plot radii ranging from 8 m to 30 m in 2 m increments. Ratio metrics were computed at fixed HTs of 0.5, 1, 1.4, 2, 2.5, …, 10 m (1.4 m coincided with DBH and instrument height). Following Solberg et al. (2009) we also included plots with a radius proportional to tree height within each plot. For variable radius plots, we used increments from 25, 50, …, 200% of plot MTH. The decision to use MTH was motivated by the availability of these data for every plot, and because MTH is well established as a measure of dominant height and productivity in stands of *P. radiata* in New Zealand (M. S. Watt et al., 2015). We also introduced the concept of a variable height threshold at which to compute ratio metrics. This was motivated by the observation that a fixed value makes no allowance for variation in canopy height across plots. We anticipated a variable HT adjusted for canopy height should be beneficial where ratio metrics reflect LAI-related crown properties. Variable HTs of 10, 20, …, 50% of the maximum height of canopy returns (99.9^{th} height percentile) for each plot and radius were used for the ratio metrics shown in Table 4.4.

We implemented all of the height, ratio, and complex metrics using lidar processing routines based on NumPy (Walt, Colbert, & Varoquaux, 2011). The software automated the calculation of all metrics at every fixed and variable plot radii and for ratio metrics, every fixed and variable HT. Where applicable, the software also computed different permutations described in Section 4.4.1.3 for the complex metrics.

4.4.3 Variable screening

Although the modelling approaches identified below in 4.4.4 were selected in part because they are robust to correlated predictors, the degree of correlation between some predictors was deemed to be excessively high. Therefore, a variable screening procedure was employed to deal with the extreme levels of correlation between several of the metrics identified in 4.4.1. Intercorrelation was evaluated by computing Pearson's correlation coefficient (r) between metrics. To constrain the number of permutations, screening was first done by computing the correlation coefficients within groups of metrics (height, ratio, and complex) and then between all remaining metrics. The problem was worst where multiple permutations of the same metric were computed. For example, the height metrics:

Percentiles, Product Percentiles, and Canopy Densities (Table 4.3) all showed very high levels of intercorrelation, as did the permutations for the complex metrics CD_zh and CC_zh (Table 4.5). We defined the threshold for exclusion as any metric with $r > 0.9$ and excluded metrics that exceeded this threshold in an iterative manner, beginning by excluding the identified metrics with multiple permutations. In these cases, we typically removed every *n*th permutation of the metric until the correlation coefficients were acceptable. This approach was primarily necessary for the subset of metrics identified above, and correlations between the filtered metrics from all groups were typically much lower. However, for some groups of predictors, the correlations were sufficiently high ($r > 0.8$) that modelling methods sensitive to intercorrelation of predictors would have been unsuitable for the statistical analysis. This process resulted in a final list of metrics with overall acceptable levels of intercorrelation and indicated that for permutation type metrics, our intervals were too fine and the software could have been adjusted to search across a coarser range of permutations without loss of information.

4.4.4 Statistical methods to estimate LAI from lidar metrics

Linear regression has been widely used for ALS-LAI model development (Griffin et al., 2008; Jensen et al., 2011, 2008; Pope & Treitz, 2013). The diversity of metrics found to be influential in the literature produced a large list of candidate predictors (*p*) for our study (Tables 4.2-4.4). Adding the standard metrics to this list, as well as multiple versions of metrics requiring tuning, placed model development into high dimensional space. Despite a relatively large number of LAI measurements (n=135), the final list of predictors made stepwise or best subsets regression computationally infeasible and undesirable due to the risk of overfitting. To address questions of variable importance and potential nonlinear relationships we chose two alternative modelling approaches. Differences in assumptions and variable selection processes prevented a direct comparison between approaches; however, the combination provided complementary information to answer the stated research questions. Fitting models to data using the increments in Section 4.4.2 introduced the possibility of obtaining similar results from adjacent values of HT and radius. In this situation, we chose to focus on the top 5% of models. This threshold captured models closest in terms of error and accounted for the differing number of fixed and variable radius models trialled.

4.4.4.1 Linear approach – elastic net regression

The success of ordinary least squares (OLS) in previous ALS-LAI work supported the use of related approaches adapted to suit high-dimensional problems such as ours. For our first

approach, we chose elastic net regression (Zou & Hastie, 2005) to model LAI as a linear function of lidar metrics. The elastic net is a form of regularised (penalised) regression offering an appealing combination of benefits from two other regularisation techniques: ridge regression, and the Lasso. Friedman, Hastie, and Tibshirani (2001) provide a detailed treatment of the aforementioned regularisation methods. Briefly, these approaches attempt to address the bias-variance trade-off where p is large (or even for $p \gg n$) by constraining the size of regression coefficients (β) while minimising the residual sum of squares. This is achieved by the introduction of a penalty on coefficient size. Given a vector of responses y and a matrix of predictors x the elastic net solves the following problem

$$\min_{(\beta_0,\beta)} \left[\frac{1}{2N} \sum_{i=1}^{N} \left(y_i - \beta_0 - x_i^{\mathrm{T}} \beta \right)^2 + \lambda P_{\propto}(\beta) \right], \tag{4.3}$$

where

$$P_{\propto}(\beta) = \frac{(1-\propto)}{2} \|\beta\|_2^2 + \alpha \|\beta\|_1 \tag{4.4}$$

$$= \sum_{j=1}^{p} \left(\frac{1-\propto}{2} \beta_j^2 + \alpha \left| \beta_j \right| \right) \tag{4.5}$$

where the first term of Eq. (4.3) is the OLS optimisation and the second is the product of the regularisation tuning parameter λ and the elastic net penalty term $P_{\propto}(\beta)$ Eq. (4.4 & 4.5) (Friedman, Hastie, & Tibshirani, 2010; Zou & Hastie, 2005). The parameter α controls the trade-off between the ridge and Lasso. When $\alpha = 0$ the penalty term simplifies such that Eq. (4.3) is equivalent to the Lasso (L_1 norm penalty). The Lasso penalty allows some coefficients in the model to be set to 0 as the shrinkage increases. In this way, Lasso can perform variable selection to produce a sparse model. However, the Lasso is known to perform poorly in the case where several predictors are highly correlated, often making a single unpredictable selection from the group (Zou & Hastie, 2005). If $\alpha = 1$ then Eq. (4.3) becomes equivalent to ridge regression (L_2 norm penalty). In ridge, coefficient size is penalised by the tuning parameter λ which forces them towards 0 as the value increases. This has the effect of introducing bias in order to reduce variance, especially in the case of highly correlated predictors whose coefficients are forced towards equality as the penalty increases. Although ridge regression handles correlated predictors well, no coefficients are precisely 0 and all variables remain in the model (Friedman et al., 2001). The elastic net ($0 < \alpha < 1$) is a compromise between these two cases. The algorithm produces sparse models through automatic variable selection, stable variance through coefficient shrinkage, and is

computationally efficient for the $p > n$ case (Friedman et al., 2010; Zou & Hastie, 2005). These properties made elastic net well suited to our problem as our data contained a large number ($p \approx n$) of correlated variables (lidar metrics) and we desired to fit many models (one at every combination of HT and radius in Section 4.4.2). Furthermore, sparsity was appealing because: (1) ALS-LAI estimation is promising for large-scale forest LAI mapping, and sparse models reduce the computational load; (2) observing patterns of selection at different plot radii and HTs would partially address our goal of comparing relative and absolute variable importance for ALS-LAI estimation.

We fitted the elastic net using the glmnet package (Friedman et al., 2010) available for R (R Core Team, 2015). Drawing on the recommendations of Friedman et al. (2010) for glmnet, we developed the following approach:

(1) The data were subset to a single combination of radius and HT.

(2) The matrix of predictors was centred and standardised in preparation for (9)

(3) A grid of α values (elastic net mixing parameter) was specified to cover the range between ridge and Lasso as follows: (α = 0.1, 0.2, …, 0.9, 0.95, 0.99).

(4) A second grid of λ values was determined based on the built-in method of glmnet.

(5) Each observation was assigned randomly to a single fold for 10-fold cross-validation (CV).

(6) An algorithm then conducted a grid search across the values of α and λ, with the elastic net mean squared error (MSE) computed by CV.

(7) Resampling was then performed by repeating 5-6 100 times.

(8) In this way, the entire grid was searched using fixed CV folds, while fold effects were reduced through resampling.

(9) The standardised model coefficients (i.e. on the scale used during fitting) were extracted at the combination of α and λ which produced the lowest MSE from CV)

Steps 1-9 were repeated to find the best model for every combination of radius and HT.

We chose a value for λ (step 6) that produced the simplest model with an MSE within 1 standard error (SE) of the model with the lowest MSE as a guard against overfitting (Friedman et al., 2001, p. 244). Elastic net does not offer a direct assessment of variable importance. Instead, we used two proxies to assess variable importance: (1) By observing

selection patterns across models, especially those included in the top 5% of models (these were nearly tied for lowest MSE); (2) we assessed variable importance and grouping effects across HT and radii by ranking the absolute magnitude of the coefficients returned from step 9. Our rationale for this was as follows: As elastic net regularisation proceeds towards the optimum, the size of important coefficients stabilises and groups of correlated but important predictors converge to be selected in groups (Grömping, 2009; Zou & Hastie, 2005). Weak predictors are pushed close to zero or excluded altogether. Although coefficient sizes at the optimum are not comparable across models, the presence (absence), rank, and grouping of variables within models provide insight into the impact of HT and radius on variable importance alongside model performance. Similar approaches have been used elsewhere to assess importance from standardised coefficient size (Finlay et al., 2015); however, our interest was constrained to the relative changes in rank. The overall performance of the best elastic net model was assessed by performing leave-one-out cross-validation (LOOCV). The elastic net model was refit at the combination of radius and HT that produced the lowest MSE using the α and λ identified in steps 1-10 and used to make predictions for the excluded observations.

4.4.4.2 Nonparametric approach – random forests

The modelling process was repeated using the ensemble learning approach of random forests (RF) (Breiman, 2001) to estimate LAI from lidar metrics at each combination of radius and HT. Statistical learning approaches such as RF have been successfully applied to model plantation productivity (M. S. Watt et al., 2015; M. S. Watt, Dash, Watt, & Bhandari, 2016), merchantable yields (Dash et al., 2015), and other variables of interest using lidar. However, these techniques have not been widely explored for ALS-LAI estimation (K. Zhao & Popescu, 2009). RF was selected as a complement to elastic net because the method is capable of discovering complex nonlinear relationships in high-dimensional data where predictors show high levels of correlation (Criminisi, Shotton, & Konukoglu, 2012). RF also offered more sophisticated measures of variable importance beyond rank and selection frequency. The random forests algorithm uses a random subset of observations for each learner (individual trees), and a random subset of predictors at each split (node) within a tree. Variable importance scores for individual predictors in RF regression are computed by randomly permuting the values of the predictor in the data withheld from each tree (out-of-bag sample). The difference in predictions on the out-of-bag observations before and after permutation is computed and averaged over all trees in the forest to give the importance score

(usually incremental %MSE for regression) (Breiman, 2001; Strobl & Zeileis, 2008). Importance scores computed in this way have been shown to overestimate the importance of highly correlated predictors (Strobl, Boulesteix, Kneib, Augustin, & Zeileis, 2008). To account for the high levels of correlation between predictors in our data we used the conditional importance scores proposed by Strobl et al. (2008) and made available in the R Party package by the same authors. This approach relies on RFs based on conditional inference trees, and we followed the recommendations of Strobl et al. (2008) and Grömping (2009) to select suitable tuning parameters for this type of RF. Firstly, the number of predictors trialled in each split (*mtry*) was varied from *mtry* = 3 up to *mtry* = *p*. Based on the minimum MSE and stability of importance scores *mtry* = *p*/3 appeared close to optimal. Then we altered the number of trees (*ntree*) and the random seed used in the software to assess the stability of results. A value of *ntree* = 4000 produced close to the lowest MSE for models and RF results that were relatively invariant to the random seed chosen.

Variable selection via the elastic net focuses on interpretability and selection of all important variables. This is in contrast to methods targeting prediction accuracy such as random forests (Grömping, 2009). Candidate predictors in our study included a mix of lidar metrics previously identified as empirically or theoretically related to LAI. We were interested in the accuracy of ALS-LAI estimates and the relative importance of theoretically meaningful metrics. The combination of approaches gave us insight into both aspects of variable importance while simultaneously identifying the best predictive models.

4.4.4.3 Semi-physical model

As will be seen, clear trends in metric selection and importance emerged. The metrics *SCI* and *LCI* (Table 4.4) were both useful predictors of LAI, with distinct trends of importance. These metrics were proposed as proxies for canopy gap fraction, which is related to LAI through the Poisson model (Section 2.3.4). In this formulation, the gap fraction is approximately measured using the lidar penetration rate through the canopy. The slope is estimated empirically using the *in situ* LAI values and can be seen as equivalent to an empirical extinction coefficient (*k*) for the lidar-based gap probability model that is influenced not just by leaf angle distribution but also canopy and species properties (Heiskanen et al., 2015). We tested these metrics in the semi-physical model proposed by Solberg et al. (2009):

$$LAI = \beta \ln(P^{-1}) \qquad 4.6$$

where *P* is the penetration rate estimated by SCI or LCI computed at a given combination of radius and HT, and β is the slope estimate obtained by fitting a regression model forced through the origin. This model has proven useful in previous studies estimating LAI from ALS data in coniferous forests (Korhonen et al., 2011; Solberg et al., 2009). We trialled SCI and LCI at all combinations of radius and HT.

For consistency, and to obtain results in units of LAI, root-mean-squared error (RMSE, Eq. 4.7) was used as the error metric for elastic net, RF, and semi-physical models. For the best elastic net and semi-physical models, a measure of model error (bias) was also computed (Eq. 4.8).

$$RMSE = \sqrt{\frac{1}{n}\sum_{i=1}^{n}(y_i - \hat{y}_i)^2} \quad 4.7$$

$$bias = \frac{\sum_{i=1}^{n}(y_i - \hat{y}_i)}{n} \quad 4.8$$

4.5 Results

A summary of plot mean LAI and associated error is given in Table 4.1. Measurements taken under diffuse skies frequently showed non-monotonic contact numbers, indicating poor readings. Masking the outer ring in these data tended to increase the LAI estimates. These problems were less frequent in measurements taken under clear sky conditions and LAI values after masking were less affected.

4.5.1 Elastic net regression – fixed radius plots

Results from the elastic net models showed the choice of fixed plot radius and height threshold had marked effects on RMSE. Fig. 4.2 shows the pattern of change in model RMSE across all combinations of HT and radius. The best model had RMSE=0.64 LAI using a radius of 20 m and HT=20% of CH. The top 5% of models had similar RMSE of 0.64–0.65. For all values of HT, the model error reduced as the radius used to extract lidar data was increased. For radii above 16 m, the choice of fixed HT became more important and increasing HTs further decreasing model error. The optimum combination of lidar parameters was between fixed radius of 20–26 m and fixed HT of 5–6 m, with several of the best models

concentrated in this region. Use of a variable HT based on a percentage of canopy height produced several models with RMSE comparable to the best fixed HT models.

The observed patterns in model error were associated with large differences in the type and number of variables selected by the elastic net algorithm. The optimum value for α (the mixing parameter) was nearly always 0.1 for weaker models using metrics from small radii and low HTs. At this value, the elastic net was closest to ridge regression. Even at this small magnitude, the introduction of an *L1* penalty meant that the maximal (and weakest) models included only ~ 30% of available variables (p=39).

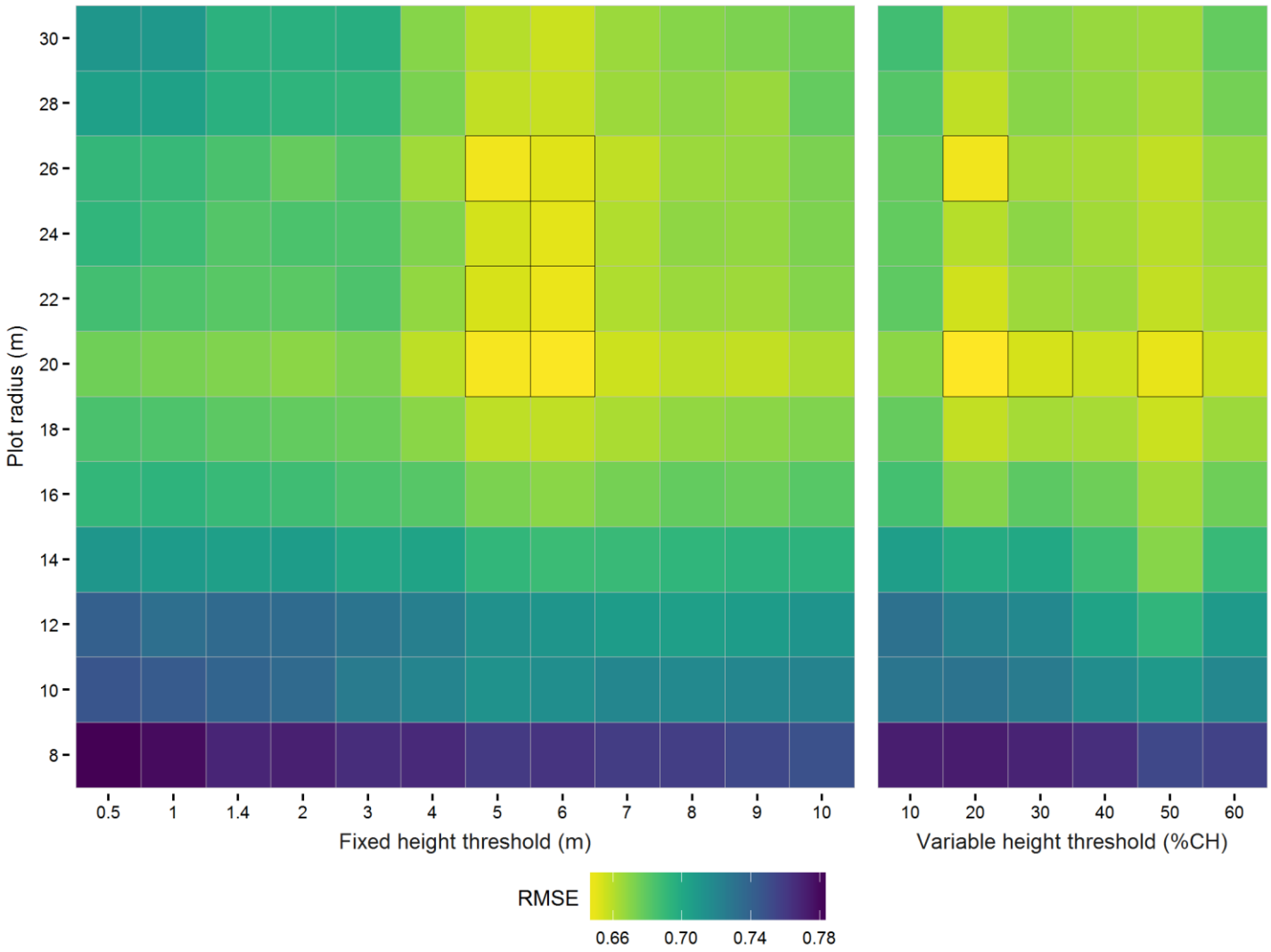

Fig. 4.2. Results from elastic net regression models estimating LAI from lidar metrics. Metrics were constructed using data extracted from a range of fixed plot radii. Ratio metrics were constructed using fixed height thresholds, and variable height thresholds as a percentage of maximum canopy height (%CH) within each plot. Outlined tiles show the top 5% of models with nearly identical RMSE (0.64–0.65).

Fig. 4.3 shows the change in model size as a percentage of the maximal model. Weaker models at radii of 8–16 m exhibited similar patterns, and models at radius=14 m are shown for reference. Above radius of 16 m model complexity decreased markedly as HT increased towards 5–6 m, and ratio metrics as a percentage of all selected metrics increased markedly. Several models in this region provided close to the lowest RMSE observed, using the smallest number of predictors. Lower RMSE was not always associated with sparsity, this was evident for models at radius=20 m and where a variable HT was used. At these values, the correlation between groups of height and ratio metrics increased (Pearson's *r* often > 0.85), and elastic net selected these larger groups of predictors together. The presence of these predictors masked the importance of ratio metrics, which still had the largest coefficients. However, regularisation meant that these variables contributed little additional error.

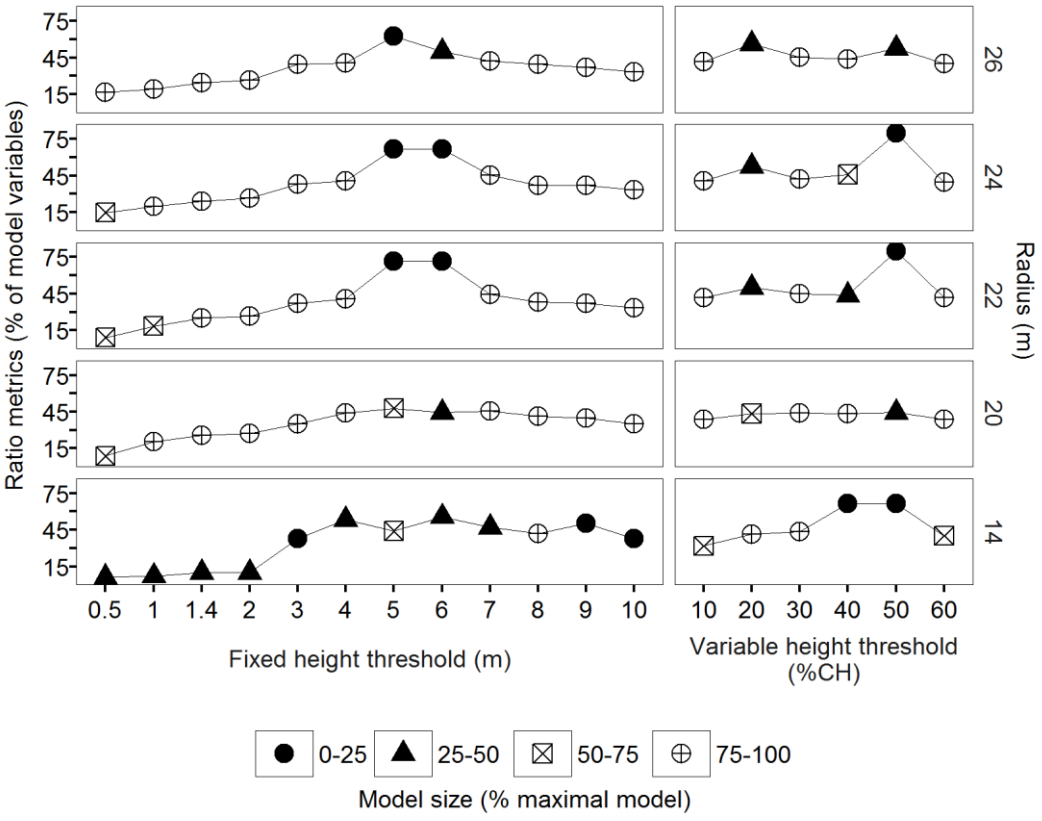

Fig. 4.3. Change in model complexity and proportion of ratio metrics selected in elastic net models of LAI using lidar data from fixed plot radii. Ratio metrics were constructed using both fixed height thresholds and height thresholds based on percentage canopy height (%CH). The top 5% of models had plot radii between 20–26 m. Models at a radius of 14 m are shown for contrast and the maximal fixed radius model had p=38.

4.5.2 Elastic net regression – variable radius plots

Elastic net models fitted to lidar metrics using data from a variable plot radius, set as a percentage of MTH, produced better results than fixed radius plots. The combination of radius=100% of MTH and HT=20% of CH performed best (RMSE=0.57 LAI). As with the fixed radius models, several combinations of HT and radius produced models very close to this value with RMSE of the top 5% of models ranging from 0.57–0.59 (Fig. 4.4). The location of these models was constrained to a narrow region (Fig. 4.2) with radius equal to 100% and 150% of MTH. Models at these radii showed lower RMSE across the range of fixed and variable HTs. The best models used ratio metrics with HTs between 4–6 m, a similar range to the best HTs in fixed radius plots, variable HTs of 20–30% of canopy height. The impact of HT was more constrained than in fixed radius models. Using a variable radius appeared to increase the importance of locating the optimum combination of radius and HT, and models chosen outside of these narrow regions had larger increases in RMSE.

Patterns of metric selection and model complexity differed from those seen in fixed radius plots (Fig. 4.5). Increasing HTs were associated with an increase in the number of ratio metrics, but the effect was not consistent across radii. Overall, trends in model complexity and fraction of ratio metrics were more varied. Inspection of the correlation coefficients and coefficient sizes from elastic net revealed that variable radius models had many small groups of 2–3 highly correlated ($r > 0.9$) height metrics that were selected together. In aggregate, this inflated the size of variable radius models and diminished the apparent importance of ratio metrics.

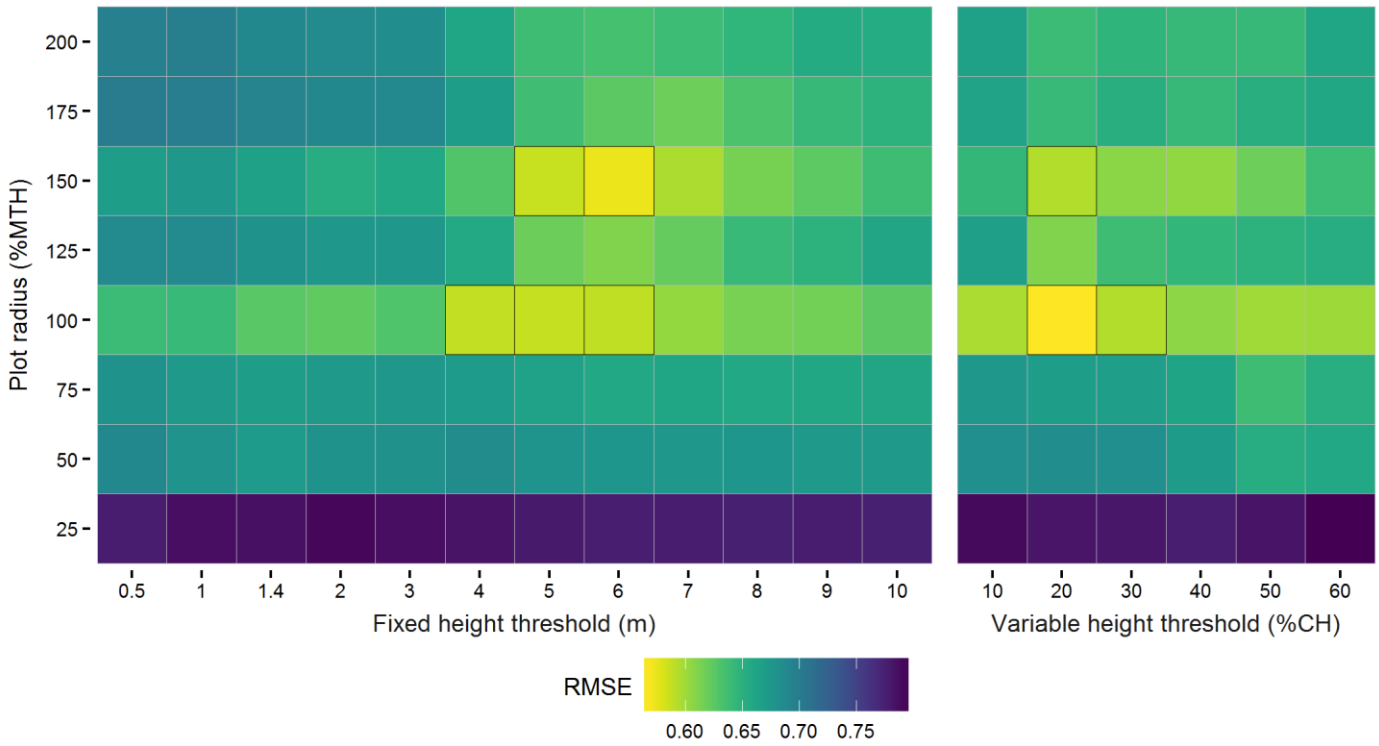

Fig. 4.4. Results from elastic net regression models estimating LAI from lidar metrics. Metrics were constructed using data extracted from a range of variable plot radii set as a percentage of mean top height (%MTH). Ratio metrics were constructed with fixed height thresholds and using variable height thresholds set as a percentage of maximum plot canopy height (%CH). Outlined tiles show the top 5% of models with similar RMSE of 0.57–0.59.

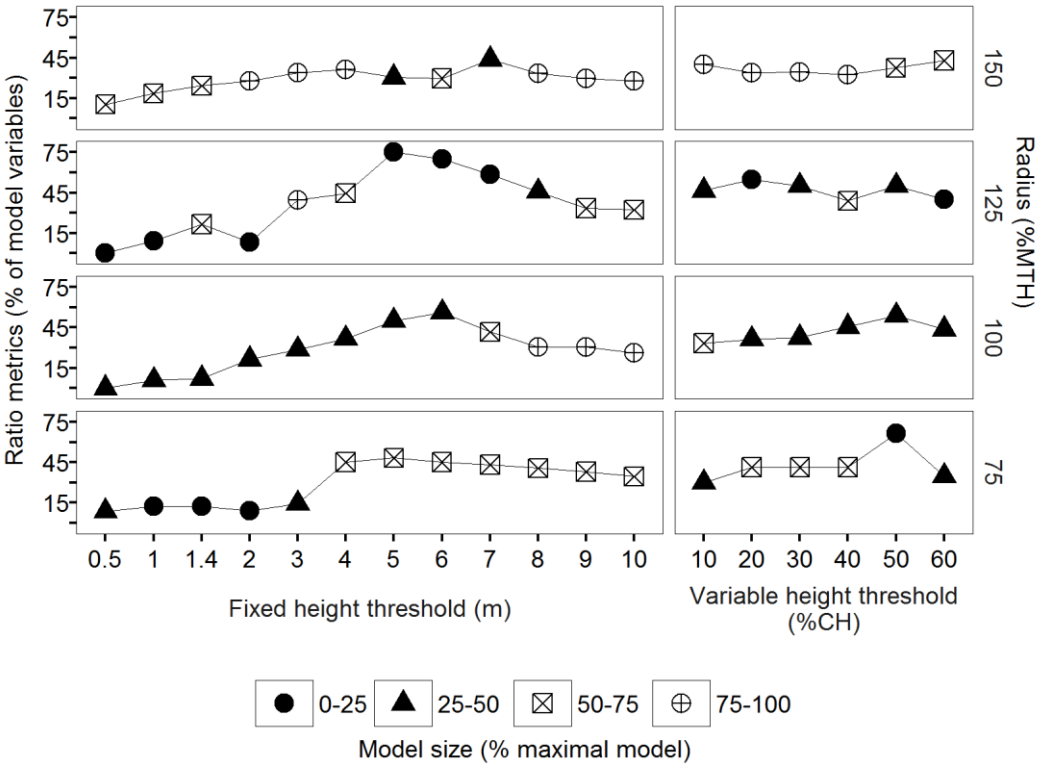

Fig. 4.5. Change in model complexity and proportion of ratio metrics selected in elastic net models of LAI using lidar data from variable plot radii set as a percentage of mean top height (%MTH). Ratio metrics were constructed using both fixed HTs and HTs based on % canopy height (%CH). The top 5% of models had plot radii of 100% and 150% of MTH. Models at radius=75% and 125% of MTH are shown for contrast. The maximal variable radius model had p=49.

The best elastic net model at radius=100% MTH and HT=20% CH showed good agreement between measured LAI and LAI predicted using leave-one-out cross-validation (Fig. 4.6) a negative bias of -0.005 indicated small underestimation of LAI. Model underestimation was most apparent when predicting LAI values towards the upper end of the range examined.

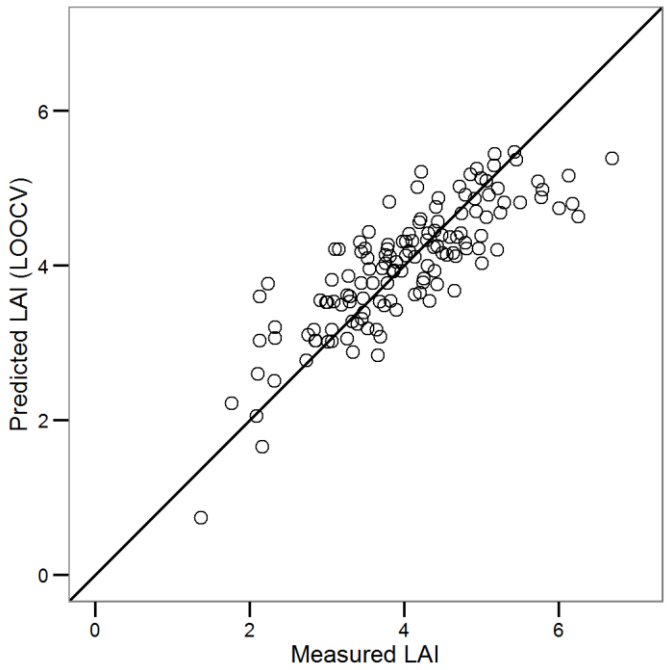

Fig. 4.6. Comparison of measured LAI and predicted LAI obtained by leave-one-out cross-validation (LOOCV) using the best elastic net model. The best model had radius=100% MTH and HT=20% CH. Model RMSE was 0.57 and bias was calculated as -0.005.

4.5.3 Elastic net – variable importance

Many of the best fixed radius models were remarkable for the fact that nearly all metrics selected were ratio metrics. Examining the frequency of metric selection in the top 5% of models highlighted several key metrics present in all of the top models (Table 4.6). A larger number of metrics were selected for occasional inclusion, especially at radius=20 m, and we focused only on those present in all of the best models. Four of the top metrics were ratio metrics, and the few important height metrics all related to the distribution of height values. Many of the metrics selected in all of the top 5% of models also had a high frequency of selection across all fixed radius models. Repeating the analysis for variable radius models showed ratio metrics to be equally influential in these models. The majority of metrics consistently selected for inclusion in the best variable radius models were ratio metrics (Table 4.6). The metrics *PFaVegMean*, LCI were selected in all of the best fixed and variable radius models.

Table 4.6. Summary of important metrics selected for inclusion in the top 5% of elastic net models. Models were fitted to lidar data from fixed and variable radius plots. Ratio metric names are in bold. Metric definitions are given in Tables 4.2–4.4. The frequency of occurrence for listed metrics in all models trialled is also shown.

Fixed radius models			Variable radius models		
Metric name	Frequency in top 5% models (%)	Frequency in all models (%)	Metric name	Frequency in top 5% models (%)	Frequency in all models (%)
PFaVegMean	100	89	**PFaVegMean**	100	83
LCI	100	77	**LCI**	100	70
SCI	100	86	**MLP**	100	72
ZP_Rig_t	100	81	**nLAI**	100	80
Lmom_Skew	100	88	**ZP_Rig_p**	100	31
Skew	100	97	b60	100	70
			CD_kurt_p5	100	20

The importance of ratio metrics was reflected in the analysis of elastic net coefficient rankings. Fig. 4.7 shows the ranked coefficients from the elastic net models fitted at the location of the top 5% of models. As height threshold increased, key ratio metrics increased in rank and displaced weaker height and ratio metrics within the best models. The model predicting LAI using widely-used defaults of plot radius equal to inventory radius (14 m) and HT set at instrument height (1.4 m) produced one of the weakest models trialled. Examining metric importance with these plot parameters would have missed all but one of the top ratio metrics (PFaVegMean, Fig. 4.7). Patterns of coefficient rank and HT were similar in the variable HT models. Increasing variable HT resulted in several ratio metrics assuming the highest coefficient rank; however, greater separation in rank was observed and some metrics responded less clearly to increased HT.

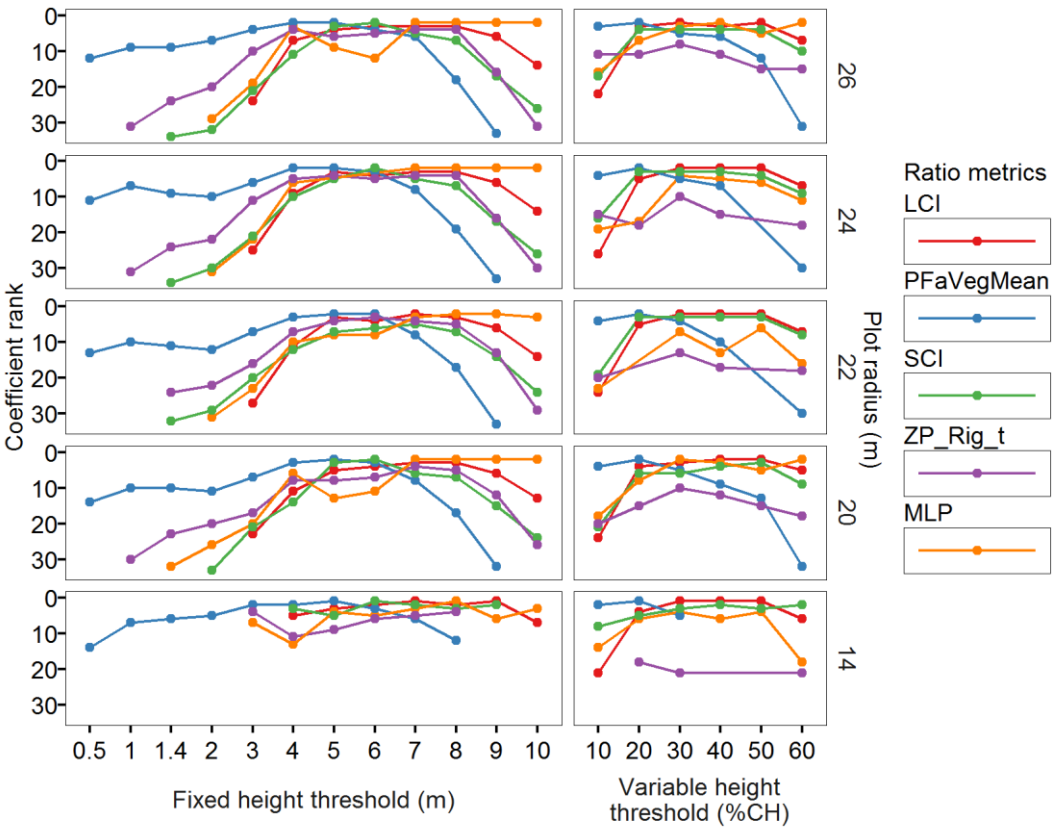

Fig. 4.7. The impact of fixed and variable height thresholds on the rank of the best ratio metrics within elastic net models fitted at the optimal fixed plot radii. Variable height thresholds for ratio metrics were set as a percentage of canopy height (%CH). Models at radius=14 m are shown for contrasts.

Coefficient ranks from variable radius elastic net models showed similar trends (Fig. 4.8). Increasing the HT across the radii at which the top 5% of models occurred (100 and 150% of MTH) increased the frequency of selection for the top ratio metrics. The rank of these metrics was generally high, frequently occupying the highest ranked positions of all coefficients in the model. The effects of increasing HT were less marked in plots with radius equal to 100% of MTH. Overall trends still showed ratio metrics to be highly ranked within the top 5% of variable radius models.

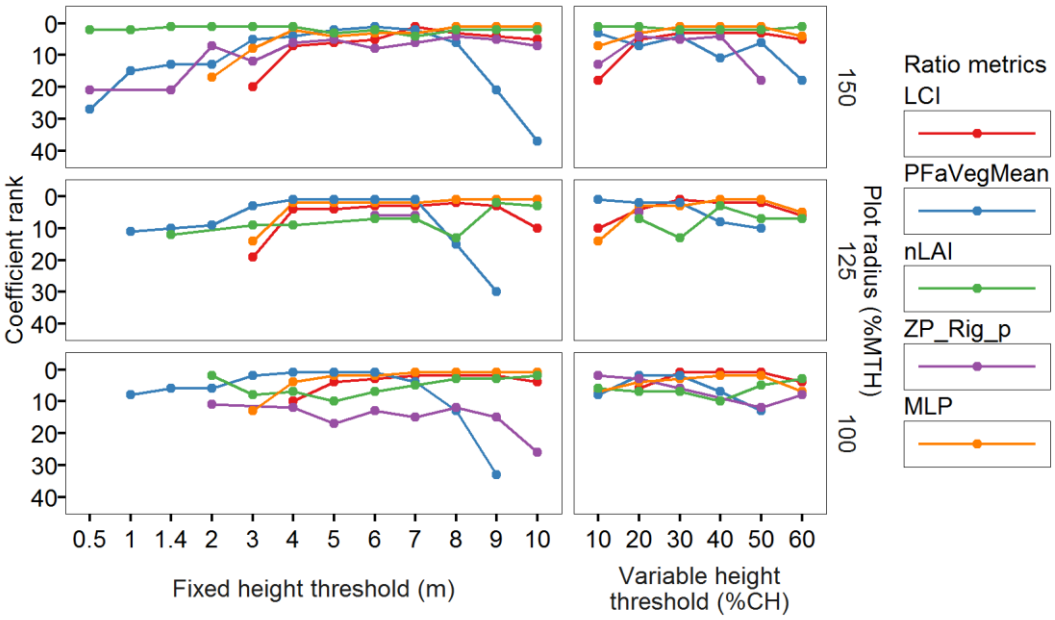

Fig. 4.8. The impact of fixed and variable height thresholds on the rank of the best ratio metrics within elastic net models fitted to data from variable radius plots. Variable radii of 100 and 150% of mean top height (%MTH) were used in all of the best elastic net models. Plots with MTH=125 and 75% MTH are shown for contrast. Variable height thresholds for ratio metrics were set as a percentage of canopy height (%CH).

4.5.4 Random forests – fixed radius plots

Random forest models estimating LAI from lidar metrics generated from fixed radius plots had similar RMSE to the fixed radius elastic net models. As with elastic net, several models were very close in terms of RMSE, and the top 5% of models trialled had RMSE=0.64–0.66 LAI. The range of RMSE for all models was 0.64–0.76 LAI. Fig. 4.9 shows the difference in RMSE between models fitted using elastic net and random forests (Enet RMSE - RF RMSE), with negative values showing combinations of radius and HT where elastic net models outperformed RF. Although elastic net found stronger relationships, the differences were quite small and broadly confined to radii above 14 m and HTs above 4 m or between 20–30% of CH. Several of the best RF models were located at radius=20 m, which also appeared important for elastic net models. Several of the top RF models used HT=50% CH for ratio metrics. We attempt to develop insight into this pattern by exploring changes in variable importance across fixed and variable HTs in Section 4.5.6.

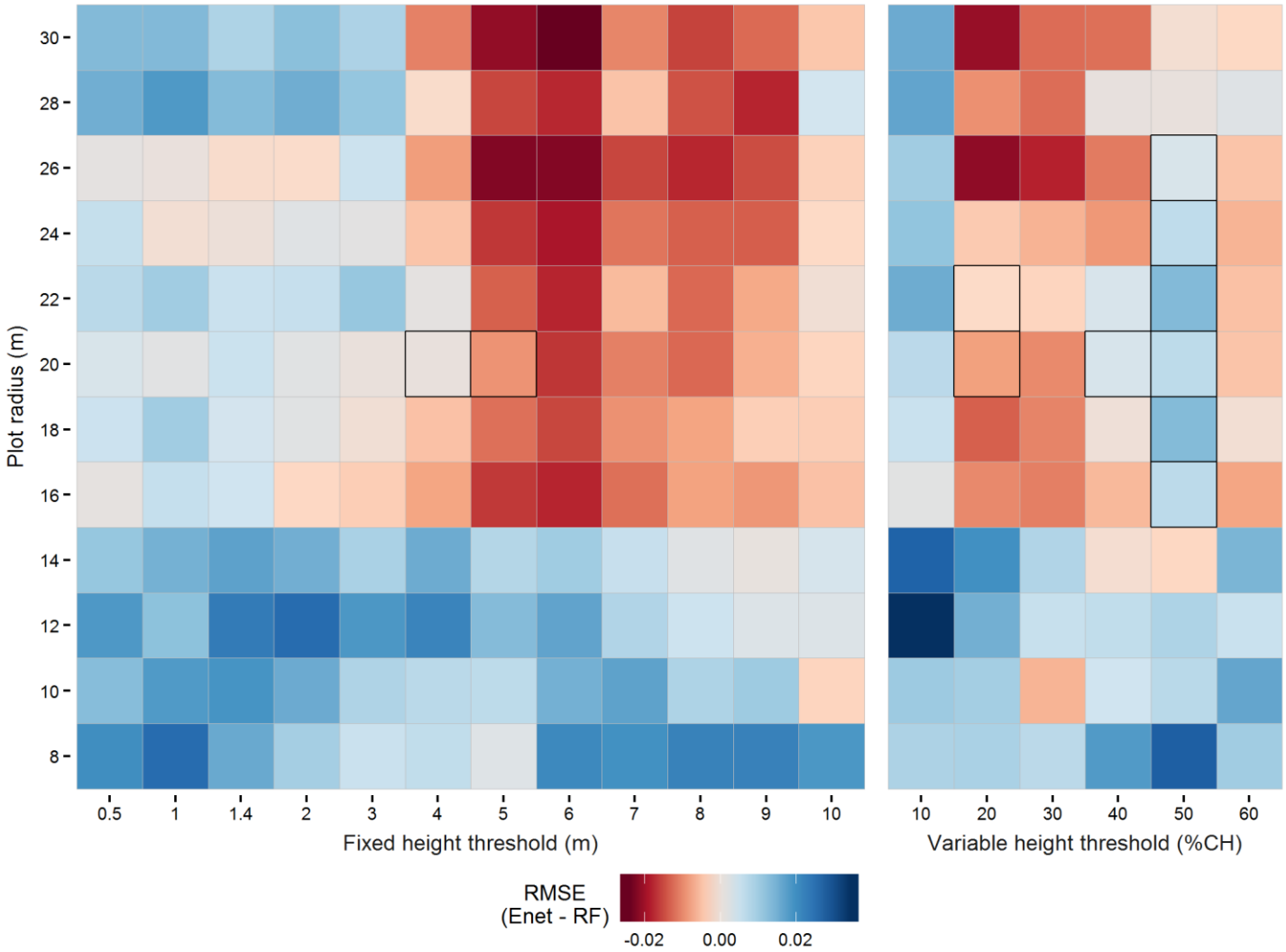

Fig. 4.9. Comparison of model RMSE from elastic net and random forests models predicting LAI from lidar metrics from fixed radius plots. Ratio metrics were computed at both fixed HTs and HTs based on percentage canopy height (%CH). Red regions show combinations of radius and HT where elastic net produced lower RMSE than random forests, and blue areas show models where random forests achieved lower RMSE. Outlined tiles show the location of the top 5% of random forests models (RMSE=0.64–0.66).

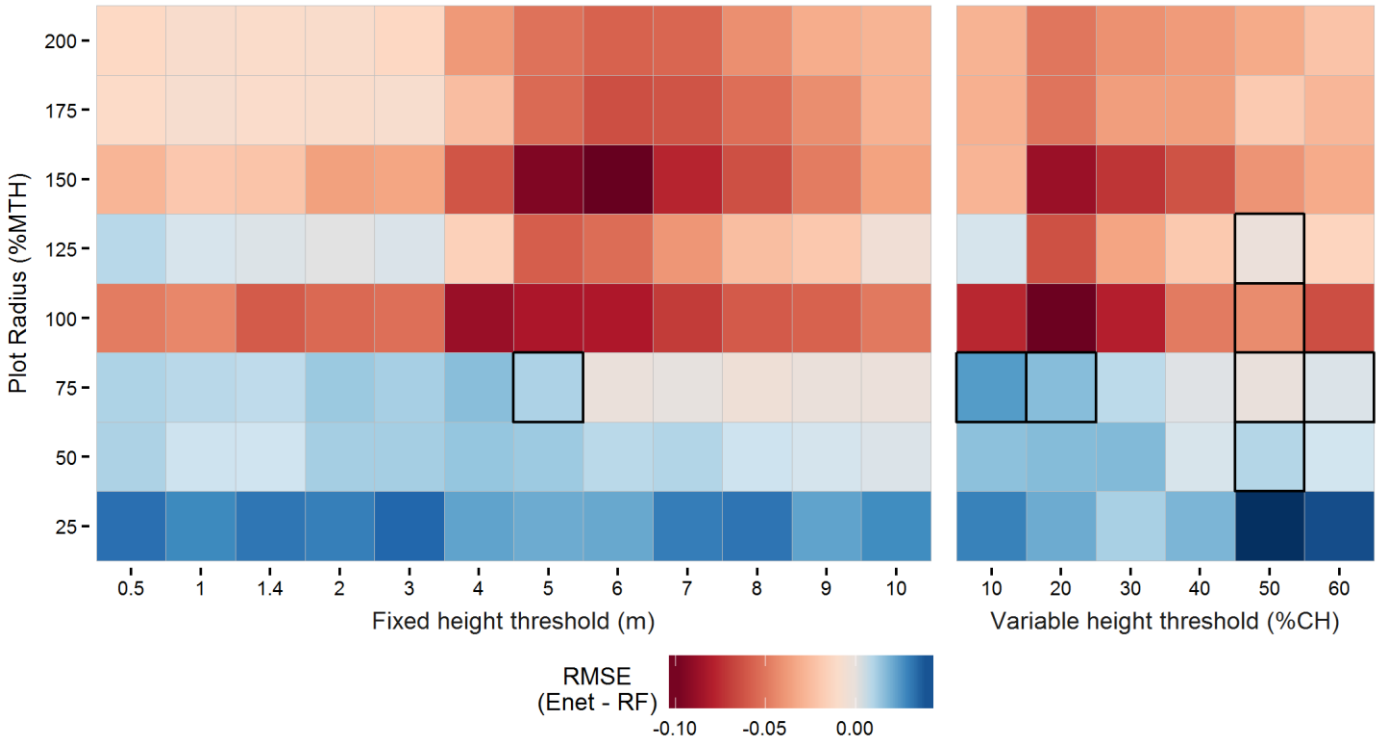

Fig. 4.10. Differences in RMSE between elastic net (Enet) models and random forests (RF) models predicting LAI from lidar metrics extracted at variable plot radii set as a percentage of mean top height (%MTH). Ratio metrics were constructed at both fixed height thresholds and using thresholds based on a percentage of maximum canopy height (%CH). Outlined tiles show the top 5% of models with similar RMSE (0.64–0.65).

4.5.5 Random forests – variable radius plots

Random forests models fitted to lidar metrics from variable radius plots (Fig. 4.10.) had RMSE ranging from 0.64–0.65. This meant for many models the difference between elastic net and random forests was more substantial than that seen with fixed radius data. The radius and HT of the best random forests models (Fig. 4.10) did not coincide with any of the top elastic net models. The radii at which random forests outperformed elastic net were largely confined to plots with a variable radius equal to 75% of MTH. As with fixed radius plots, several of the top random forests models were located where ratio metrics used an HT of 50% of CH.

4.5.6 Random forests - variable importance

Extraction of the conditional variable importance scores for all variables (lidar metrics) in each of the random forest models fitted added significantly to the computation time required. Summary statistics by metric were used to construct box plots (Fig. 4.11) that revealed large fluctuations in importance for some metrics at different combinations of radius and HT. Ranking metrics by mean importance within the top 5% of models highlighted the key metrics for fixed and variable radius data. Metrics with mean importance below those shown in Fig. 4.11 decreased markedly in mean and maximum importance score and were excluded from further analysis. In most cases, the apparent outliers shown in the all-model boxplots were the importance scores from the top 5% of models. This emphasised the strong response in importance scores when models used metrics constructed at the optimum radii and HTs. However, in other cases, the outliers reflected large localised increases in importance outside of the top models. For example, in the fixed radius models *nLAI*, *PAaVegMean*, and *Lmom_Skew* had instances of high importance outside of the location of top 5% of models. These fluctuations in importance were similar to the trends observed in elastic net metric selection where a general relationship could be established between metric selection, coefficient rank, and model performance, but results there also showed localised fluctuations at particular combinations of radius and HT.

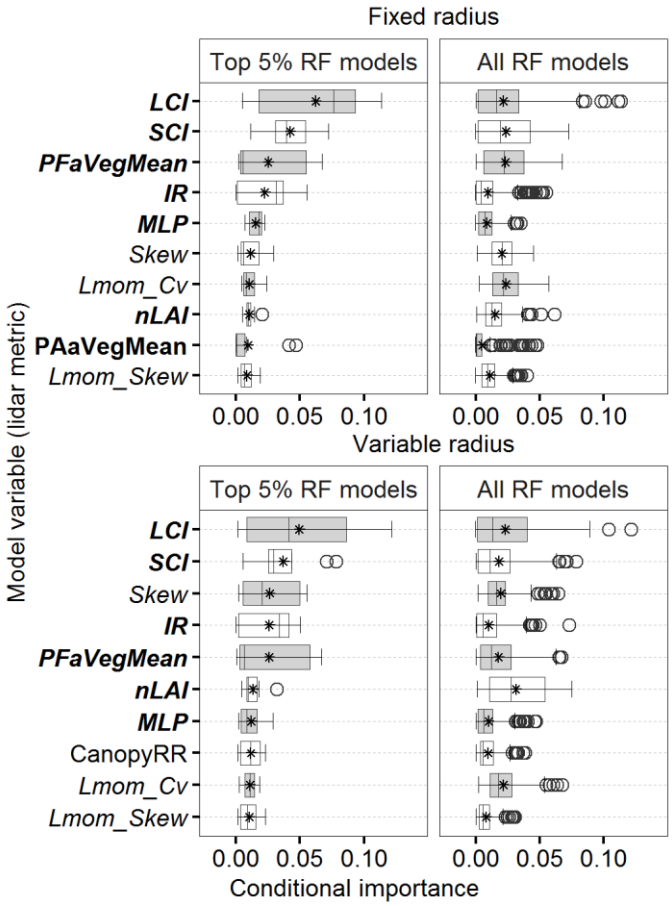

Fig. 4.11. Boxplots of conditional variable importance from random forests models fitted to lidar data from fixed and variable radius plots. Variables are arranged in descending order of mean importance (*) within the top 5% of models by RMSE. Metrics important in both fixed and variable radii plots are italicised and ratio metrics are indicated in bold.

For the fixed radius models, the list of important metrics was composed primarily of ratio metrics. The highest mean, median, and maximum scores were also obtained from ratio metrics. A nearly identical (9/10) set of metrics had the highest mean importance in the top 5% of models fitted to variable radius plots. With the exception of *Skew*, the mean and distribution of metric importance scores were also reasonably similar across the best fixed and variable radius models. The metrics Skew, *Lmom_Cv*, and Lmom_skew had the highest mean importance scores of all height metrics across fixed and variable radii. All of these metrics describe the distribution of lidar return heights, and both Skew and Lmom_Skew were included in all of the top fixed radius elastic net models. The importance scores of these height metrics were expected to be sensitive only to the choice of plot radius; however, their importance scores appeared to decrease where higher HTs increased the importance of the best ratio metrics. These changes in importance score reflected the changes in metric

selection observed in elastic net models, where higher values of HT (especially fixed HTs) decreased the number of height metrics selected.

Patterns of changing importance with HT and radius were particularly evident in the importance scores of the ratio metrics LCI, SCI, *PFaVegMean*, and to a lesser extent IR (Fig. 4.12). These metrics were identified because the mean and maximum importance scores from both fixed and variable plots were higher than those of the remaining ratio metrics and because the distribution of importance scores indicated high variability in response to radius and HT. The metrics LCI and SCI showed increased importance when a variable HT of 50% of CH was used. For fixed HTs, only PFaVegMean and SCI showed increasing in importance as HT increased. The optimum regions for these metrics broadly overlapped the optimal fixed HTs identified by elastic net (4–6 m).

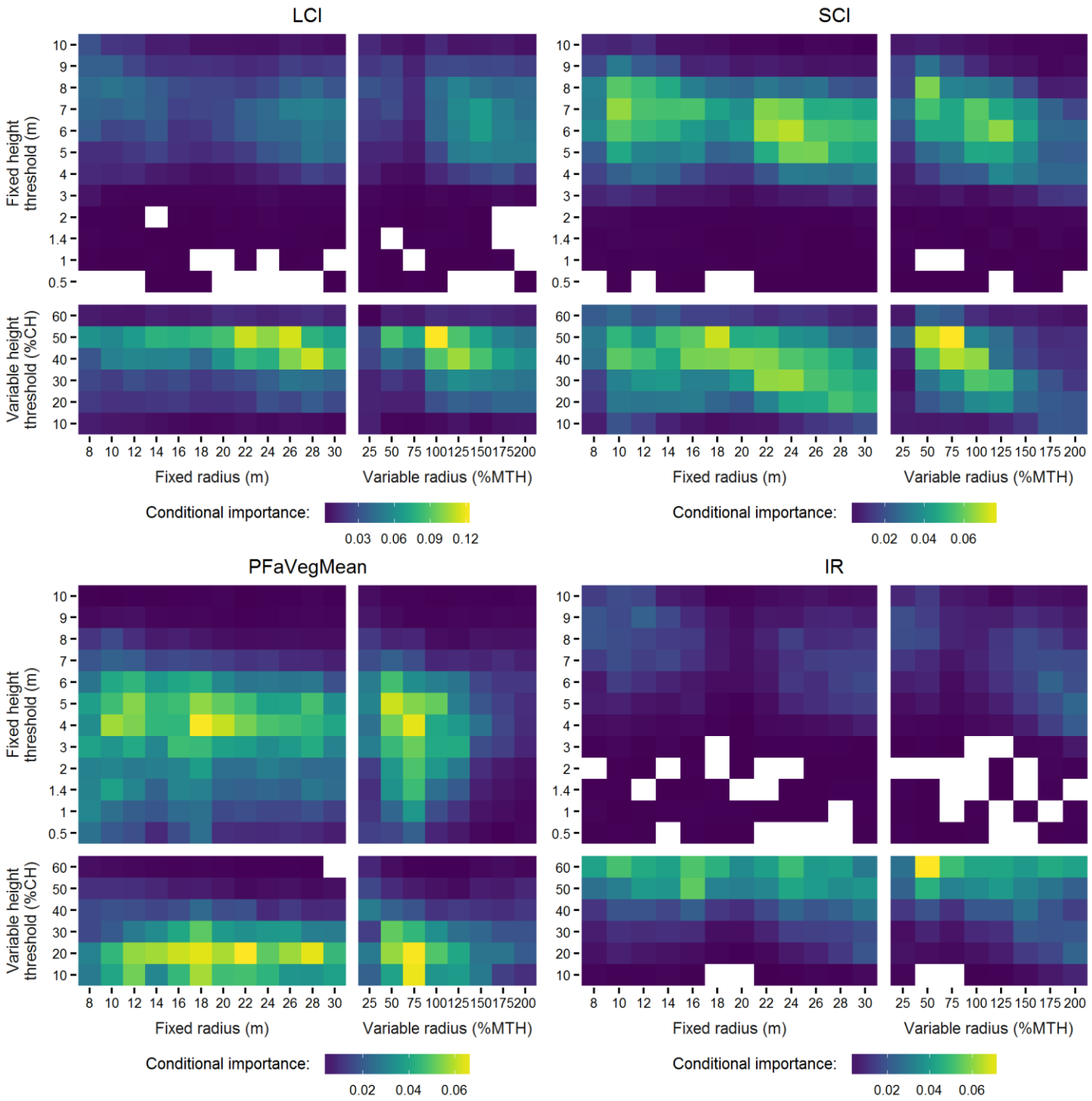

Fig. 4.12. Random forests conditional importance scores for key ratio metrics. Lidar metrics were computed from data extracted from fixed radius plots and variable radius plots set as a percentage of mean top height (%MTH). Ratio metrics were computed using both fixed height thresholds, and height thresholds set as a percentage of maximum canopy height (%CH). Empty tiles show negative conditional importance scores. Note: scales are set per metric for visual clarity.

4.5.7 Semi-physical models

The semi-physical model fitted using LCI proved weak, producing high RMSE at any combination of plot radius and HT. In contrast, models using SCI performed well across a range of combinations of HT and radius. For fixed radius plots, models with radius above 18 m and HT of 5–6 m or 20–50% of CH showed good agreement (RMSE=0.73–0.81 LAI). Models fitted to data from variable radius plots were slightly improved. The best model (R^2=0.97, RMSE=0.72 LAI) used radius=100% of MTH and HT 50% of CH. Predictions from this model showed a small overall positive bias of 0.11 indicating an overestimation of LAI (Fig. 4.13), and the size of the residuals appeared to increase when predicting higher values of LAI. The clustering of top RF models at HT=50% of CH coinciding with the increased importance of SCI and LCI suggested a potential nonlinear relationship. However, there was no evidence of reduced RMSE at this HT in the semi-physical model trialled. Instead, models using SCI had similar performance across the combinations of radii and HTs seen in elastic net (Fig. 4.2 and Fig. 4.4). However, the impact of HT was greater on the semi-physical models. A notable increase in RMSE and a decline in R^2 was observed for all models either side of the optimum range for fixed or variable HT.

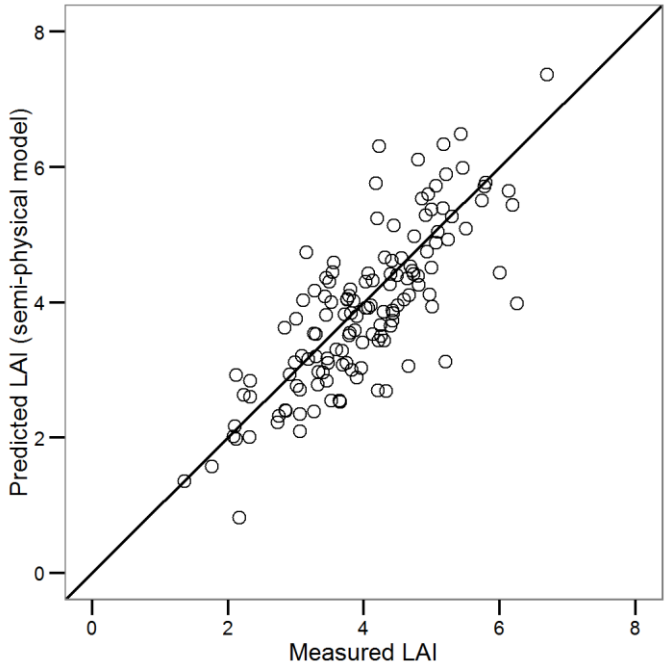

Fig. 4.13. Comparison of measured and predicted values of LAI from a no-intercept nonlinear model. The model estimated LAI from the SCI metric at a radius of 100% mean top height and height threshold set at 50% of canopy height. The model had R^2=0.97 and RMSE=0.72 LAI. The positive bias of 0.11 indicated an overestimation of LAI.

4.6 Discussion

Our findings demonstrate that LAI can be estimated from lidar data in planted forests of pure *Pinus radiata*. Similar results in stands of loblolly pine in the US (Peduzzi et al., 2012) and planted Scots pine in Spain (Riaño et al., 2004) suggest that ALS-LAI estimation is a viable tool for large-scale assessment of LAI in managed forests of this type. A key finding was the sensitivity of model performance to the chosen plot parameters. The combination of instrument height as the HT in ratio metrics and fixed radius set to the field plot size considerably increased model error. Under these assumptions, key metrics were seldom selected for inclusion in elastic net models and had reduced importance in random forests. Trialling a range of values proved useful for determining the optimal location of both fixed and variable radii and HTs. The process highlighted that similar model accuracy could be obtained across a range of plot parameters. For fixed radius plots, our results showed a gradual decrease in model error with increasing radius. There was no evidence of a sharp asymptote, and models with comparable error covered a range of 6 meters in radius. This finding agrees well with results from previous studies examining fixed radius increments (Richardson et al., 2009; Solberg et al., 2009; K. Zhao & Popescu, 2009) and suggests that trialling radii at relatively coarse increments is sufficient to identify close to the optimal size for fixed radius plots.

Models developed using variable radius plots clearly improved on the approach of setting a single fixed radius for all plots. This supports similar findings from ALS-LAI studies in a range of forest types (Riaño et al., 2004; Solberg et al., 2009). Use of a plot radius based on canopy height is appealing because it offers the possibility to derive LAI related lidar metrics from data coincident with the instrument view distance. With the outer ring masked, and without accounting for foliage density, the maximum distance viewable in our plots would be approximately $\tan 58.1°$ or 160% of canopy height (LI-COR, 2015). Several of the best elastic net models were located close to this value (150% of MTH), and it is conceivable that differences in stand density could partially account for the location of several top models at 100% of MTH, although we did not test for this.

Instrument characteristics posed some limitations on the analysis. The physically defined annulus rings of the LI-COR did not allow us to trial and match zenith view to the lidar data ‘cylinder’ (e.g. K. Zhao & Popescu, 2009). Furthermore, a view cap was always required to reduce the required size of clearings for above canopy readings and to block the sun. This meant all measurements in our plots were limited to 90° or 180° views of the canopy and

these were always facing in the same direction, preventing a full hemispherical view as may be obtained with HCP. These limitations prevented us from establishing a direct link between lidar data extracted from variable radius plots and the canopy viewed by the optical LAI measurements. Nonetheless, the variable radius plots produced the best ALS-LAI models, adding to previous results identifying optimum plot sizes close to instrument view distance.

We hypothesise that use of variable radius plots close to instrument view distance both increased correlation between metrics and strengthened links between LAI and important metrics. At 100% & 150% of MTH, the average plot size would be at or greater than 30 m (Table 4.1), and the greater averaging of forest conditions could be expected to decrease variability between related metrics. This would help to explain the large increase in the number of small, highly correlated groups of predictors selected together in the elastic net model fitting. The absence of a marked decrease in RMSE from models using a fixed radius of 30 m provides some support for the notion that a plot radius closer to the actual canopy area viewed strengthens the relationship between LAI and important metrics. We chose to cover a large range of variable radii by using relatively coarse increments. For example, a 25% change in the MTH of the mean plot was equal to a 7 m change in radius. Given the large decrease in model accuracy outside of the optimal range, it may have been preferable to exclude values at the extremes in favour of finer increments close to canopy height.

Ratio metrics were the most important group of predictors trialled, being most frequently selected in fixed and variable elastic net models and having the highest conditional importance scores in RF. Previous ALS-LAI work has demonstrated the importance of ratio metrics (Korhonen et al., 2011; Morsdorf, 2006; Solberg et al., 2009, 2006), but these studies have often relied on low HTs (often instrument height). Our study confirms that the optimum HT for many ratio metrics may lie considerably above these typical heights. Zhao & Popescu (2009) identified a much higher (3.6 m) HT as the optimal value for ratio metrics used in their study and reached a similar conclusion that prior studies using lower HTs may not have achieved the strongest result possible. Our methodology trialling models at all combinations of radius and HT provided additional insight into patterns of covariate importance. We observed that using ratio metrics generated using the best HTs identified greatly increased the selection frequency in elastic net and importance score in RF of ratio metrics above a minimum plot size.

Interestingly, several of the ALS penetration proxy ratio metrics (e.g. SCI, LCI, MLP) discarded information from intermediate returns, focusing only on first or last returns. Indeed,

even PFaVegMean relied principally on first returns (although the mean is computed from all returns). Korhonen et al. (2011) omitted intermediate returns when devising LCI on the basis that these returns provide little additional information. The importance of these metrics in our study adds support to the idea that penetration type metrics forming a proxy for canopy gap fraction do not benefit substantially from the addition of intermediate returns. In contrast, the few height metrics highlighted as important did appear to benefit from intermediate returns. Most of the important height metrics related to the distribution of elevation values from all return types. It could be argued that these metrics also reflect canopy gap fraction and hence LAI by reflecting shifts in point distribution due to changes in canopy openness. These metrics were highly correlated with each other and had lower importance than ratio metrics. It is conceivable that model accuracy would not have been greatly impacted if the majority were excluded from model building. Of the more complex metrics, only the canopy density metric *CD_kurt_p5* of Peduzzi et al. (2012) was selected or ranked with high importance. This was the only complex metric developed and trialled in a planted forest, with the remainder being useful in studies conducted in natural forests (e.g. Griffin et al., 2008; Pope & Treitz, 2013) and it is conceivable that these metrics are better suited to these conditions.

Our objective was not to directly compare RF and elastic net, and we did not perform the prerequisite intermediate variable selection steps required to improve RF interpretability (e.g. Genuer, Poggi, & Tuleau-Malot, 2010). However, despite substantial differences in the assumptions and methods of RF and elastic net, the results often showed very similar patterns. Many metrics with high conditional importance were also those most frequently selected by elastic net. Both approaches showed ratio metrics increasing in importance (or selection and rank in elastic net) across the optimum HTs and an associated decrease in height metric importance at the same locations. One notable difference was evident in the series of RF models located at 50% of CH across fixed and variable radii. Few of the top elastic net models were located here, and the nonlinear semi-physical model did not improve using this HT. One possible explanation may be that certain covariates using this HT allowed RF models to avoid the bias shown by semi-physical and elastic net models for high LAI values. Regardless, the best elastic net model had lower RMSE and showed good overall predictive ability - albeit with some bias evident for high LAI values. The RMSE from 10-fold CV also agreed well with that obtained from LOOCV using the identified tuning parameters. Overall, the linear approach of elastic net was appealing for the accuracy and interpretability of models, and our results support those of other studies employing linear

methods for developing empirical models of LAI from ALS data (e.g. Beets et al., 2011; Morsdorf, 2006; Peduzzi et al., 2012; Pope & Treitz, 2013).

Given its simplicity, the semi-physical model was remarkable for its accuracy and our results supported this approach as a reliable method to estimate LAI by relating lidar penetration to gap fraction theory. The SCI metric of Solberg et al. (2009) was specifically proposed as a proxy to measure the canopy gap fraction through pulse penetration for use in the chosen semi-physical model. The combination performed well across a broad range of LAI values (LAI≈2–5). However, as with the best elastic net model, there was some evidence of underestimation of high LAI values (LAI>5) and the lower accuracy was also evident in the magnitude of the residuals. Overall, our results confirm those of other studies identifying SCI as an important metric with strong links to LAI (Härkönen et al., 2013; Korhonen et al., 2011; Solberg et al., 2009). Indeed, SCI was also highlighted as important in elastic net and random forests models. Tuning of the weighting applied by SCI to multiple return pulses did not appear beneficial over the default value of λ=0.5.

Aside from SCI, several other ratio metrics that have some relation to gap fraction were highlighted by both empirical approaches. Of these, PFaVegMean appeared to be particularly influential in the elastic net models, which had the lowest RMSE. This metric was based on a simpler metric: *percentage of first returns above the mean height*. The modified form removed the impact of ground returns and, as the HT increases, returns from the lower canopy. This allows the mean height to be more closely related to the central mass of vegetation returns and the metric begins to reflect canopy openness near this region. Several other metrics that attempt to establish links between ALS pulse penetration and LAI theory, such as LCI, SCI, ZP_Rig_t, and MLP, were also notable for their importance in both elastic net and RF, and our results confirm that these ratio metrics appear to have strong links to LAI but that they are sensitive to the selection of an appropriate HT.

The importance of ratio-based metrics across empirical and semi-physical models can be explained by the clear connection between these metrics and canopy gap fraction, which is nonlinearly related to canopy LAI through the Beer-Lambert law. Indeed, optical instruments such as the LAI-2200 use gap fraction to estimate LAI through inversion of the Poisson model (Section 2.3.6) and so it is not surprising that ratio (penetration) metrics that are sensitive to canopy gap fraction can be used to predict LAI. The approach of Solberg et al. (2009) and others to use regression to estimate an empirical extinction coefficient (the slope β in Eq. 4.6) may offer several advantages in the context of *P. radiata* forests. The coefficient

estimated in this way incorporates species-specific properties such as leaf angle distribution and crown properties that affect the interception of lidar by the forest canopy (Heiskanen et al., 2015). It has been proposed that knowledge of the coefficient would allow extrapolation of this approach to similar forest types without the need for re-calibration and therefore could be used generally within forest types (Heiskanen et al., 2015, 2015). This is particularly relevant in New Zealand, where most of the commercial estate is single-species forest, often managed using similar silvicultural regimes. Further research may reveal that a single coefficient could be used to estimate LAI in this forest type without the need for re-calibration. As discussed, the impact of plot radius on the performance of gap fraction related metrics can be understood through the fact that the ground instrument view distance is related to canopy height. In our study, the instrument was masked by up to 270°; however, in this homogenous forest type, gap fraction would be strongly influenced by tree spacing, which is relatively uniform within stands. Furthermore, our sampling strategy averaged many measurements of gap fraction, including many samples specifically targeting the areas that would be excluded from the instrument view when located at plot centre. Therefore, it is likely that gap fraction would be similar across most azimuthal directions and the sampling strategy would include measurements of gap fraction from all sectors of the plot, leaving a smaller mismatch between the lidar plot radius and the effective area observed by the LAI-2200C after masking the outer ring.

The impact of height threshold on the performance of the key ratio metrics is less well understood. Other studies have observed similar effects (K. Zhao & Popescu, 2009) but did not offer an explanation. The HT serves primarily to separate ground from canopy returns and our results strongly point to higher fixed or variable HTs improving the lidar ratio metrics relationship to LAI. One possibility is that the instrument measures of gap fraction are dominated by the large between-canopy gaps and that high HTs serve to better capture this aspect of canopy structure by characterising penetration at a level in the canopy that would be close to or just below the lower base of the canopy – the same region that would likely define the larger between-canopy gaps within the sensors field of view. The introduction of a variable HT based on maximum canopy height was primarily introduced to allow the HT to be set at different locations along the canopy profile while accounting for differences in height across plots. Use of this approach appeared beneficial, with several of the top models located at 20% of CH across all radius and modelling scenarios. It is worth noting that for many of our plots 20% of CH would be close to 4–6 m which coincided with

many of the best models achieved with a fixed HT. We did not have detailed crown descriptions; however, in this forest type, 20% of CH would be below the height of green crown in all but the youngest, unpruned stands. For many stands, this HT would reasonably separate the largest volume of light (and pulse) obscuring biomass from understory and below canopy returns. Canopy height models or convex hull tree detection and outlining methods may offer a means of further exploring this link by allowing the relationship between gap fraction from optical field measurements and the between-canopy gaps identified at different heights from the lidar methods to be compared.

Despite these promising results, discrete lidar is not as well suited to retrieval of LAI using gap probability theory as waveform methods. This is because discrete methods necessarily sample only a limited portion of the canopy and cannot reliably resolve gaps below the footprint size or gaps that are not sampled at all. Waveform profile techniques record the cumulative reflected energy from all canopy and ground elements and, once decomposed, very accurate measures of gap fraction can be obtained without the need for site-specific calibration (Armston et al., 2013; X. T. Chen et al., 2014). However, these sensors are not yet commonly used for terrain characterisation or forest inventory assessment in New Zealand and calibrated, discrete ALS-LAI methods remain the only practical path to achieve large-scale LAI estimation.

It must be noted that all the modelling approaches trialled in our study were likely to have been impacted by a degree of measurement error. Although Pearse et al. (2016) found strong agreement between measurements taken under clear and diffuse sky, the generally higher mean estimates from clear sky measurements would have affected 43% of the plots in our study. The requirement of previous generations of the instrument to measure LAI only under diffuse skies can greatly restrict field data collection (e.g. Solberg et al., 2009). The clear-sky scattering correction model of Kobayashi et al. (2013) greatly expanded the number of LAI plots available for measurement in our study during the (largely) dormant season. Therefore, we judged the introduced error worth the expansion in sample size achieved in this time period. Despite this potential source of error, the only evidence of systematic bias appeared more closely related to high LAI values, and the overall model performance clearly demonstrated a strong relationship between ALS metrics and measured LAI.

4.7 Conclusions

Our results demonstrate that ALS data offer an effective method to estimate LAI in planted forests of *Pinus radiata*. Using the default plot parameters of lidar radius equal to inventory plot size and HT equal to DBH or instrument height produced some of the weakest models observed. For fixed radius plots, our findings supported previous work favouring larger fixed radii. However, use of a variable plot radius close to the expected instrument view distance produced the best results. These results appeared to support proposed links between instrument view distance and the optimum plot radius. Our results emphasised the importance of ratio metrics that use pulse penetration as a proxy for gap fraction for ALS-LAI estimation. Our approach demonstrated that beyond a minimum fixed or variable plot size, the optimal choice of HT for ratio metrics had a much greater impact on model sparsity and accuracy. Near the optimal fixed HT (4–6 m in our study) several ratio metrics alone were nearly sufficient to predict LAI in several of the best linear elastic net models. Conditional variable importance scores from RF showed ratio metrics at higher HTs to have the highest importance of all metrics trialled. Our study also trialled the use of a variable HT for ratio metrics set as a percentage of the maximum canopy height within each plot. Several of the best models were located where ratio metrics used an HT equal to 20% of canopy height, supporting the use of this approach. Empirically derived elastic net models produced the best ALS-LAI models. However, the semi-physical models and metrics proposed by Solberg et al (2009) appear well suited to ALS-LAI estimation, especially considering the relative simplicity of the metric and model required. These metrics directly relate lidar penetration to LAI through gap probability theory and may offer the potential to estimate LAI without empirical calibration in similar forest types.

4.8 Acknowledgements

This research was supported by the Growing Confidence in Forestry's Future (GCFF) research program administered by Scion New Zealand Ltd. The corresponding author received additional support in the form of a scholarship from the University of Canterbury, New Zealand. We would like to thank Timberlands Ltd. and their helpful staff for providing access to the forest and associated data.

Chapter 5 - Summary and Conclusions

5.1 Acquiring field measurements of LAI

The over-arching goal of this thesis was to develop methods for estimating LAI from lidar data in New Zealand's unique *P. radiata* forests. In order to accomplish this, it was necessary to address the first research question by validating the use of the new LAI-2200C and accompanying scattering correction model. The strong agreement observed between results after masking the outer ring and parameterising the model with measured values for reflectance and transmittance were encouraging. Other studies estimating LAI from lidar have been limited by the need to sample only under diffuse skies (Solberg et al., 2009) and this would have been no different in the sampling carried out for this thesis. Being constrained to sampling only under diffuse skies would have reduced the number of plots to 77 instead of the combined total of 135. Instead, by being able to sample under clear and diffuse skies this study was able to utilise one of the largest datasets collected for development of ALS-LAI models. For example, Zhao and Popescu (2009) relied on 53 LAI plots, while Solberg at al. (2009) and Korhonen et al. (2011) used 35 and 64 plots respectively, measured with a combination of HCP and LAI. Peduzzi et al. (2012) were able to measure 104 plots with the LAI-2000 but measurements crossed seasons, and changes in LAI necessitated adjustments to some measurements. It is clear that the advent of the scattering correction model can greatly assist future work requiring field estimates of LAI.

Despite these advantages, hemispherical photography should not be overlooked as a potential method for future studies relying on field measurements of LAI. The field of HCP image acquisition and processing is advancing rapidly and in the time elapsed during the preparation of this thesis advances have been made in theoretical methods for removing the influence of woody material on LAI estimates from canopy images (Woodgate, Disney, et al., 2015; Woodgate et al., 2016). In the same brief time period, advances have been made that may allow detailed sky reconstruction from HCP images in order to better segment sky and canopy pixels regardless of sky condition, potentially allowing for images to be acquired under an even greater range of sampling conditions than those afforded by the LAI-2200C (Hwang et al., 2016). If successfully validated, these methods may allow unconstrained

sampling with the additional benefits of HCP such as improved estimation of clumping index (Leblanc et al., 2005), identification of stems (Piayda et al., 2015), and defining custom image segments for analysis. Furthermore, HCP-based instruments are generally cheaper and do not require large open clearings for above canopy reference measurements. Nonetheless, until these methods mature, the LAI-2200C offers a robust means of measuring LAI under the broadest range of sky conditions. The reduced error in the outer ring and generally higher LAI values obtained suggests that the scattering correction model may actually improve LAI estimates and a comparison of clear sky LAI measurements and reference values from destructive harvesting would be a valuable addition to the literature. Finally, the reduction in potential measurement error when sampling under clear skies cannot be overlooked. Experience in the field revealed that uniform overcast days are rare in the region where the thesis study was conducted, and unobserved sky changes are almost inevitable when the sensors are separated by some distance. Although stray clouds were also an issue in clear skies, these could easily be seen visually. Clear sky changes were also relatively easy to identify when examining the raw data from the reference sensor. This was not true with overcast days where intra-ring variation could be as high as inter-temporal changes in the transmittance values recorded by the LAI-2200C. The reasons for this are unclear, but the implications are that clear sky LAI measurement may offer both reduced instrument error resulting from scattered light and reduced measurement error resulting from unstable sky conditions.

Previously, measured needle spectra were principally required for radiative transfer modelling or for use in hyperspectral studies (Coops & Stone, 2005; Stone, Chisholm, & McDonald, 2003). However, with the advent of the scattering correction model, there is likely to be increased need to acquire accurate spectra from needle-leaved species. Research questions 2-3 were chosen to identify the value of acquiring measured spectra and potential methods to acquire these should they prove important. While results in this study showed that use of the default reflectance (0.05) and transmittance (0.01) still produced good agreement with diffuse sky LAI (R^2=0.78) the use of measured values was still justified, producing stronger agreement (R^2=.87) and reducing the size of the residuals. This is important where LAI measurement taken under both diffuse and clear skies are to be pooled – a principle advantage of the new instrument. Therefore, the advent of the method proposed by Noda et al. (2013) for overcoming the many challenges of acquiring accurate spectra from needle-leaved species is timely. Although further testing in other species will be required, the

stability of the spectra acquired for this thesis suggests that it may be possible to re-use measured spectra for a species in subsequent applications of the scattering correction model. It is very likely that the noise and instability of transmittance values were due to instrument error. Overall, the method was very efficient and required minimal sample preparation – keeping sample degradation to a minimum.

5.2 Estimating LAI from lidar

The literature review presented in Chapter 2 clearly highlighted the advantages of using lidar to estimate LAI. However, the summary of different approaches and metrics presented in Chapter 4 identified many uncertainties in selecting the best approach when attempting to predict LAI from lidar. In the context of this thesis, where there was no established body of work to build on, this necessitated a much more in-depth process to develop models than was initially envisioned. Early results using the most promising methods from other forest types produced poor results and alternative methods had to be sought. It was immediately evident from the literature that the list of candidate lidar metrics precluded analysis using standard lidar processing tools such as FUSION (McGaughey, 2015) and this problem was formulated as research question 4. The scale of the problem was greatly increased by the added uncertainty around the optimum choice of plot parameters such as choice of height threshold and fixed or variable radius plots. The development of a dedicated software tool greatly facilitated the analysis and the thesis results presented are the first to simultaneously address lidar metric selection, plot parameters, and modelling approach (research questions 4-6 respectively). The results showed that the analysis was worthwhile as the 'default' parameters (radius set at inventory plot size of 14 m and height threshold set at instrument height of 1.4 m) produced some of the weakest results of all models trialled. Furthermore, using these values failed to identify any of the key predictive metrics. The best model results with RMSE=0.57 LAI compared favourably to other research in the area. For example, Peduzzi et al. (2012) found the best model in their study estimating LAI from lidar in *P. taeda* plantations to have RMSE=0.46, while Zhao and Popescu (2009) found a model with RMSE=0.29 from a smaller study with several plots located in planted pine forests. Indeed, the results from this thesis are likely to be biased towards higher error. This is because when selecting methods for cross-validation and the elastic net, the choices were always towards pessimistic assessment of model performance (for example using the 1-standard error rule in Section 4-3.3). The LAI values observed in plots measured for this thesis ranged from 1 to

nearly 7. This range is much larger than that seen in many other ALS-LAI studies. This is significant because even at the maximum LAI, only weak evidence for increased bias was observed (-0.005 overall). Taken together, these results strongly suggest that ALS-LAI estimation is a viable tool for large-scale assessment of LAI, offering accurate predictions across the full range of LAI values found in intensively managed pine forests. A significant finding from this thesis was the detection of very high levels of inter-correlation between classes of lidar metrics. The levels of correlation observed between predictors were severe enough to pose serious limitations to statistical approaches sensitive to these effects. This has significant implications for past and future studies, as undetected inter-correlation of this magnitude would likely impact the validity and robustness of the results obtained.

The observation that larger fixed radii (4-6 m) improved ALS-LAI models was consistent with results from the few studies examining the question (K. Zhao & Popescu, 2009), as was the finding that a variable radius produced better overall results (Riaño et al., 2004; Solberg et al., 2009). However, what was significant from the thesis results was the degree of interaction observed between the choice of plot radius and height threshold. This interaction has not previously been explored and the results showed that above a minimum fixed radius the choice of a higher height threshold was relatively more important. The implications of this finding are that reasonable combinations of fixed plot parameters may be obtained by trialling relatively coarse increments of radius and height threshold. However, the improved results from variable radii plots strongly suggests these should be trialled in future work. Interestingly, work done subsequent to this thesis has examined the transferability of results from ALS-LAI models to metrics derived in new settings. Results from this work appeared to suggest that only a limited number of lidar metrics were applicable outside of the site where they were developed (Sumnall et al., 2016). This suggests that a framework such as the one used in this thesis is likely to be called for when developing ALS-LAI models elsewhere. The recommendations in Section 4-6 may provide some general guidelines for future work in this area.

5.3 Operational implications

The primary goal of the thesis was to attempt to develop methods for large-scale estimation of LAI from ALS data captured over production forests. This was achieved with a reasonable level of accuracy, and several of the findings may help to guide similar efforts.

Acquisition of LAI field measurements is required to calibrate the empirical models and to estimate the extinction coefficient (slope of the no-intercept regression). The LAI-2200C offers the strong advantage of expanding sampling conditions to include clear sky conditions. However, for other species, it is recommended that measured needle spectra are acquired and that the outer ring is masked when pooling data acquired under both diffuse and clear sky conditions. Based on the findings in Chapter 3, this approach will minimise the differences between measurements. The use of hemispherical canopy photography (HCP) should also be examined. Although measurements are best acquired under diffuse skies, new developments in software may expand the range of suitable conditions to include some clear sky conditions (Hwang et al., 2016). HCP has the advantage of observing the entire hemisphere whereas the LAI-2200C must usually be operated with a view restrictor due to the presence of direct sunlight and very few large clearings available for matching 'above' canopy readings. HCP also offers the ability to limit retrieval of gap fraction to any defined region of the hemisphere, allowing issues such as the selection of an appropriate HT and plot radius to be carefully examined. This ability also allows LAI to be retrieved at the zenith region centred on 57°, where the projection coefficient is insensitive to the (often unknown) leaf angle distribution. More accurate methods to extract clumping index from gap fraction data are also available in HCP software and these are likely to improve LAI estimates in *P. radiata* or other coniferous forest types with highly clumped canopy architecture.

The findings in Chapter 4 suggest that empirical models estimating LAI from ALS data perform well in this forest type. Generation of metrics does not need to include the full list outlined in this study. Instead, ratio metrics (e.g. SCI, LCI, MLP, PFaVegMean) should be strongly favoured, with a limited set of distributional and descriptive height metrics suggested as well. Use of a variable plot radius based on the instrument view distance is well supported by the literature and the findings of this thesis. If HCP is used to measure LAI then it may be possible to adjust the view zenith range to better improve the alignment between lidar plot radius and instrument view distance, although this approach could not be tested using the LAI-2200C. Although the mechanism is not clear, choice of height threshold strongly impacts the strength of the relationship between ratio metrics and LAI in both the empirical and theoretical approach. Findings from this thesis and the broader literature suggest that the optimum HT may be some distance above instrument height and the use of a variable HT based on canopy height should be explored to identify the optimum HT for the important ratio-based metrics.

Care should be taken when selecting modelling methods as high levels of inter-correlation between lidar metrics was observed in the results of this study. A smaller set of metrics will likely alleviate some of these issues; however, methods such as regularised regression or random forests are well suited to modelling LAI from ALS and include methods to compensate for intercorrelation and overfitting. This contrasts with linear regression which is very likely to overfit models when used with a large number of predictors, while the correlation levels would make the estimated coefficients unstable.

Models produced using the empirical approach are likely to be site and campaign specific and the process may well need to be repeated in new locations or with different ALS data. Where simplicity is desired, the semi-physical model presented in Chapter 4 appears to provide good estimates of LAI based on the use of the SCI metric. This approach uses a metric that measures canopy penetration from lidar in a model that inverts the widely-used Poisson gap probability model to obtain LAI. Further development of the semi-physical model may offer an opportunity to overcome the site-dependence of empirical models requiring calibration with *in situ* LAI measurements. Other studies using the semi-physical model have observed that because only a single parameter (β - the slope estimate) is required it may be possible to reuse estimates between similar forest types (Härkönen et al., 2013; Korhonen et al., 2011). The proposed link between β and the foliage projection coefficient (and hence leaf angle distribution – see Section 2.3.4) is partially supported by observations that stratification is beneficial when applying the SCI-based model across forest types with different leaf angle distributions (Heiskanen et al., 2015). This line of research is particularly appealing in the context of plantation forestry. Foliage projection and leaf angle distribution and are often highly variable in natural forests (Stenberg, 2006), but it is plausible that values may be more stable, and hence reusable without calibration, in relatively homogenous forest types. Indeed, there is even the potential to explore stratification of β values according to other factors that may be linked to the foliage projection coefficient such as age class or stand density. Success in this area would allow LAI to be repeatedly estimated from ALS data across large areas of New Zealand's planted forest estate without calibration data and with the potential to instead explore adjustment of the β coefficient according to influential auxiliary data such as stand density. The information provided by such an approach would be a valuable tool for researchers and forest managers alike.

References

Amponsah, I. G., Comeau, P. G., Brockley, R. P., & Lieffers, V. J. (2005). Effects of repeated fertilization on needle longevity, foliar nutrition, effective leaf area index, and growth characteristics of lodgepole pine in interior British Columbia, Canada. *Canadian Journal of Forest Research, 35*(2), 440–451. https://doi.org/10.1139/x04-200

Anderson, K., Hancock, S., Disney, M., & Gaston, K. J. (2016). Is waveform worth it? A comparison of LiDAR approaches for vegetation and landscape characterization. *Remote Sensing in Ecology and Conservation, 2*(1), 5–15. https://doi.org/10.1002/rse2.8

Armston, J., Disney, M., Lewis, P., Scarth, P., Phinn, S., Lucas, R., … Goodwin, N. (2013). Direct retrieval of canopy gap probability using airborne waveform lidar. *Remote Sensing of Environment, 134*, 24–38. https://doi.org/10.1016/j.rse.2013.02.021

Asrar, G., Fuchs, M., Kanemasu, E. T., & Hatfield, J. L. (1984). Estimating Absorbed Photosynthetic Radiation and Leaf Area Index from Spectral Reflectance in Wheat. *Agronomy Journal*, *76*(2), 300–306. https://doi.org/10.2134/agronj1984.00021962007600020029x

Balster, N. J., & Marshall, J. D. (2000). Eight-year responses of light interception, effective leaf area index, and stemwood production in fertilized stands of interior Douglas-fir (Pseudotsuga menziesii var. glauca). *Canadian Journal of Forest Research, 30*(5), 733–743. https://doi.org/10.1139/x00-002

References

Baltsavias, E. . (1999). Airborne laser scanning: basic relations and formulas. *ISPRS Journal of Photogrammetry and Remote Sensing*, *54*(2–3), 199–214. https://doi.org/10.1016/S0924-2716(99)00015-5

Barilotti, A., Turco, S., & Alberti, G. (2006). LAI determination in forestry ecosystem by LiDAR data analysis. Presented at the Workshop on 3D Remote Sensing in Forestry, Vienna, Austria. Retrieved from http://www.rali.boku.ac.at/fileadmin/data/H03000/H85000/H85700/workshops/3drsforestry/presentations/8b.3-barilotti.pdf

Bartelink, H. H. (1996). Allometric relationships on biomass and needle area of Douglas-fir. *Forest Ecology and Management*, *86*(1–3), 193–203. https://doi.org/10.1016/S0378-1127(96)03783-8

Beckschäfer, P., Seidel, D., Kleinn, C., & Xu, J. (2013). On the exposure of hemispherical photographs in forests. *iForest - Biogeosciences and Forestry*, *6*(4), 228–237. https://doi.org/10.3832/ifor0957-006

Beets, P. N. (1977). Determination of the fascicle surface area for Pinus radiata. *NZJ For. Sci*, *7*(3), 397–407.

Beets, P. N., Reutebuch, S., Kimberley, M. O., Oliver, G. R., Pearce, S. H., & McGaughey, R. J. (2011). Leaf Area Index, Biomass Carbon and Growth Rate of Radiata Pine Genetic Types and Relationships with LiDAR. *Forests*, *2*(4), 637–659. https://doi.org/10.3390/f2030637

Beets, P. N., & Whitehead, D. (1996). Carbon partitioning in Pinus radiata stands in relation to foliage nitrogen status. *Tree Physiology*, *16*(1–2), 131–138. https://doi.org/10.1093/treephys/16.1-2.131

Béland, M., Baldocchi, D. D., Widlowski, J.-L., Fournier, R. A., & Verstraete, M. M. (2014). On seeing the wood from the leaves and the role of voxel size in determining leaf area

distribution of forests with terrestrial LiDAR. *Agricultural and Forest Meteorology*, *184*, 82–97. https://doi.org/10.1016/j.agrformet.2013.09.005

Béland, M., Widlowski, J.-L., & Fournier, R. A. (2014). A model for deriving voxel-level tree leaf area density estimates from ground-based LiDAR. *Environmental Modelling & Software*, *51*, 184–189. https://doi.org/10.1016/j.envsoft.2013.09.034

Bland, J. M., & Altman, D. (1986). Statistical methods for assessing agreement between two methods of clinical measurement. *The Lancet*, *327*(8476), 307–310. https://doi.org/10.1016/S0140-6736(86)90837-8

Bréda, N. J. J. (2003). Ground-based measurements of leaf area index: a review of methods, instruments and current controversies. *Journal of Experimental Botany*, *54*(392), 2403–2417. https://doi.org/10.1093/jxb/erg263

Bréda, N. J. J. (2008). Leaf Area Index. In Editors-in-Chief: Sven Erik Jorgensen & Brian Fath (Eds.), *Encyclopedia of Ecology* (pp. 2148–2154). Oxford: Academic Press. Retrieved from http://www.sciencedirect.com/science/article/pii/B9780080454054008491

Breiman, L. (2001). Random Forests. *Machine Learning*, *45*(1), 5–32. https://doi.org/10.1023/A:1010933404324

Brix, H., & Mitchell, A. K. (1983). Thinning and nitrogen fertilization effects on sapwood development and relationships of foliage quantity to sapwood area and basal area in Douglas-fir. *Canadian Journal of Forest Research*, *13*(3), 384–389. https://doi.org/10.1139/x83-057

Broge, N. ., & Leblanc, E. (2001). Comparing prediction power and stability of broadband and hyperspectral vegetation indices for estimation of green leaf area index and canopy chlorophyll density. *Remote Sensing of Environment*, *76*(2), 156–172. https://doi.org/10.1016/S0034-4257(00)00197-8

References

Brown, L., Chen, J. M., Leblanc, S. G., & Cihlar, J. (2000). A Shortwave Infrared Modification to the Simple Ratio for LAI Retrieval in Boreal Forests: An Image and Model Analysis. *Remote Sensing of Environment*, *71*(1), 16–25. https://doi.org/10.1016/S0034-4257(99)00035-8

Carlson, T. N., & Ripley, D. A. (1997). On the relation between NDVI, fractional vegetation cover, and leaf area index. *Remote Sensing of Environment*, *62*(3), 241–252. https://doi.org/10.1016/S0034-4257(97)00104-1

Carlyle, J. C. (1998). Relationships between nitrogen uptake, leaf area, water status and growth in an 11-year-old Pinus radiata plantation in response to thinning, thinning residue, and nitrogen fertiliser. *Forest Ecology and Management*, *108*(1–2), 41–55. https://doi.org/10.1016/S0378-1127(97)00333-2

Carter, G. A., & Knapp, A. K. (2001). Leaf optical properties in higher plants: linking spectral characteristics to stress and chlorophyll concentration. *American Journal of Botany*, *88*(4), 677–684.

Chasmer, L., Hopkinson, C., Smith, B., & Treitz, P. (2006). Examining the influence of changing laser pulse repetition frequencies on conifer forest canopy returns. *Photogrammetric Engineering and Remote Sensing*, *72*(12), 1359.

Chen, J. M. (1996). Optically-based methods for measuring seasonal variation of leaf area index in boreal conifer stands. *Agricultural and Forest Meteorology*, *80*(2–4), 135–163. https://doi.org/10.1016/0168-1923(95)02291-0

Chen, J. M., & Black, T. A. (1992). Defining leaf area index for non-flat leaves. *Plant, Cell & Environment*, *15*(4), 421–429. https://doi.org/10.1111/j.1365-3040.1992.tb00992.x

Chen, J. M., Black, T. A., & Adams, R. S. (1991). Evaluation of hemispherical photography for determining plant area index and geometry of a forest stand. *Agricultural and Forest Meteorology*, *56*(1), 129–143. https://doi.org/10.1016/0168-1923(91)90108-3

References

Chen, J. M., & Cihlar, J. (1995). Quantifying the effect of canopy architecture on optical measurements of leaf area index using two gap size analysis methods. *IEEE Transactions on Geoscience and Remote Sensing*, *33*(3), 777–787. https://doi.org/10.1109/36.387593

Chen, J. M., & Cihlar, J. (1996). Retrieving leaf area index of boreal conifer forests using Landsat TM images. *Remote Sensing of Environment*, *55*(2), 153–162. https://doi.org/10.1016/0034-4257(95)00195-6

Chen, J. M., Govind, A., Sonnentag, O., Zhang, Y., Barr, A., & Amiro, B. (2006). Leaf area index measurements at Fluxnet-Canada forest sites. *Agricultural and Forest Meteorology*, *140*(1–4), 257–268. https://doi.org/10.1016/j.agrformet.2006.08.005

Chen, J. M., Rich, P. M., Gower, S. T., Norman, J. M., & Plummer, S. (1997). Leaf area index of boreal forests: Theory, techniques, and measurements. *Journal of Geophysical Research: Atmospheres*, *102*(D24), 29429–29443. https://doi.org/10.1029/97JD01107

Chen, X. T., Disney, M. I., Lewis, P., Armston, J., Han, J. T., & Li, J. C. (2014). Sensitivity of direct canopy gap fraction retrieval from airborne waveform lidar to topography and survey characteristics. *Remote Sensing of Environment*, *143*, 15–25. https://doi.org/10.1016/j.rse.2013.12.010

Chianucci, F., & Cutini, A. (2012). Digital hemispherical photography for estimating forest canopy properties: current controversies and opportunities. *iForest - Biogeosciences and Forestry*, *5*(6), 290–295. https://doi.org/10.3832/ifor0775-005

Cohen, W. B., Maiersperger, T. K., Yang, Z., Gower, S. T., Turner, D. P., Ritts, W. D., … Running, S. W. (2003). Comparisons of land cover and LAI estimates derived from ETM+ and MODIS for four sites in North America: a quality assessment of

2000/2001 provisional MODIS products. *Remote Sensing of Environment*, *88*(3), 233–255. https://doi.org/10.1016/j.rse.2003.06.006

Coops, N. C., Hilker, T., Wulder, M. A., St-Onge, B., Newnham, G., Siggins, A., & Trofymow, J. A. (Tony). (2007). Estimating canopy structure of Douglas-fir forest stands from discrete-return LiDAR. *Trees*, *21*(3), 295–310. https://doi.org/10.1007/s00468-006-0119-6

Coops, N. C., & Stone, C. (2005). A comparison of field-based and modelled reflectance spectra from damaged Pinus radiata foliage. *Australian Journal of Botany*, *53*(5), 417–429. https://doi.org/10.1071/BT04129

Criminisi, A., Shotton, J., & Konukoglu, E. (2012). Decision forests: A unified framework for classification, regression, density estimation, manifold learning and semi-supervised learning. *Foundations and Trends in Computer Graphics and Vision*, *7*(2–3), 81–227. https://doi.org/10.1561/0600000035

Curran, P. J., Dungan, J. L., & Gholz, H. L. (1992). Seasonal LAI in slash pine estimated with landsat TM. *Remote Sensing of Environment*, *39*(1), 3–13. https://doi.org/10.1016/0034-4257(92)90136-8

Danson, F. M., Gaulton, R., Armitage, R. P., Disney, M., Gunawan, O., Lewis, P., … Ramirez, A. F. (2014). Developing a dual-wavelength full-waveform terrestrial laser scanner to characterize forest canopy structure. *Agricultural and Forest Meteorology*, *198–199*, 7–14. https://doi.org/10.1016/j.agrformet.2014.07.007

Danson, F. M., Hetherington, D., Morsdorf, F., Koetz, B., & Allgower, B. (2007). Forest Canopy Gap Fraction From Terrestrial Laser Scanning. *IEEE Geoscience and Remote Sensing Letters*, *4*(1), 157–160. https://doi.org/10.1109/LGRS.2006.887064

References

Dash, J. P., Marshall, H. M., & Rawley, B. (2015). Methods for estimating multivariate stand yields and errors using k-NN and aerial laser scanning. *Forestry*, *88*(2), 237–247. https://doi.org/10.1093/forestry/cpu054

Dassot, M., Constant, T., & Fournier, M. (2011). The use of terrestrial LiDAR technology in forest science: application fields, benefits and challenges. *Annals of Forest Science*, *68*(5), 959–974. https://doi.org/10.1007/s13595-011-0102-2

Daughtry, C. S. T., Biehl, L. L., & Ranson, K. J. (1989). A new technique to measure the spectral properties of conifer needles. *Remote Sensing of Environment*, *27*(1), 81–91. https://doi.org/10.1016/0034-4257(89)90039-4

Disney, M. I., Kalogirou, V., Lewis, P., Prieto-Blanco, A., Hancock, S., & Pfeifer, M. (2010). Simulating the impact of discrete-return lidar system and survey characteristics over young conifer and broadleaf forests. *Remote Sensing of Environment, 114*(7), 1546–1560. https://doi.org/10.1016/j.rse.2010.02.009

Doane, D. P., & Seward, L. E. (2011). Measuring skewness: a forgotten statistic. *Journal of Statistics Education*, *19*(2), 1–18.

Douglas, E. S., Strahler, A., Martel, J., Cook, T., Mendillo, C., Marshall, R., … Lovell, J. (2012). DWEL: A Dual-Wavelength Echidna Lidar for ground-based forest scanning. In *Geoscience and Remote Sensing Symposium (IGARSS), 2012 IEEE International* (pp. 4998–5001). https://doi.org/10.1109/IGARSS.2012.6352489

Dubayah, R., Goetz, S. J., Blair, J. B., Fatoyinbo, T. E., Hansen, M., Healey, S. P., … Luthcke, S. B. (2014). The global ecosystem dynamics investigation. In *AGU Fall Meeting Abstracts* (Vol. 1, p. 07).

Fang, H., & Liang, S. (2008). Leaf Area Index Models. In Editors-in-Chief: Sven Erik Jorgensen & Brian Fath (Eds.), *Encyclopedia of Ecology* (pp. 2139–2148). Oxford:

Academic Press. Retrieved from http://www.sciencedirect.com/science/article/pii/B9780080454054001907

Fassnacht, K. S., Gower, S. T., Norman, J. M., & McMurtric, R. E. (1994). A comparison of optical and direct methods for estimating foliage surface area index in forests. *Agricultural and Forest Meteorology*, *71*(1–2), 183–207. https://doi.org/10.1016/0168-1923(94)90107-4

Fife, D. N., & Nambiar, E. K. S. (1997). Changes in the canopy and growth of Pinus radiata in response to nitrogen supply. *Forest Ecology and Management*, *93*(1–2), 137–152. https://doi.org/10.1016/S0378-1127(96)03917-5

Finlay, K., Vogt, R. J., Bogard, M. J., Wissel, B., Tutolo, B. M., Simpson, G. L., & Leavitt, P. R. (2015). Decrease in CO2 efflux from northern hardwater lakes with increasing atmospheric warming. *Nature*, *519*(7542), 215–218. https://doi.org/10.1038/nature14172

Friedman, J., Hastie, T., & Tibshirani, R. (2001). *The elements of statistical learning* (Vol. 1). Springer series in statistics Springer, Berlin.

Friedman, J., Hastie, T., & Tibshirani, R. (2010). Regularization Paths for Generalized Linear Models via Coordinate Descent. *Journal of Statistical Software*, *33*(1), 22. https://doi.org/10.18637/jss.v033.i01

Gatziolis, D., & Andersen, H.-E. (2008). *A guide to LiDAR data acquisition and processing for the forests of the Pacific Northwest*. US Department of Agriculture, Forest Service, Pacific Northwest Research Station. Retrieved from http://www.arlis.org/docs/vol1/A/276932054.pdf

Genuer, R., Poggi, J.-M., & Tuleau-Malot, C. (2010). Variable selection using random forests. *Pattern Recognition Letters*, *31*(14), 2225–2236. https://doi.org/10.1016/j.patrec.2010.03.014

References

Gower, S. T., Kucharik, C. J., & Norman, J. M. (1999). Direct and Indirect Estimation of Leaf Area Index, fAPAR, and Net Primary Production of Terrestrial Ecosystems. *Remote Sensing of Environment*, *70*(1), 29–51. https://doi.org/10.1016/S0034-4257(99)00056-5

Graham, L. (2012). The LAS 1.4 specification. *Photogrammetric Engineering and Remote Sensing*, *78*(2), 93–102.

Griffin, A. M., Popescu, S., & Zhao, K. (2008). Using LIDAR and normalized difference vegetation index to remotely determine LAI and percent canopy cover. In *Proceedings of SilviLaser*. Retrieved from http://geography.swan.ac.uk/silvilaser/papers/poster_papers/Griffin.pdf

Grömping, U. (2009). Variable Importance Assessment in Regression: Linear Regression versus Random Forest. *The American Statistician*, *63*(4), 308–319. https://doi.org/10.1198/tast.2009.08199

Hancock, S., Lewis, P., Foster, M., Disney, M., & Muller, J.-P. (2012). Measuring forests with dual wavelength lidar: A simulation study over topography. *Agricultural and Forest Meteorology*, *161*, 123–133. https://doi.org/10.1016/j.agrformet.2012.03.014

Harding, D. J., & Carabajal, C. C. (2005). ICESat waveform measurements of within-footprint topographic relief and vegetation vertical structure. *Geophysical Research Letters*, *32*(21), L21S10. https://doi.org/10.1029/2005GL023471

Härkönen, S., Tokola, T., Packalén, P., Korhonen, L., & Mäkelä, A. (2013). Predicting forest growth based on airborne light detection and ranging data, climate data, and a simplified process-based model. *Canadian Journal of Forest Research*, *43*(4), 364–375. https://doi.org/10.1139/cjfr-2012-0295

Heiskanen, J., Korhonen, L., Hietanen, J., & Pellikka, P. K. E. (2015). Use of airborne lidar for estimating canopy gap fraction and leaf area index of tropical montane forests.

International Journal of Remote Sensing, *36*(10), 2569–2583. https://doi.org/10.1080/01431161.2015.1041177

Hilker, T., van Leeuwen, M., Coops, N. C., Wulder, M. A., Newnham, G. J., Jupp, D. L. B., & Culvenor, D. S. (2010). Comparing canopy metrics derived from terrestrial and airborne laser scanning in a Douglas-fir dominated forest stand. *Trees*, *24*(5), 819–832. https://doi.org/10.1007/s00468-010-0452-7

Holmgren, J., Nilsson, M., & Olsson, H. (2003). Simulating the effects of lidar scanning angle for estimation of mean tree height and canopy closure. *Canadian Journal of Remote Sensing*, *29*(5), 623–632. https://doi.org/10.5589/m03-030

Hopkinson, C., & Chasmer, L. (2007a). Modelling canopy gap fraction from lidar intensity. In *ISPRS Workshop on Laser Scanning 2007 and SilviLaser 2007* (pp. 190–194). Retrieved from http://www.isprs.org/proceedings/XXXVI/3-W52/final_papers/Hopkinson_2007.pdf

Hopkinson, C., & Chasmer, L. (2007b). Using discrete laser pulse return intensity to model canopy transmittance. *The Photogrammetric Journal of Finland*, *20*(2), 16–26.

Hopkinson, C., & Chasmer, L. (2009). Testing LiDAR models of fractional cover across multiple forest ecozones. *Remote Sensing of Environment*, *113*(1), 275–288. https://doi.org/10.1016/j.rse.2008.09.012

Hosking, J. R. M. (1990). L-Moments: Analysis and Estimation of Distributions Using Linear Combinations of Order Statistics. *Journal of the Royal Statistical Society. Series B (Methodological)*, *52*(1), 105–124.

Hosoi, F., & Omasa, K. (2006). Voxel-Based 3-D Modeling of Individual Trees for Estimating Leaf Area Density Using High-Resolution Portable Scanning Lidar. *IEEE Transactions on Geoscience and Remote Sensing*, *44*(12), 3610–3618. https://doi.org/10.1109/TGRS.2006.881743

References

Hosoi, F., & Omasa, K. (2007). Factors contributing to accuracy in the estimation of the woody canopy leaf area density profile using 3D portable lidar imaging. *Journal of Experimental Botany*, *58*(12), 3463–3473. https://doi.org/10.1093/jxb/erm203

Huang, P., & Pretzsch, H. (2010). Using terrestrial laser scanner for estimating leaf areas of individual trees in a conifer forest. *Trees*, *24*(4), 609–619. https://doi.org/10.1007/s00468-010-0431-z

Huete, A., Didan, K., Miura, T., Rodriguez, E. ., Gao, X., & Ferreira, L. . (2002). Overview of the radiometric and biophysical performance of the MODIS vegetation indices. *Remote Sensing of Environment*, *83*(1–2), 195–213. https://doi.org/10.1016/S0034-4257(02)00096-2

Hwang, Y., Ryu, Y., Kimm, H., Jiang, C., Lang, M., Macfarlane, C., & Sonnentag, O. (2016). Correction for light scattering combined with sub-pixel classification improves estimation of gap fraction from digital cover photography. *Agricultural and Forest Meteorology*, *222*, 32–44. https://doi.org/10.1016/j.agrformet.2016.03.008

Jakubowski, M. K., Guo, Q., & Kelly, M. (2013). Tradeoffs between lidar pulse density and forest measurement accuracy. *Remote Sensing of Environment*, *130*, 245–253. https://doi.org/10.1016/j.rse.2012.11.024

Jensen, J. L. R., Humes, K. S., Hudak, A. T., Vierling, L. A., & Delmelle, E. (2011). Evaluation of the MODIS LAI product using independent lidar-derived LAI: A case study in mixed conifer forest. *Remote Sensing of Environment*, *115*(12), 3625–3639. https://doi.org/10.1016/j.rse.2011.08.023

Jensen, J. L. R., Humes, K. S., Vierling, L. A., & Hudak, A. T. (2008). Discrete return lidar-based prediction of leaf area index in two conifer forests. *Remote Sensing of Environment*, *112*(10), 3947–3957. https://doi.org/10.1016/j.rse.2008.07.001

References

Johnson, J. D. (1984). A Rapid Technique for Estimating Total Surface Area of Pine Needles. *Forest Science*, *30*(4), 913–921.

Jonckheere, I., Fleck, S., Nackaerts, K., Muys, B., Coppin, P., Weiss, M., & Baret, F. (2004). Review of methods for in situ leaf area index determination: Part I. Theories, sensors and hemispherical photography. *Agricultural and Forest Meteorology*, *121*(1–2), 19–35. https://doi.org/10.1016/j.agrformet.2003.08.027

Jupp, D. L. B., Culvenor, D. S., Lovell, J. L., Newnham, G. J., Strahler, A. H., & Woodcock, C. E. (2009). Estimating forest LAI profiles and structural parameters using a ground-based laser called 'Echidna®. *Tree Physiology*, *29*(2), 171–181. https://doi.org/10.1093/treephys/tpn022

Kaasalainen, S., Pyysalo, U., Krooks, A., Vain, A., Kukko, A., Hyyppä, J., & Kaasalainen, M. (2011). Absolute Radiometric Calibration of ALS Intensity Data: Effects on Accuracy and Target Classification. *Sensors*, *11*(12), 10586–10602. https://doi.org/10.3390/s111110586

Kamal, M., Phinn, S., & Johansen, K. (2016). Assessment of multi-resolution image data for mangrove leaf area index mapping. *Remote Sensing of Environment*, *176*, 242–254. https://doi.org/10.1016/j.rse.2016.02.013

Kimberley, M., West, G., Dean, M., & Knowles, L. (2005). The 300 Index–a volume productivity index for radiata pine. *New Zealand Journal of Forestry*, *50*(2), 13–18.

Knyazikhin, Y., Martonchik, J. V., Diner, D. J., Myneni, R. B., Verstraete, M., Pinty, B., & Gobron, N. (1998). Estimation of vegetation canopy leaf area index and fraction of absorbed photosynthetically active radiation from atmosphere-corrected MISR data. *Journal of Geophysical Research: Atmospheres*, *103*(D24), 32239–32256. https://doi.org/10.1029/98JD02461

References

Knyazikhin, Y., Martonchik, J. V., Myneni, R. B., Diner, D. J., & Running, S. W. (1998). Synergistic algorithm for estimating vegetation canopy leaf area index and fraction of absorbed photosynthetically active radiation from MODIS and MISR data. *Journal of Geophysical Research: Atmospheres*, *103*(D24), 32257–32275. https://doi.org/10.1029/98JD02462

Kobayashi, H., Ryu, Y., Baldocchi, D. D., Welles, J. M., & Norman, J. M. (2013). On the correct estimation of gap fraction: How to remove scattered radiation in gap fraction measurements? *Agricultural and Forest Meteorology*, *174–175*, 170–183. https://doi.org/10.1016/j.agrformet.2013.02.013

Korhonen, L., Korpela, I., Heiskanen, J., & Maltamo, M. (2011). Airborne discrete-return LIDAR data in the estimation of vertical canopy cover, angular canopy closure and leaf area index. *Remote Sensing of Environment*, *115*(4), 1065–1080. https://doi.org/10.1016/j.rse.2010.12.011

Küßner, R., & Mosandl, R. (2000). Comparison of direct and indirect estimation of leaf area index in mature Norway spruce stands of eastern Germany. *Canadian Journal of Forest Research*, *30*(3), 440–447. https://doi.org/10.1139/x99-227

Kuusk, A., Lang, M., Kodar, A., & Sims, A. (2015). Estimation of Leaf Area Index of Hemiboreal Forests. *The Open Remote Sensing Journal*, *6*(1), 1–10. https://doi.org/10.2174/1875413901506010001

Lang, A. R. G. (1986). Leaf-Area and Average Leaf Angle From Transmission of Direct Sunlight. *Australian Journal of Botany*, *34*(3), 349–355. https://doi.org/10.1071/BT9860349

Lang, A. R. G., & Yueqin, X. (1986). Estimation of leaf area index from transmission of direct sunlight in discontinuous canopies. *Agricultural and Forest Meteorology*, *37*(3), 229–243. https://doi.org/10.1016/0168-1923(86)90033-X

References

Law, B. E., Arkebauer, T., Campbell, J. L., Chen, J., Sun, O., Schwartz, M., … Verma, S. (2008). Terrestrial carbon observations: Protocols for vegetation sampling and data submission. *FAO, Rome*. Retrieved from http://www.fao.org/gtos/doc/pub55.pdf

Le Dantec, V., Dufrêne, E., & Saugier, B. (2000). Interannual and spatial variation in maximum leaf area index of temperate deciduous stands. *Forest Ecology and Management*, *134*(1–3), 71–81. https://doi.org/10.1016/S0378-1127(99)00246-7

Leathwick, J. R., Wilson, G., & Stephens, R. T. . (2002). *Climate Surfaces for New Zealand* (No. LC9798/126). Landcare Research.

Leblanc, S. G. (2004). *Digital Hemispherical Photography Manual*. Saint-Hubert, Québec: Canada Centre for Remote Sensing. Retrieved from ftp://ftp.ccrs.nrcan.gc.ca/ftp/ad/EMS/butson/DHP%20MANUAL.pdf

Leblanc, S. G., & Chen, J. M. (2001). A practical scheme for correcting multiple scattering effects on optical LAI measurements. *Agricultural and Forest Meteorology*, *110*(2), 125–139. https://doi.org/10.1016/S0168-1923(01)00284-2

Leblanc, S. G., Chen, J. M., Fernandes, R., Deering, D. W., & Conley, A. (2005). Methodology comparison for canopy structure parameters extraction from digital hemispherical photography in boreal forests. *Agricultural and Forest Meteorology*, *129*(3–4), 187–207. https://doi.org/10.1016/j.agrformet.2004.09.006

Leeuwen, M. van, & Nieuwenhuis, M. (2010). Retrieval of forest structural parameters using LiDAR remote sensing. *European Journal of Forest Research*, *129*(4), 749–770. https://doi.org/10.1007/s10342-010-0381-4

Lefsky, M. A., Cohen, W. B., Acker, S. A., Parker, G. G., Spies, T. A., & Harding, D. (1999). Lidar Remote Sensing of the Canopy Structure and Biophysical Properties of Douglas-Fir Western Hemlock Forests. *Remote Sensing of Environment*, *70*(3), 339–361. https://doi.org/10.1016/S0034-4257(99)00052-8

References

Lefsky, M. A., Cohen, W. B., Parker, G. G., & Harding, D. J. (2002). Lidar Remote Sensing for Ecosystem Studies: Lidar, an emerging remote sensing technology that directly measures the three-dimensional distribution of plant canopies, can accurately estimate vegetation structural attributes and should be of particular interest to forest, landscape, and global ecologists. *BioScience*, *52*(1), 19–30. https://doi.org/10.1641/0006-3568(2002)052[0019:LRSFES]2.0.CO;2

Li, Y., Guo, Q., Tao, S., Zheng, G., Zhao, K., Xue, B., & Su, Y. (2016). Derivation, Validation, and Sensitivity Analysis of Terrestrial Laser Scanning-Based Leaf Area Index. *Canadian Journal of Remote Sensing*, *42*(6), 719–729. https://doi.org/10.1080/07038992.2016.1220829

Liang, S., & Li, X. (2012). *Advanced remote sensing*. Amsterdam ; Boston: Academic Press. Retrieved from http://www.sciencedirect.com.ezproxy.canterbury.ac.nz/science/book/9780123859549

LI-COR. (2015). LAI-2200C Plant Canopy Analyzer: Instruction Manual. LI-COR Inc., Lincoln, Nebraska. Retrieved from ftp://ftp.licor.com/perm/env/LAI-2200/Manual/LAI-2200_Manual.pdf

Lilburne, L. R., Hewitt, A. E., & Webb, T. W. (2012). Soil and informatics science combine to develop S-map: A new generation soil information system for New Zealand. *Geoderma*, *170*, 232–238. https://doi.org/10.1016/j.geoderma.2011.11.012

Lim, K., Treitz, P., Wulder, M., St-Onge, B., & Flood, M. (2003). LiDAR remote sensing of forest structure. *Progress in Physical Geography*, *27*(1), 88–106. https://doi.org/10.1191/0309133303pp360ra

Lovell, J. L., Jupp, D. L. B., Culvenor, D. S., & Coops, N. C. (2003). Using airborne and ground-based ranging lidar to measure canopy structure in Australian forests.

Canadian Journal of Remote Sensing, *29*(5), 607–622. https://doi.org/10.5589/m03-026

Macfarlane, C., Grigg, A., & Evangelista, C. (2007). Estimating forest leaf area using cover and fullframe fisheye photography: Thinking inside the circle. *Agricultural and Forest Meteorology*, *146*(1–2), 1–12. https://doi.org/10.1016/j.agrformet.2007.05.001

Macfarlane, C., Hoffman, M., Eamus, D., Kerp, N., Higginson, S., McMurtrie, R., & Adams, M. (2007). Estimation of leaf area index in eucalypt forest using digital photography. *Agricultural and Forest Meteorology*, *143*(3–4), 176–188. https://doi.org/10.1016/j.agrformet.2006.10.013

Macfarlane, C., Ryu, Y., Ogden, G. N., & Sonnentag, O. (2014). Digital canopy photography: Exposed and in the raw. *Agricultural and Forest Meteorology*, *197*, 244–253. https://doi.org/10.1016/j.agrformet.2014.05.014

Magnussen, S., & Boudewyn, P. (1998). Derivations of stand heights from airborne laser scanner data with canopy-based quantile estimators. *Canadian Journal of Forest Research*, *28*(7), 1016–1031. https://doi.org/10.1139/x98-078

Majasalmi, T., Rautiainen, M., Stenberg, P., & Lukeš, P. (2013). An assessment of ground reference methods for estimating LAI of boreal forests. *Forest Ecology and Management*, *292*, 10–18. https://doi.org/10.1016/j.foreco.2012.12.017

Majasalmi, T., Rautiainen, M., Stenberg, P., & Rita, H. (2012). Optimizing the sampling scheme for LAI-2000 measurements in a boreal forest. *Agricultural and Forest Meteorology*, *154–155*, 38–43. https://doi.org/10.1016/j.agrformet.2011.10.002

Mason, E. G., Diepstraten, M., Pinjuv, G. L., & Lasserre, J.-P. (2012). Comparison of direct and indirect leaf area index measurements of Pinus radiata D. Don. *Agricultural and Forest Meteorology*, *166–167*, 113–119. https://doi.org/10.1016/j.agrformet.2012.06.013

References

McGaughey, R. J. (2015). FUSION (Version 3.42). Washington, USA: USDA. Retrieved from http://forsys.cfr.washington.edu/fusion/fusionlatest.html

McGaughey, R. J., Andersen, H., & Reutebuch, S. E. (2006). Considerations for planning, acquiring, and processing LIDAR data for forestry applications. In *11th Biennial USDA Forest Service Remote Sensing Applications Conference, Salt Lake City, UT*. Retrieved from http://forsys.cfr.washington.edu/JFSP06/publications/McGaughey_et_al_2006.pdf

McLaren, R. G., & Cameron, K. C. (1996). *Soil science: sustainable production and environmental protection*. Auckland; New York: Oxford University Press.

Miller, J. B. (1967). A formula for average foliage density. *Australian Journal of Botany, 15*(1), 141–144.

Monsi, M., & Saeki, T. (1953). Uber den Lichtfaktor in den Pflanzengesellschaften und seine Bedeutung fur die Stoffproduktion. *Japanese Journal of Botany, 14*(1), 22–52.

Monsi, M., & Saeki, T. (2005). On the Factor Light in Plant Communities and its Importance for Matter Production. *Annals of Botany, 95*(3), 549–567. https://doi.org/10.1093/aob/mci052

Moorthy, I., Miller, J. R., Hu, B., Chen, J., & Li, Q. (2008). Retrieving crown leaf area index from an individual tree using ground-based lidar data. *Canadian Journal of Remote Sensing, 34*(3), 320–332. https://doi.org/10.5589/m08-027

Morgenroth, J., & Visser, R. (2013). Uptake and barriers to the use of geospatial technologies in forest management. *New Zealand Journal of Forestry Science, 43*(1), 1–9. https://doi.org/10.1186/1179-5395-43-16

Morrison, H., Hopkinson, C., Chasmer, L., & Kljun, N. (2011). Generating an automated approach to optimize effective leaf area index by Canadian boreal forest species using airborne LiDAR. In *Silvilaser 11th International Conference on LiDAR Applications*

for Assessing Forest Ecosystems. Retrieved from http://www.locuscor.net/silvilaser2011/papers/060_Morrison.pdf

Morsdorf, F. (2006). *LIDAR remote sensing for estimation of biophysical vegetation parameters*. University of Zurich, Zurich. Retrieved from http://doi.org/10.5167/uzh-3756

Morsdorf, F., Frey, O., Meier, E., Itten, K. I., & Allgöwer, B. (2008). Assessment of the influence of flying altitude and scan angle on biophysical vegetation products derived from airborne laser scanning. *International Journal of Remote Sensing*, *29*(5), 1387–1406. https://doi.org/10.1080/01431160701736349

Morsdorf, F., Kötz, B., Meier, E., Itten, K. I., & Allgöwer, B. (2006). Estimation of LAI and fractional cover from small footprint airborne laser scanning data based on gap fraction. *Remote Sensing of Environment*, *104*(1), 50–61. https://doi.org/10.1016/j.rse.2006.04.019

MPI. (2012). *National Exotic Forest Description as at 1 April 2012* (No. 1170–5191). Wellington: MPI. Retrieved from http://www.mpi.govt.nz/document-vault/3951

Mu, Q., Heinsch, F. A., Zhao, M., & Running, S. W. (2007). Development of a global evapotranspiration algorithm based on MODIS and global meteorology data. *Remote Sensing of Environment*, *111*(4), 519–536. https://doi.org/10.1016/j.rse.2007.04.015

Nackaerts, K., Coppin, P., Muys, B., & Hermy, M. (2000). Sampling methodology for LAI measurements with LAI-2000 in small forest stands. *Agricultural and Forest Meteorology*, *101*(4), 247–250. https://doi.org/10.1016/S0168-1923(00)00090-3

Næsset, E. (2002). Predicting forest stand characteristics with airborne scanning laser using a practical two-stage procedure and field data. *Remote Sensing of Environment*, *80*(1), 88–99. https://doi.org/10.1016/S0034-4257(01)00290-5

References

Neilsen, W. A., Pataczek, W., Lynch, T., & Pyrke, R. (1992). Growth response of Pinus radiata to multiple applications of nitrogen fertilizer and evaluation of the quantity of added nitrogen remaining in the forest system. *Plant and Soil*, *144*(2), 207–217. https://doi.org/10.1007/BF00012877

Nilson, T. (1971). A theoretical analysis of the frequency of gaps in plant stands. *Agricultural Meteorology*, *8*, 25–38. https://doi.org/10.1016/0002-1571(71)90092-6

Nilson, T. (1999). Inversion of gap frequency data in forest stands. *Agricultural and Forest Meteorology*, *98–99*, 437–448. https://doi.org/10.1016/S0168-1923(99)00114-8

Noda, H. M., Motohka, T., Murakami, K., Muraoka, H., & Nasahara, K. N. (2013). Accurate measurement of optical properties of narrow leaves and conifer needles with a typical integrating sphere and spectroradiometer. *Plant, Cell & Environment*, *36*(10), 1903–1909. https://doi.org/10.1111/pce.12100

Økland, T., & Næsset, E. (2002). Estimating tree height and tree crown properties using airborne scanning laser in a boreal nature reserve. *Remote Sensing of Environment*, *79*(1), 105–115. https://doi.org/10.1016/S0034-4257(01)00243-7

Pearse, G. D., Moltchanova, E., & Bloomberg, M. (2015). Assessment of the accuracy of profile available water and potential rooting depth estimates held within New Zealand's fundamental soil layers geo-database. *Soil Research*, *53*(7), 737–744. https://doi.org/10.1071/SR14012

Pearse, G. D., Watt, M. S., & Morgenroth, J. (2016). Comparison of optical LAI measurements under diffuse and clear skies after correcting for scattered radiation. *Agricultural and Forest Meteorology*, *221*, 61–70. https://doi.org/10.1016/j.agrformet.2016.02.001

Peduzzi, A., Wynne, R. H., Fox, T. R., Nelson, R. F., & Thomas, V. A. (2012). Estimating leaf area index in intensively managed pine plantations using airborne laser scanner

data. *Forest Ecology and Management*, *270*, 54–65. https://doi.org/10.1016/j.foreco.2011.12.048

Peñuelas, J., & Filella, I. (1998). Visible and near-infrared reflectance techniques for diagnosing plant physiological status. *Trends in Plant Science*, *3*(4), 151–156. https://doi.org/10.1016/S1360-1385(98)01213-8

Perry, S. G., Fraser, A. B., Thomson, D. W., & Norman, J. M. (1988). Indirect sensing of plant canopy structure with simple radiation measurements. *Agricultural and Forest Meteorology*, *42*(2–3), 255–278. https://doi.org/10.1016/0168-1923(88)90082-2

Piayda, A., Dubbert, M., Werner, C., Vaz Correia, A., Pereira, J. S., & Cuntz, M. (2015). Influence of woody tissue and leaf clumping on vertically resolved leaf area index and angular gap probability estimates. *Forest Ecology and Management*, *340*, 103–113. https://doi.org/10.1016/j.foreco.2014.12.026

Pinheiro, J., Bates, D., DebRoy, S., Sarkar, D., & R Core Team. (2015). *nlme: Linear and Nonlinear Mixed Effects Models*. Retrieved from http://CRAN.R-project.org/package=nlme

Pisek, J., Ryu, Y., & Alikas, K. (2011). Estimating leaf inclination and G-function from leveled digital camera photography in broadleaf canopies. *Trees*, *25*(5), 919–924. https://doi.org/10.1007/s00468-011-0566-6

Pont, D., Kimberley, M. O., Brownlie, R. K., Sabatia, C. O., & Watt, M. S. (2015). Calibrated tree counting on remotely sensed images of planted forests. *International Journal of Remote Sensing*, *36*(15), 3819–3836. https://doi.org/10.1080/01431161.2015.1054048

Pope, G., & Treitz, P. (2013). Leaf Area Index (LAI) Estimation in Boreal Mixedwood Forest of Ontario, Canada Using Light Detection and Ranging (LiDAR) and WorldView-2 Imagery. *Remote Sensing*, *5*(10), 5040–5063. https://doi.org/10.3390/rs5105040

References

Popescu, S., & Zhao, K. (2008). A voxel-based lidar method for estimating crown base height for deciduous and pine trees. *Remote Sensing of Environment*, *112*(3), 767–781. https://doi.org/10.1016/j.rse.2007.06.011

Popescu, S., Zhao, K., Neuenschwander, A., & Lin, C. (2011). Satellite lidar vs. small footprint airborne lidar: Comparing the accuracy of aboveground biomass estimates and forest structure metrics at footprint level. *Remote Sensing of Environment*, *115*(11), 2786–2797. https://doi.org/10.1016/j.rse.2011.01.026

Pu, R., & Cheng, J. (2015). Mapping forest leaf area index using reflectance and textural information derived from WorldView-2 imagery in a mixed natural forest area in Florida, US. *International Journal of Applied Earth Observation and Geoinformation*, *42*, 11–23. https://doi.org/10.1016/j.jag.2015.05.004

R Core Team. (2015). R: A Language and Environment for Statistical Computing (Version 3.1.3). Vienna, Austria: R Foundation for Statistical Computing. Retrieved from http://www.R-project.org

Radtke, P. J., & Bolstad, P. V. (2001). Laser point-quadrat sampling for estimating foliage-height profiles in broad-leaved forests. *Canadian Journal of Forest Research*, *31*(3), 410–418. https://doi.org/10.1139/x00-182

Raison, R. J., & Myers, B. J. (1992). The Biology of Forest Growth experiment: linking water and nitrogen availability to the growth of Pinus radiata. *Forest Ecology and Management*, *52*(1–4), 279–308. https://doi.org/10.1016/0378-1127(92)90506-5

Riaño, D., Valladares, F., Condés, S., & Chuvieco, E. (2004). Estimation of leaf area index and covered ground from airborne laser scanner (Lidar) in two contrasting forests. *Agricultural and Forest Meteorology*, *124*(3–4), 269–275. https://doi.org/10.1016/j.agrformet.2004.02.005

References

Rich, P. M. (1990). Characterizing plant canopies with hemispherical photographs. *Remote Sensing Reviews*, *5*(1), 13–29. https://doi.org/10.1080/02757259009532119

Richardson, J. J., Moskal, L. M., & Kim, S.-H. (2009). Modeling approaches to estimate effective leaf area index from aerial discrete-return LIDAR. *Agricultural and Forest Meteorology*, *149*(6–7), 1152–1160. https://doi.org/10.1016/j.agrformet.2009.02.007

Roberts, S. D., Dean, T. J., Evans, D. L., McCombs, J. W., Harrington, R. L., & Glass, P. A. (2005). Estimating individual tree leaf area in loblolly pine plantations using LiDAR-derived measurements of height and crown dimensions. *Forest Ecology and Management*, *213*(1–3), 54–70. https://doi.org/10.1016/j.foreco.2005.03.025

Rombouts, J., Ferguson, I. S., & Leech, J. W. (2010). Campaign and site effects in LiDAR prediction models for site-quality assessment of radiata pine plantations in South Australia. *International Journal of Remote Sensing*, *31*(5), 1155–1173. https://doi.org/10.1080/01431160903380573

Rosette, J., North, P. R. J., Rubio-Gil, J., Cook, B., Los, S., Suarez, J., … Blair, J. B. (2013). Evaluating Prospects for Improved Forest Parameter Retrieval From Satellite LiDAR Using a Physically-Based Radiative Transfer Model. *IEEE Journal of Selected Topics in Applied Earth Observations and Remote Sensing*, *6*(1), 45–53. https://doi.org/10.1109/JSTARS.2013.2244199

Rubilar, R. A., Albaugh, T. J., Allen, H. L., Alvarez, J., Fox, T. R., & Stape, J. L. (2013a). Foliage development and leaf area duration in Pinus radiata. *Forest Ecology and Management*, *304*, 455–463. https://doi.org/10.1016/j.foreco.2013.05.044

Rubilar, R. A., Albaugh, T. J., Allen, H. L., Alvarez, J., Fox, T. R., & Stape, J. L. (2013b). Influences of silvicultural manipulations on above- and belowground biomass accumulations and leaf area in young Pinus radiata plantations, at three contrasting sites in Chile. *Forestry*, *86*(1), 27–38. https://doi.org/10.1093/forestry/cps055

References

Ryu, Y., Nilson, T., Kobayashi, H., Sonnentag, O., Law, B. E., & Baldocchi, D. D. (2010). On the correct estimation of effective leaf area index: Does it reveal information on clumping effects? *Agricultural and Forest Meteorology*, *150*(3), 463–472. https://doi.org/10.1016/j.agrformet.2010.01.009

Schutz, B. E., Zwally, H. J., Shuman, C. A., Hancock, D., & DiMarzio, J. P. (2005). Overview of the ICESat Mission. *Geophysical Research Letters*, *32*(21), L21S01. https://doi.org/10.1029/2005GL024009

Seidel, D., Fleck, S., & Leuschner, C. (2012). Analyzing forest canopies with ground-based laser scanning: A comparison with hemispherical photography. *Agricultural and Forest Meteorology*, *154–155*, 1–8. https://doi.org/10.1016/j.agrformet.2011.10.006

Sellers, P. J. (1985). Canopy reflectance, photosynthesis and transpiration. *International Journal of Remote Sensing*, *6*(8), 1335–1372. https://doi.org/10.1080/01431168508948283

Sellers, P. J., Berry, J. A., Collatz, G. J., Field, C. B., & Hall, F. G. (1992). Canopy reflectance, photosynthesis, and transpiration. III. A reanalysis using improved leaf models and a new canopy integration scheme. *Remote Sensing of Environment*, *42*(3), 187–216. https://doi.org/10.1016/0034-4257(92)90102-P

Smith, N. J. (1991). Predicting Radiation Attenuation in Stands of Douglas-Fir. *Forest Science*, *37*(5), 1213–1223.

Solberg, S., Brunner, A., Hanssen, K. H., Lange, H., Næsset, E., Rautiainen, M., & Stenberg, P. (2009). Mapping LAI in a Norway spruce forest using airborne laser scanning. *Remote Sensing of Environment*, *113*(11), 2317–2327. https://doi.org/10.1016/j.rse.2009.06.010

Solberg, S., Næsset, E., Hanssen, K. H., & Christiansen, E. (2006). Mapping defoliation during a severe insect attack on Scots pine using airborne laser scanning. *Remote*

Sensing of Environment, *102*(3–4), 364–376. https://doi.org/10.1016/j.rse.2006.03.001

Song, C. (2013). Optical remote sensing of forest leaf area index and biomass. *Progress in Physical Geography*, *37*(1), 98–113. https://doi.org/10.1177/0309133312471367

Soudani, K., François, C., le Maire, G., Le Dantec, V., & Dufrêne, E. (2006). Comparative analysis of IKONOS, SPOT, and ETM+ data for leaf area index estimation in temperate coniferous and deciduous forest stands. *Remote Sensing of Environment*, *102*(1–2), 161–175. https://doi.org/10.1016/j.rse.2006.02.004

Stenberg, P. (2006). A note on the G-function for needle leaf canopies. *Agricultural and Forest Meteorology*, *136*(1–2), 76–79. https://doi.org/10.1016/j.agrformet.2006.01.009

Stenberg, P., Linder, S., Smolander, H., & Flower-Ellis, J. (1994). Performance of the LAI-2000 plant canopy analyzer in estimating leaf area index of some Scots pine stands. *Tree Physiology*, *14*(7-8–9), 981–995. https://doi.org/10.1093/treephys/14.7-8-9.981

Stenberg, P., Rautiainen, M., Manninen, T., Voipio, P., & Smolander, H. (2004). Reduced simple ratio better than NDVI for estimating LAI in Finnish pine and spruce stands. *Silva Fennica*, *38*(1), 3–14. https://doi.org/10.14214/sf.431

Stone, C., Chisholm, L., & McDonald, S. (2003). Spectral reflectance characteristics of Pinus radiata needles affected by dothistroma needle blight. *Canadian Journal of Botany*, *81*(6), 560–569. https://doi.org/10.1139/b03-053

Strobl, C., Boulesteix, A.-L., Kneib, T., Augustin, T., & Zeileis, A. (2008). Conditional variable importance for random forests. *BMC Bioinformatics*, *9*, 307. https://doi.org/10.1186/1471-2105-9-307

References

Strobl, C., & Zeileis, A. (2008). Danger: high power!–exploring the statistical properties of a test for random forest variable importance, *17*. Retrieved from http://nbn-resolving.de/urn/resolver.pl?urn=nbn:de:bvb:19-epub-2111-8

Sumnall, M., Peduzzi, A., Fox, T. R., Wynne, R. H., Thomas, V. A., & Cook, B. (2016). Assessing the transferability of statistical predictive models for leaf area index between two airborne discrete return LiDAR sensor designs within multiple intensely managed Loblolly pine forest locations in the south-eastern USA. *Remote Sensing of Environment, 176*, 308–319. https://doi.org/10.1016/j.rse.2016.02.012

Tang, H., Brolly, M., Zhao, F., Strahler, A. H., Schaaf, C. L., Ganguly, S., … Dubayah, R. (2014). Deriving and validating Leaf Area Index (LAI) at multiple spatial scales through lidar remote sensing: A case study in Sierra National Forest, CA. *Remote Sensing of Environment, 143*, 131–141. https://doi.org/10.1016/j.rse.2013.12.007

Tang, H., Dubayah, R., Swatantran, A., Hofton, M., Sheldon, S., Clark, D. B., & Blair, B. (2012). Retrieval of vertical LAI profiles over tropical rain forests using waveform lidar at La Selva, Costa Rica. *Remote Sensing of Environment, 124*, 242–250. https://doi.org/10.1016/j.rse.2012.05.005

Trotter, C. M., & Hosking, G. R. (1998). *Diagnostic Spectral Features of Pinus Radiata Foliage* (No. LC9798/127). Palmerston North: Landcare Research.

Tucker, C. J. (1979). Red and photographic infrared linear combinations for monitoring vegetation. *Remote Sensing of Environment*, *8*(2), 127–150. https://doi.org/10.1016/0034-4257(79)90013-0

Turner, D. P., Cohen, W. B., Kennedy, R. E., Fassnacht, K. S., & Briggs, J. M. (1999). Relationships between Leaf Area Index and Landsat TM Spectral Vegetation Indices across Three Temperate Zone Sites. *Remote Sensing of Environment*, *70*(1), 52–68. https://doi.org/10.1016/S0034-4257(99)00057-7

References

Van Ewijk, K. (2015, April 28). *Estimating Forest Structure from LiDAR and High Spatial Resolution Imagery for the Prediction of Succession and Species Composition*. Queen's University. Retrieved from http://hdl.handle.net/1974/13014

van Gardingen, P. ., Jackson, G. ., Hernandez-Daumas, S., Russell, G., & Sharp, L. (1999). Leaf area index estimates obtained for clumped canopies using hemispherical photography. *Agricultural and Forest Meteorology*, *94*(3–4), 243–257. https://doi.org/10.1016/S0168-1923(99)00018-0

Vose, J. M., Dougherty, P. M., Long, J. N., Smith, F. W., Gholz, H. L., & Curran, P. J. (1994). Factors Influencing the Amount and Distribution of Leaf Area of Pine Stands. *Ecological Bulletins*, (43), 102–114. https://doi.org/10.2307/20113135

Walt, S. van der, Colbert, S. C., & Varoquaux, G. (2011). The NumPy Array: A Structure for Efficient Numerical Computation. *Computing in Science & Engineering*, *13*(2), 22–30. https://doi.org/10.1109/MCSE.2011.37

Wang, W.-M., Li, Z.-L., & Su, H.-B. (2007). Comparison of leaf angle distribution functions: Effects on extinction coefficient and fraction of sunlit foliage. *Agricultural and Forest Meteorology*, *143*(1–2), 106–122. https://doi.org/10.1016/j.agrformet.2006.12.003

Wang, X., Cheng, X., Gong, P., Huang, H., Li, Z., & Li, X. (2011). Earth science applications of ICESat/GLAS: a review. *International Journal of Remote Sensing*, *32*(23), 8837–8864. https://doi.org/10.1080/01431161.2010.547533

Wang, Y., Woodcock, C. E., Buermann, W., Stenberg, P., Voipio, P., Smolander, H., … Myneni, R. B. (2004). Evaluation of the MODIS LAI algorithm at a coniferous forest site in Finland. *Remote Sensing of Environment*, *91*(1), 114–127. https://doi.org/10.1016/j.rse.2004.02.007

Watt, M. S., Dash, J. P., Bhandari, S., & Watt, P. J. (2015). Comparing parametric and non-parametric methods of predicting Site Index for radiata pine using combinations of

data derived from environmental surfaces, satellite imagery and airborne laser scanning. *Forest Ecology and Management*, *357*, 1–9. https://doi.org/10.1016/j.foreco.2015.08.001

Watt, M. S., Dash, J. P., Watt, P. J., & Bhandari, S. (2016). Multi-sensor modelling of a forest productivity index for radiata pine plantations. *New Zealand Journal of Forestry Science*, *46*(1), 1–14. https://doi.org/10.1186/s40490-016-0065-z

Watt, M. S., Palmer, D. J., Kimberley, M. O., Höck, B. K., Payn, T. W., & Lowe, D. J. (2010). Development of models to predict Pinus radiata productivity throughout New Zealand. *Canadian Journal of Forest Research*, *40*(3), 488–499. https://doi.org/10.1139/X09-207

Watt, P. J., & Watt, M. S. (2013). Development of a national model of Pinus radiata stand volume from lidar metrics for New Zealand. *International Journal of Remote Sensing*, *34*(16), 5892–5904. https://doi.org/10.1080/01431161.2013.798053

Wehr, A., & Lohr, U. (1999). Airborne laser scanning—an introduction and overview. *ISPRS Journal of Photogrammetry and Remote Sensing*, *54*(2–3), 68–82. https://doi.org/10.1016/S0924-2716(99)00011-8

Weiskittel, A. R., & Maguire, D. A. (2007). Response of Douglas-fir leaf area index and litterfall dynamics to Swiss needle cast in north coastal Oregon, USA. *Annals of Forest Science*, *64*(2), 121–132. https://doi.org/10.1051/forest:2006096

Weiss, M., Baret, F., Smith, G. J., Jonckheere, I., & Coppin, P. (2004). Review of methods for in situ leaf area index (LAI) determination: Part II. Estimation of LAI, errors and sampling. *Agricultural and Forest Meteorology*, *121*(1–2), 37–53. https://doi.org/10.1016/j.agrformet.2003.08.001

References

Welles, J. M., & Cohen, S. (1996). Canopy structure measurement by gap fraction analysis using commercial instrumentation. *Journal of Experimental Botany*, *47*(9), 1335–1342. https://doi.org/10.1093/jxb/47.9.1335

Welles, J. M., & Norman, J. M. (1991). Instrument for Indirect Measurement of Canopy Architecture. *Agronomy Journal*, *83*(5), 818–825. https://doi.org/10.2134/agronj1991.00021962008300050009x

Wilson, J. W. (1959). Analysis of the Spatial Distribution of Foliage by Two-Dimensional Point Quadrats. *New Phytologist*, *58*(1), 92–99. https://doi.org/10.1111/j.1469-8137.1959.tb05340.x

Wilson, J. W. (1960). Inclined Point Quadrats. *New Phytologist*, *59*(1), 1–7. https://doi.org/10.1111/j.1469-8137.1960.tb06195.x

Woodgate, W., Armston, J. D., Disney, M., Jones, S. D., Suarez, L., Hill, M. J., … Soto-Berelov, M. (2016). Quantifying the impact of woody material on leaf area index estimation from hemispherical photography using 3D canopy simulations. *Agricultural and Forest Meteorology*, *226–227*, 1–12. https://doi.org/10.1016/j.agrformet.2016.05.009

Woodgate, W., Disney, M., Armston, J. D., Jones, S. D., Suarez, L., Hill, M. J., … Mellor, A. (2015). An improved theoretical model of canopy gap probability for Leaf Area Index estimation in woody ecosystems. *Forest Ecology and Management*, *358*, 303–320. https://doi.org/10.1016/j.foreco.2015.09.030

Woodgate, W., Jones, S. D., Suarez, L., Hill, M. J., Armston, J. D., Wilkes, P., … Mellor, A. (2015). Understanding the variability in ground-based methods for retrieving canopy openness, gap fraction, and leaf area index in diverse forest systems. *Agricultural and Forest Meteorology*, *205*, 83–95. https://doi.org/10.1016/j.agrformet.2015.02.012

References

Wulder, M. A., White, J. C., Nelson, R. F., Næsset, E., Ørka, H. O., Coops, N. C., … Gobakken, T. (2012). Lidar sampling for large-area forest characterization: A review. *Remote Sensing of Environment*, *121*, 196–209. https://doi.org/10.1016/j.rse.2012.02.001

Xing, Y., de Gier, A., Zhang, J., & Wang, L. (2010). An improved method for estimating forest canopy height using ICESat-GLAS full waveform data over sloping terrain: A case study in Changbai mountains, China. *International Journal of Applied Earth Observation and Geoinformation*, *12*(5), 385–392. https://doi.org/10.1016/j.jag.2010.04.010

Yanez-Rausell, L., Malenovsky, Z., Clevers, J. G. P. W., & Schaepman, M. E. (2014). Minimizing Measurement Uncertainties of Coniferous Needle-Leaf Optical Properties. Part II: Experimental Setup and Error Analysis. *IEEE Journal of Selected Topics in Applied Earth Observations and Remote Sensing*, *7*(2), 406–420. https://doi.org/10.1109/JSTARS.2013.2292817

Yanez-Rausell, L., Schaepman, M. E., Clevers, J. G. P. W., & Malenovsky, Z. (2014). Minimizing Measurement Uncertainties of Coniferous Needle-Leaf Optical Properties, Part I: Methodological Review. *IEEE Journal of Selected Topics in Applied Earth Observations and Remote Sensing*, *7*(2), 399–405. https://doi.org/10.1109/JSTARS.2013.2272890

Yang, W., Tan, B., Huang, D., Rautiainen, M., Shabanov, N. V., Wang, Y., … Myneni, R. B. (2006). MODIS leaf area index products: from validation to algorithm improvement. *IEEE Transactions on Geoscience and Remote Sensing*, *44*(7), 1885–1898. https://doi.org/10.1109/TGRS.2006.871215

Yu, X., Hyyppä, J., Hyyppä, H., & Maltamo, M. (2004). Effects of flight altitude on tree height estimation using airborne laser scanning. In *International Conference*

NATSCAN "Laser-Scanners for Forest and Landscape Assessment – Instruments, Processing Methods and Applications" (Vol. XXXVI, pp. 96–101). Freiburg, Germany: International Archives of Photogrammetry, Remote Sensing and Spatial Information Sciences. Retrieved from http://citeseerx.ist.psu.edu/viewdoc/download?doi=10.1.1.151.611&rep=rep1&type=pdf

Zarco-Tejada, P. J., Miller, J. R., Harron, J., Hu, B., Noland, T. L., Goel, N., … Sampson, P. (2004). Needle chlorophyll content estimation through model inversion using hyperspectral data from boreal conifer forest canopies. *Remote Sensing of Environment*, *89*(2), 189–199. https://doi.org/10.1016/j.rse.2002.06.002

Zhang, Y., Chen, J. M., & Miller, J. R. (2005). Determining digital hemispherical photograph exposure for leaf area index estimation. *Agricultural and Forest Meteorology*, *133*(1–4), 166–181. https://doi.org/10.1016/j.agrformet.2005.09.009

Zhao, F., Strahler, A. H., Schaaf, C. L., Yao, T., Yang, X., Wang, Z., … Newnham, G. J. (2012). Measuring gap fraction, element clumping index and LAI in Sierra Forest stands using a full-waveform ground-based lidar. *Remote Sensing of Environment*, *125*, 73–79. https://doi.org/10.1016/j.rse.2012.07.007

Zhao, F., Yang, X., Schull, M. A., Román-Colón, M. O., Yao, T., Wang, Z., … Strahler, A. H. (2011). Measuring effective leaf area index, foliage profile, and stand height in New England forest stands using a full-waveform ground-based lidar. *Remote Sensing of Environment*, *115*(11), 2954–2964. https://doi.org/10.1016/j.rse.2010.08.030

Zhao, K., & Popescu, S. (2009). Lidar-based mapping of leaf area index and its use for validating GLOBCARBON satellite LAI product in a temperate forest of the southern USA. *Remote Sensing of Environment*, *113*(8), 1628–1645. https://doi.org/10.1016/j.rse.2009.03.006

References

Zheng, G., & Moskal, L. M. (2009). Retrieving Leaf Area Index (LAI) Using Remote Sensing: Theories, Methods and Sensors. *Sensors*, *9*(4), 2719–2745. https://doi.org/10.3390/s90402719

Zheng, G., & Moskal, L. M. (2012). Computational-Geometry-Based Retrieval of Effective Leaf Area Index Using Terrestrial Laser Scanning. *IEEE Transactions on Geoscience and Remote Sensing*, *50*(10), 3958–3969. https://doi.org/10.1109/TGRS.2012.2187907

Zheng, G., Moskal, L. M., & Kim, S.-H. (2013). Retrieval of Effective Leaf Area Index in Heterogeneous Forests With Terrestrial Laser Scanning. *IEEE Transactions on Geoscience and Remote Sensing*, *51*(2), 777–786. https://doi.org/10.1109/TGRS.2012.2205003

Zou, H., & Hastie, T. (2005). Regularization and variable selection via the elastic net. *Journal of the Royal Statistical Society: Series B (Statistical Methodology)*, *67*(2), 301–320. https://doi.org/10.1111/j.1467-9868.2005.00503.x